NASA TECHNICAL REPORT

NASA TR R-374

NASA TR R-374
C.1

CALCULATION OF NONLINEAR CONICAL FLOWS BY THE METHOD OF LINES

by E. B. Klunker, Jerry C. South, Jr., and Ruby M. Davis

Langley Research Center
Hampton, Va. 23365

NATIONAL AERONAUTICS AND SPACE ADMINISTRATION • WASHINGTON, D. C. • OCTOBER 1971

1. Report No.	2. Government Accession No.	3. Recipient's Catalog No.
NASA TR R-374		

4. Title and Subtitle
CALCULATION OF NONLINEAR CONICAL FLOWS BY THE METHOD OF LINES

5. Report Date
October 1971

6. Performing Organization Code

7. Author(s)
E. B. Klunker, Jerry C. South, Jr., and Ruby M. Davis

8. Performing Organization Report No.
L-7813

9. Performing Organization Name and Address
NASA Langley Research Center
Hampton, Va. 23365

10. Work Unit No.
136-13-05-01

11. Contract or Grant No.

12. Sponsoring Agency Name and Address
National Aeronautics and Space Administration
Washington, D.C. 20546

13. Type of Report and Period Covered
Technical Report

14. Sponsoring Agency Code

15. Supplementary Notes

16. Abstract

A computational technique, called the method of lines, is developed for computing the flow field about conical configurations at incidence in a supersonic flow. The method, which makes use of the self-similarity property, is developed for the nonlinear flow equations. The method has proved to be an efficient and versatile procedure for constructing the numerical solutions to conical flow problems. It has been successful in computing the flow about circular and elliptic cones at conditions where small regions of supersonic cross flow develop and for the conical delta wings where the region of supersonic cross flow is extensive. The calculations made for circular and elliptic cones as well as for the compression side of various conical delta wings are in good agreement with experiment except in regions where viscous effects become important.

17. Key Words (Suggested by Author(s))	18. Distribution Statement
Method of lines Conical flow Entropy layer Delta wings	Unclassified – Unlimited

19. Security Classif. (of this report)	20. Security Classif. (of this page)	21. No. of Pages	22. Price*
Unclassified	Unclassified	80	$3.00

*For sale by the National Technical Information Service, Springfield, Virginia 22151

CONTENTS

	Page
SUMMARY	1
INTRODUCTION	1
BACKGROUND	3
Nonlinear Conical Methods	3
Method of Lines	5
SYMBOLS	6
METHOD	9
Conical Coordinates	9
Differential Equations	10
Transformation to a rectangular region	11
Geometric Parameters	14
The Method of Lines	15
Symmetry and Boundary Conditions	16
Symmetry conditions	16
Flow tangency at surface	16
Shock-wave conditions	17
Attached shock at wing leading edge	17
Determination of the Shock Shape	17
Newton iteration for shock shape	17
Modified Newton iteration procedure	18
Approximate starting shock shapes	19
Extrapolation to Surface	21
Corrected isentropic surface values	21
Computation of the surface entropy	22
Stability and Error Growth	22
Force Coefficients	23
RESULTS AND DISCUSSION	24
Circular Cone	24
Difficulties at large relative incidence	25
Extrapolation of surface pressures to large angles of incidence	28
Artificial hump on leeward side	29
Entropy Layer and Vortical Singularities	31
Entropy layer	32
Vortical singularity lift-off	34

Page

Elliptic Cone 36
Extrapolated surface pressures 37
Cross-flow streamline pattern 38
Computation history 39
Effect of number of lines 41
Elliptic cone with large axis ratio 41
Comparison of an elliptic cone computation with other methods 44
Elliptic cone at yaw 44
Conical Delta Wings 49
Parabolic-arc cross section 50
Circular-arc cross section 52
Flat delta wing 53
Wing with reverse curvature 57
Convergence history 59
Convergence with increasing N 59
Variable Line Spacing 61

CONCLUDING REMARKS 61

APPENDIX A – GEOMETRICAL RELATIONS 63
Arc Length 63
Direction Cosines 65

APPENDIX B – FLOW PROPERTIES BEHIND SHOCK WAVE 67
Shock Conditions 67
Attached Shock at Wing Leading Edge 69

APPENDIX C – FORCE AND MOMENT COEFFICIENTS 71

REFERENCES 74

CALCULATION OF NONLINEAR CONICAL FLOWS BY THE METHOD OF LINES

By E. B. Klunker, Jerry C. South, Jr., and Ruby M. Davis
Langley Research Center

SUMMARY

A computational technique, called the method of lines, is developed for computing the flow field about conical configurations at incidence in a supersonic flow. The method, which makes use of the self-similarity property, is developed for the nonlinear flow equations. The basic idea is to discretize all but one of the independent variables in the partial differential equations so that a coupled system of approximate, simultaneous, ordinary differential-difference equations is obtained. Initial values of these differential-difference equations are determined from the shock relations after the shock shape is estimated or otherwise specified. The system of equations is integrated numerically and an iterative process is utilized for adjusting the shock shape to satisfy the boundary condition of flow tangency on the body.

The method has proved to be an efficient and versatile procedure for constructing the numerical solutions to conical flow problems. It has been successful in computing the flow about circular and elliptic cones at conditions where small regions of supersonic cross flow develop and for the conical delta wings where the region of supersonic cross flow is extensive. The calculations made for circular and elliptic cones as well as for the compression side of various conical delta wings are in good agreement with experiment except in regions where viscous effects become important.

INTRODUCTION

In 1935 Busemann (ref. 1) introduced the concept of a general conical flow field as one in which the fluid properties are constant along any ray emanating from a common point in the flow. Solutions for such self-similar conical flows are of great importance to the aerodynamicist since (1) significant regions of the flow about many practical configurations are conical, or nearly so; (2) conical bodies and wings are the simplest class of three-dimensional shapes and thereby provide "benchmark" cases for both theoretical and experimental studies in supersonic and hypersonic flow.

Although the self-similarity property of conical flow allows the reduction of the problem from three to two space dimensions, the analyst finds himself confronted with a formidable free-boundary problem for nonlinear partial differential equations of elliptic

or mixed type. Hence until the last decade, most conical solutions have been obtained only for the simplest cases or after linearization or other approximations to the equations. However, recent advances in speed and storage of digital computers have spurred the development of numerical solutions of the full nonlinear equations, to the point where solutions to very general conical flow problems can be obtained in a few minutes.

A particularly efficient numerical technique for solving conical flow problems has been reported in references 2 to 4. The method is semidiscrete, wherein one independent variable is discretized while the other remains as a continuous variable. This method is referred to as the method of lines, to distinguish it from grid or network computations where all independent variables are discretized.

The method of lines is "direct" in the sense that the body shape is given and is one of the bounding coordinate surfaces; yet, the shock wave is another bounding coordinate surface, and the governing differential equations are solved by integrating inward from the shock. Thus, in that respect, the method is like the inverse methods. The technique employed for solving this free boundary problem has three distinguishing features: (1) the coordinate transformation which maps the region between the shock and body onto a rectangle, (2) the solution of the equations by the semidiscrete method of lines, and (3) an iteration procedure for satisfying the boundary conditions. None of these features are new; yet when combined, they prove to be an efficient means of solving free boundary problems such as the supersonic blunt-body problem or conical flows. The basic idea of the method of lines is to discretize all but one of the independent variables in the partial differential equations so that a system of approximate, simultaneous, ordinary, differential-difference equations is obtained. Initial values for the system of equations are estimated, or otherwise specified, and the system of equations is integrated numerically. An iterative process is utilized to satisfy the boundary conditions; thus, the initial values are subsequently altered and the equations are again integrated. The success of the method of lines as a computational tool hinges upon (1) formulation of the problem in a form which requires relatively few lines, (2) use of an efficient integration routine that yields good accuracy with relatively large integration steps, and (3) development of an efficient interative process to satisfy the boundary conditions. The first requirement is largely met through the choice of the coordinate system and the second can be satisfied with any of a number of integration schemes such as a fourth-order Runge-Kutta method. The computational time and the utility of the method depend to a large part on the iterative process.

The present paper expands upon the material in reference 4; further details and refinements of the method are presented, together with numerous applications to a variety of conical flow problems. Comparisons of the present calculations with other theories and experiment are given for circular and elliptic cones, and conical delta wings.

The stream velocity vector lies in a plane of symmetry for all the configurations; however, this restriction is not a limitation of the method itself. Some of the more theoretical aspects of conical flow are touched on, such as the inviscid entropy layer with the attendant steep gradients adjacent to the surface, and the nodal-type singularities of the cross-flow streamline patterns.

To aid the reader, numerous headings and subsections are employed. A separate section "Background" is included which cites most of the recent work in nonlinear conical flow theory, in particular, the related work in the U.S.S.R. which seems to have gone relatively unnoticed.

BACKGROUND

In this section, a review of past work in nonlinear supersonic conical flow theory is given. No effort has been made to consider the large body of literature which concerns linearized conical flow theory.

Nonlinear Conical Methods

The earliest treatment of nonaxisymmetric conical flow was given by Stone (ref. 5) together with the numerical computations carried out under the direction of Kopal (ref. 6), where the flow about circular cones at small incidence was constructed as a perturbation about the axisymmetric nonlinear Taylor-Maccoll solution (ref. 7). Ferri (ref. 8) recognized the singularities of these conical flows, which were not accounted for in the Stone solution, and discussed the general features of the streamlines. The many analytical papers published since (refs. 9 to 11 and many other papers referenced in these works) have been concerned largely with the construction of solutions to conical flows by means of matched asymptotic expansions. These papers have concentrated primarily on the theoretical development; consequently, there has been relatively little computational work presented.

Two basic approaches are available for the numerical development of exact nonlinear conical solutions:[1]

(1) Distance-asymptotic methods, where some initial distribution of the flow variables and shock-wave shape is used near the apex as initial values for continuing the calculation downstream by some three-dimensional computation scheme. The calculation proceeds until conical similarity conditions are sufficiently satisfied.

[1]Exact in the sense that the only approximation made is the reduction of the governing partial differential equations to ordinary differential equations or algebraic equations by using finite-difference expressions for the derivatives with respect to one or more of the coordinates.

(2) Methods which invoke the conical self-similarity and thereby reduce to two the number of independent variables are referred to simply as "conical" methods for brevity.

Both general approaches have their merits. The distance-asymptotic techniques develop the solution as a well-posed initial-boundary problem for equations of hyperbolic type, and convergence is "almost" guaranteed from both physical and theoretical considerations. However, to achieve a satisfactory solution in many problems where a fine mesh is needed, these methods require a large amount of computer storage and time. The conical methods reduce the problem to one in two dimensions but in the more difficult form of a free boundary problem for equations of elliptic or mixed type. In fact, many of the conical methods are similar to methods used for solving the blunt-body problem.

The methods of references 12 to 20 are examples of the distance-asymptotic method. References 12, 13, and 14 considered circular cones at angle of attack, references 15 and 16 included cones of elliptic cross section, and reference 17 presents calculations for the compression side of conical delta wings with the shock wave attached not only at the apex, but also along the swept leading edges. More recently, a three-dimensional characteristic method has been developed to compute the flow about some delta-wing configurations, also with an attached leading-edge shock (ref. 18). In references 19 and 20, a method is presented which is essentially a distance-asymptotic method, and which treats shock waves not as discontinuities, but as rapid but continuous compressions. This method appears to be most promising for problems in which complicated embedded shock patterns may occur. Reference 19 presents results not only for circular cones at incidence, but also for a conical wing-body configuration. Reference 20 includes results for both the expansion and compression sides of planar delta wings with shock attached at the leading edge.

Examples of conical methods appear as early as 1929, when Busemann (ref. 21) constructed the axisymmetric conical flow by numerical-graphical construction in the hodograph plane. Reference 22 (pp. 526-536) cites many of the approximate and exact conical methods documented up to about 1964; therefore, they are not all discussed in the present paper. Most recent conical methods are of the "inverse" type, in which a simple analytic function is assumed for the conical shock wave, and the governing partial differential equations are solved by marching inward until some body shape is obtained. Various inverse methods are reported in references 23 to 27. These methods have not been successful in constructing solutions for body shapes which produce a shock wave requiring many parameters for an adequate description; only circular-cross-section cones at incidence have been amenable whereas solutions for elliptic cones have been obtained only painstakingly. Other conical methods have used the method of relaxation in regions where the cross flow (velocity component normal to a conical ray) is subsonic,

and the governing differential equations are of the elliptic type; a two-dimensional method of characteristics is used in supersonic cross-flow regions where the equations are hyperbolic. Such approaches are developed in references 28 to 30 in which flat delta wings with attached leading-edge shocks are considered. It is not known whether these methods can be easily coded for efficient machine calculation for nonflat conical wings.

Method of Lines

The method of lines is somewhat similar to the better-known (in the United States) method of integral relations (ref. 31) in that both methods are semidiscrete. The method of integral relations, in its usual formulation (refs. 31 to 35), requires new algebraic development for each higher approximation (that is, more lines) and the equations grow more complex; whereas the method of lines system is written recursively with arbitrary number and spacing of lines.

Liskovets (ref. 36) presents a general review of the method of lines as applied to linear equations of elliptic, parabolic, and hyperbolic types. It is of interest to note that the method apparently dates from 1939 with an application to the solution of the Laplace equation by M. G. Slobodyanskii. An extensive bibliography (covering the work done in the U.S.S.R. up to 1965) is presented in reference 36.

In reference 37, the work of Telenin and his coworkers is cited, in which they used the method of lines for constructing numerical solutions to the axisymmetric, supersonic blunt-body problem. That work was extended to the three-dimensional blunt-body problem and reported in reference 38.[2] More details of the preceding work are given in reference 39.

Makhin and Syagayev (ref. 40) recognized the difficulties associated with Syagayev's earlier inverse method (ref. 27) and applied the transformation discussed previously in which the body and shock become bounding coordinate surfaces. Their procedure was essentially the method of lines. They used a first-order Euler method to integrate toward the body and to maintain accuracy, a small integration step size was required (1/64th of the local shock-layer thickness). The modification allowed them to solve the direct elliptic-cone problem, which was intractable by the earlier inverse approach.

Bazzhin and Chelysheva (ref. 41) applied the method to conical bodies at large angles of attack, where regions of supersonic cross flow always occur. Their procedure was very similar to approaches to the blunt-body problem; they used the method of lines on the windward, high-pressure side of the conical body up to, and beyond, the region where the cross flow becomes supersonic. A conical, two-dimensional method of characteristics was used to continue the solutions of the supersonic cross-flow region. More

[2]The word "Attached" in the title of reference 38 is an obvious error in translation, and should read "Detached."

results, with emphasis on the characteristics solutions, are given in reference 42. An interesting result in reference 42 was that in some instances, it was possible to continue the characteristics solution through the leeward plane of symmetry of elliptic cones at large incidence; thus, symmetry conditions were violated and indicated the impossibility of flow without embedded shocks in the general case. Neither reference 41 nor 42 suggests using the method of lines for the small-to-moderate incidences in which the cross flow is everywhere subsonic, nor was any mention given to the application in reference 40.

Jones (ref. 2) reported a method similar in many ways to the present procedure. He obtained solutions for circular and elliptic cones and a conical body with a four-parameter, smooth cross-section contour having both concave and convex portions. The method was shown to be accurate and efficient, and he was able to experiment numerically with some of the more theoretical questions concerning conical flows such as the "lift-off" of the vortical singularity (refs. 8 and 9). Ndefo (ref. 3) has applied the Telenin approach to the computation of conical flows. His development of the method of lines, which is similar in many respects to that of Jones and the present work, has been applied only to the computation of the flow about circular cones. In reference 4, the method of lines was applied to circular and elliptic cones, and to conical delta wings with attached leading-edge shocks. The present paper develops the method further and presents additional computations.

SYMBOLS

a	semimajor axis of ellipse
b	semiminor axis of ellipse
C_D	drag coefficient
C_L	lift coefficient
$C_{m,x}$	pitching-moment coefficient about X-axis
C_p	pressure coefficient
C_Y	normal-force coefficient
C_Z	axial-force coefficient

c	ratio of speed of sound to critical speed, $\sqrt{\frac{\gamma p}{\rho}}$
c^*	ratio of critical speed to free-stream speed, $\sqrt{\frac{\gamma - 1}{\gamma + 1} + \frac{2}{(\gamma + 1)M_\infty{}^2}}$
D/Dt	differential operator
$\bar{e}_\tau, \bar{e}_\eta, \bar{e}_r$	unit vectors along τ, η, and r
h	scale factor for τ coordinate at $r = 1$
i,j	indices indicating line number
$\bar{i},\bar{j},\bar{k}$	unit vectors along X-, Y-, and Z-directions
K	mean curvature of surface η = Constant
K_B	mean curvature of conical body given by equation (3)
M_∞	free-stream Mach number
M_c	cross-flow Mach number, $\frac{\sqrt{v^2 + w^2}}{c}$
N	number of lines
p	pressure, referenced to product of stream density and square of critical speed
r	distance along ray
S	entropy
u,v,w	components of velocity in r-, η-, and τ-directions, respectively, referenced to critical speed
u_c, v_c, w_c	cylindrical components of velocity in axial, radial, and azimuthal directions, respectively, referenced to critical speed
V	total velocity, referenced to critical speed

X,Y,Z	Cartesian coordinates
$x = \frac{X}{Z}$	
$\bar{x}$	nondimensional spanwise coordinate, $\frac{x}{x_{max}}$
$y = \frac{Y}{Z}$	
α	angle of attack or incidence
β	shock angle
γ	ratio of specific heats
ϵ	convergence criterion on normal velocity at conical surface
$\zeta = \frac{\eta}{\eta_s}$	
η	angle measured in plane normal to body from ray on surface of body to ray in field
η_s	value of η at shock
θ	conical apex angle of body in horizontal plane $Y = 0$
θ_o	conical apex angle of body in plane of symmetry containing free-stream velocity vector
Λ	sweep angle
ξ	transformed arc length variable
ρ	density, referenced to stream density
σ	angle between shock normal and η-direction (fig. 38)
τ	arc length along intersection of unit sphere with conical body

ϕ polar angle in cylindrical coordinates (fig. 2)

ψ yaw angle

Subscripts:

n normal to leading edge

o body surface coordinate

r,η,τ indicates directions associated with these components

∞ free stream

METHOD

Conical Coordinates

The equations governing supersonic, inviscid flow of an ideal gas are written in a body-oriented, orthogonal, conical coordinate system (r,η,τ) as developed in reference 43 where r is the distance along a conical ray, η is the angle measured from the body surface to the ray in a plane τ = Constant, and τ is a measure of the arc length[3] along the intersection of the body surface with a sphere of radius r centered at the body apex. (See fig. 1.) The body is the conical surface $\eta = 0$, and the contour along which τ is measured is a plane curve only in the special cases of a circular cone or a flat delta wing. This coordinate system has the advantage that the associated velocity components in the r-, η-, and τ-directions are the natural conical components u, v, and w; the v-component is zero at the surface $\eta = 0$ and $\sqrt{v^2 + w^2}$, the magnitude of the velocity component normal to a conical ray (hereafter called the "cross-flow" component), governs the type (elliptic or hyperbolic) of the partial differential equations of the conical flow. Furthermore, certain singularities appear where the cross-flow component vanishes $\left(\sqrt{v^2 + w^2} = 0\right)$, and it is extremely important that such points be recognized and interpreted correctly. These coordinates prove to be advantageous from the computational point of view as well except for bodies with concave curvature.

---

[3]In reference 4 both ξ and τ are arc length variables where the duplicity arises because of a coordinate transformation. In the present development the variable τ is the arc length and $\xi = \xi(\tau)$ is a transformed coordinate which can be selected to vary the line spacing.

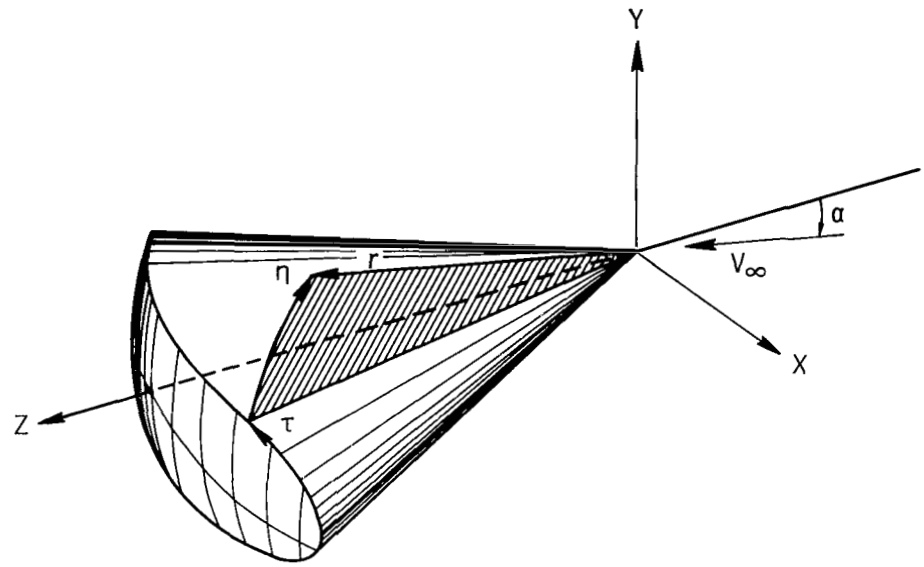

Figure 1.- Body-oriented conical coordinates.

Differential Equations

With the conical similarity $\left(\frac{\partial}{\partial r} = 0\right)$, the partial differential equations which describe the flow involve two independent variables, η and τ. Consequently, the solution can be developed on the spherical surface $r = 1$. The equations of continuity, momentum, and conservation of entropy S along a stream surface in these coordinates (ref. 43) become

$$\left.\begin{aligned}
&\frac{1}{\rho}\frac{D\rho}{Dt} + h\frac{\partial v}{\partial \eta} + \frac{\partial w}{\partial \tau} + 2uh - hKv = 0 \\
&\frac{Du}{Dt} - h\left(v^2 + w^2\right) = 0 \\
&\frac{Dv}{Dt} + \frac{h}{\rho}\frac{\partial p}{\partial \eta} + huv + hKw^2 = 0 \\
&\frac{Dw}{Dt} + \frac{1}{\rho}\frac{\partial p}{\partial \tau} + huw - hKvw = 0 \\
&\frac{DS}{Dt} = 0
\end{aligned}\right\} \qquad (1)$$

where the total derivative is

$$\frac{D}{Dt} = hv \frac{\partial}{\partial \eta} + w \frac{\partial}{\partial \tau}$$

The scale factor h for the τ coordinate and the mean curvature K of the surface η = Constant at $r = 1$ are

$$h = \cos \eta - K_B \sin \eta$$

$$K = -\frac{1}{h} \frac{\partial h}{\partial \eta} = \frac{1}{h}\left(\sin \eta + K_B \cos \eta\right)$$

where K_B is the mean body curvature.

Transformation to a rectangular region.- The integration of the system of equations, as discussed previously, is facilitated by a coordinate transformation which maps the region bounded by the shock and the body into a rectangular domain as shown in figure 2. For this purpose the transformed variables are taken as

$$\zeta = \frac{\eta}{\eta_s}$$

$$\xi = \xi(\tau)$$

where $\eta = \eta_s(\tau)$ is the shock surface. Thus, $\zeta = 0$ on the body and $\zeta = 1$ on the shock. The transformation to the new independent variable ξ permits a local

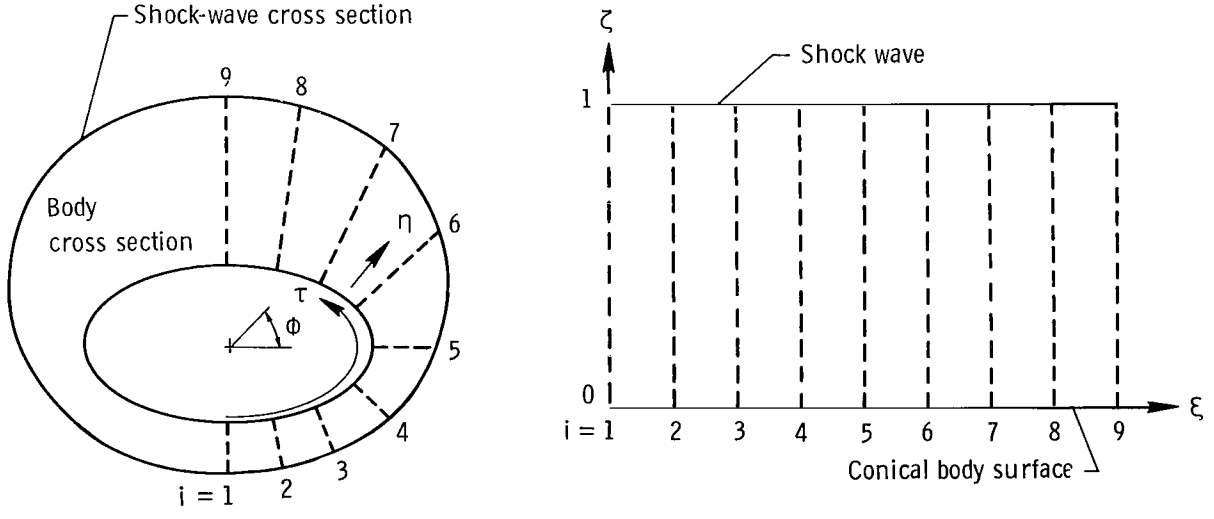

Figure 2.- Layout of computational lines.

stretching of the arc length coordinate. The chain rule gives

$$\frac{\partial}{\partial \eta} = \frac{1}{\eta_s} \frac{\partial}{\partial \zeta}$$

$$\frac{\partial}{\partial \tau} = \xi_\tau \left(\frac{\partial}{\partial \xi} - \frac{\zeta}{\eta_s} \frac{d\eta_s}{d\xi} \frac{\partial}{\partial \zeta} \right)$$

where

$$\xi_\tau = \frac{d\xi}{d\tau}$$

For a perfect gas the derivative of the density in the continuity equation is replaced by one involving the pressure through the use of the equation for the conservation of entropy along a stream line. Thus,

$$\frac{D\rho}{Dt} = \frac{1}{c^2} \frac{Dp}{Dt}$$

where c is the ratio of the speed of sound to the critical speed. Then the equations (1) in the new coordinates can be written as

$$\left.\begin{aligned}
\frac{\partial p}{\partial \zeta} &= \frac{\rho}{D} \left(F_1 g - F_2 h + F_3 \zeta \xi_\tau \frac{d\eta_s}{d\xi} \right) \\
\frac{\partial v}{\partial \zeta} &= -\frac{1}{g} \left(\frac{h}{\rho} \frac{\partial p}{\partial \zeta} + F_2 \right) \\
\frac{\partial w}{\partial \zeta} &= \frac{1}{g} \left[\left(\zeta \xi_\tau \frac{d\eta_s}{d\xi} \right) \frac{1}{\rho} \frac{\partial p}{\partial \zeta} - F_3 \right] \\
\frac{\partial u}{\partial \zeta} &= \frac{f}{g} \\
\frac{\partial S}{\partial \zeta} &= -\eta_s \xi_\tau \frac{w}{g} \frac{\partial S}{\partial \xi}
\end{aligned}\right\} \qquad (2)$$

where

$$g = hv - w\zeta \xi_\tau \frac{d\eta_s}{d\xi}$$

$$D = h^2 + \left(\zeta \xi_\tau \frac{d\eta_s}{d\xi}\right)^2 - \frac{g^2}{c^2}$$

$$F_1 = \eta_s\left(\frac{w\xi_\tau}{\rho c^2}\frac{\partial p}{\partial \xi} + \xi_\tau \frac{\partial w}{\partial \xi} + 2uh - hKv\right)$$

$$F_2 = \eta_s\left(w\xi_\tau \frac{\partial v}{\partial \xi} + huv + hKw^2\right)$$

$$F_3 = \eta_s\left(\frac{\xi_\tau}{\rho}\frac{\partial p}{\partial \xi} + w\xi_\tau \frac{\partial w}{\partial \xi} + huw - hKvw\right)$$

$$f = \eta_s\left[h\left(v^2 + w^2\right) - w\xi_\tau \frac{\partial u}{\partial \xi}\right]$$

and the entropy is related to the pressure and density by

$$S = \log\left(\gamma M_\infty{}^2 c^{*2} \frac{p}{\rho^\gamma}\right)$$

where

$$c^* = \sqrt{\frac{\gamma - 1}{\gamma + 1} + \frac{2}{(\gamma + 1)M_\infty{}^2}}$$

is the ratio of the critical speed to the free-stream speed. The Bernoulli equation

$$\frac{2\gamma}{\gamma - 1}\frac{p}{\rho} + u^2 + v^2 + w^2 = \frac{\gamma + 1}{\gamma - 1}$$

provides an additional relation between the flow variables. The velocities are nondimensionalized with the critical speed, the density with the stream density, and the pressure with the product of the stream density and the square of the critical speed.

The right-hand members of equations (2) involve the unknown shock shape, the velocity components, pressure, density, and the derivatives of these quantities with respect to the variable ξ. The density can be computed from the value of the entropy and the pressure in the integration of the system of equations (2) or through the use of the Bernoulli equation.

The problem in the η,τ coordinates is thus transformed to the solution of a system of equations in a rectangular domain with coordinates ζ,ξ. The shock wave and the body

surface are mapped onto the lines $\zeta = 1$ and $\zeta = 0$, respectively. The origin of the arc length τ as well as the transformed variable ξ are taken in the windward plane of symmetry; the terminal value of ξ is taken in the leeward plane of symmetry for circular and elliptic cones and at the leading edge of the conical wing configurations.

Geometric Parameters

The body geometry enters the system of equations (2) through the body curvature and the arc length τ along the intersection of the conical body with the spherical surface $r = 1$. These quantities are evaluated from the equation defining the shape of the body. The body is defined in the Cartesian coordinate system shown in figure 1. The body axis is in the Z-direction and the angle of incidence α is measured relative to the Z-axis. From the conical similarity, the flow is constant along each ray defined by $\frac{X}{Z} = \text{Constant}$, $\frac{Y}{Z} = \text{Constant}$. Let

$$x = \frac{X}{Z}$$

$$y = \frac{Y}{Z}$$

and let the subscript o denote values on the body. Then the conical body can be defined by an equation of the form

$$G(x_o, y_o) = 0$$

The mean body curvature at $r = 1$, which is required for the evaluation of the scale factor h and the coordinate curvature K (ref. 44), is

$$K_B = -\left(G_y{}^2 G_{xx} + G_x{}^2 G_{yy} - 2G_x G_y G_{xy}\right)\left(\frac{A_1}{A_2}\right)^{3/2} \tag{3}$$

where the single and double subscripts on G denote the first and second derivatives of G with respect to the indicated variables x_o and y_o and

$$A_1 = 1 + x_o{}^2 + y_o{}^2$$

$$A_2 = G_x{}^2 + G_y{}^2 + \left(x_o G_x + y_o G_y\right)^2$$

The differentials of the arc length at $r = 1$ and the transformed coordinate ξ are (appendix A)

$$\left.\begin{aligned} d\tau &= -A_1^{-1}A_2^{1/2}G_y^{-1}dx_o = A_1^{-1}A_2^{1/2}G_x^{-1}dy_o \\ d\xi &= \xi_\tau\, d\tau \end{aligned}\right\} \tag{4}$$

The origin of the arc length is taken in the plane of symmetry; thus, the initial values are $x_o(0) = 0$, $y_o = y_o(0)$, and $\tau = 0$. Integration of these equations then determines the arc length in terms of the body coordinates.

In practice equations (4) are integrated numerically to obtain values of τ and ξ at the leeward plane of symmetry for the circular and elliptic cones or values of τ and ξ at the leading edge of wing configurations. The line spacing is specified in terms of ξ and equations (4) are again integrated to compute the values of x_o and y_o at each line. The quantities $\sqrt{A_1}$ and $\sqrt{A_2}$ (appendix A) are the normalizing factors for the vectors normal to the spherical surface $r = 1$ and the conical surface $G(x_o,y_o) = 0$, respectively.

The relation between unit vectors $\bar{e}_\eta$, $\bar{e}_\tau$, and $\bar{e}_r$ in the η-, τ-, and r-directions and the Cartesian unit vectors $\bar{i}$, $\bar{j}$, and $\bar{k}$ is required for the development of the shock relations and for the computation of the Cartesian coordinates of points in the flow field. The direction cosines are given in appendix A.

The Method of Lines

The region of interest in the ζ,ξ-plane is divided by N lines parallel to the ζ-axis ($N + 1$ lines for the delta wings with attached leading-edge shocks); the line $i = 1$ is taken in the windward plane of symmetry. The stream velocity vector lies in a plane of symmetry for all the results presented; however, this is not a limitation on the method itself. It is not necessary that the distance between lines be of equal width since the spacing of the lines in the physical η,τ-plane can be adjusted through the selection of the coordinate transformation $\xi = \xi(\tau)$. Figure 2 illustrates the division in the physical η,τ coordinates and the transformed ζ,ξ coordinates with $\xi = \tau$ for an elliptic cone with nine lines. Also shown is the cylindrical polar angle ϕ; ϕ is $-\pi/2$ in the windward symmetry plane and $\pi/2$ in the leeward symmetry plane for conical configurations at incidence. For the elliptic cone at yaw, $\phi = 0$ in the windward symmetry plane and $\phi = \pi$ in the leeward symmetry plane.

At each strip boundary or line, the system of equations (2) is reduced to a set of ordinary differential-difference equations by replacing the derivative $\partial/\partial\xi$ by finite

differences. The derivative of the Lagrange interpolation polynomial (ref. 45, for example) was used in the computer program with an equal number of lines on either side of the line at which $\partial/\partial\xi$ is computed; therefore, central differencing is obtained when the line spacing is equal. In forming ξ-derivatives at lines near the leading edge of wings with an attached leading-edge shock (the leading edge is line $i = N + 1$), the number of points used in the derivative formulas is reduced, if necessary, to retain an equal number of lines on either side of the line at which $\partial/\partial\xi$ is computed. A five-point formula was used for most computations.

The system of equations (2) is integrated simultaneously along each line $i = 1, \ldots, N$ with the derivatives in the right-hand members evaluated with the Lagrange formula for derivatives. This polynomial approximation for $\partial/\partial\xi$ causes the differential equations along any line to be coupled to those along the other lines. The system of equations (2) thus becomes a system of 5N ordinary differential equations which are integrated by a Runge-Kutta or similar method. A fourth-order Runge-Kutta integration has been employed in the computer program, and the integration step size was generally in increments of -0.1 from the shock to a value of ξ of 0.1 and by increments of -0.05 and -0.025 thereafter, except in calculations where details of the entropy layer are sought. Note that the system of equations (2) is of order 4N if the density is computed with the Bernoulli equation and the equation for the conservation of entropy is deleted. The system of 5N equations has been employed in the computations presented herein.

Symmetry and Boundary Conditions

Symmetry conditions.- The Y,Z-plane is the plane of symmetry (fig. 1) which contains the stream velocity vector for all configurations other than the elliptic cone at yaw. The stream velocity vector lies in the plane of the major axis (X,Z-plane) for the yawed cone. The origin of the arc length τ and the transformed variable ξ is taken in the windward plane of symmetry. The symmetry conditions require that all the flow quantities other than w are symmetric and the circumferential component of velocity w is antisymmetric about the plane of symmetry. Symmetry is accounted for in the formula for the ξ derivatives by properly reflecting points (lines) about the symmetry plane. For the elliptic cone both the windward ($i = 1$) and leeward ($i = N$) lines correspond to symmetry planes. For the compression side of delta wings, the line $i = 1$ is a symmetry plane.

Flow tangency at surface.- The natural coordinate system has been employed in part to simplify the form of the boundary conditions on the body. The condition of flow tangency on the body surface $\zeta = 0$ requires that the normal component of velocity v must vanish. Thus,

$$v(0,\tau) = 0 \tag{5}$$

Since the system of equations (2) is integrated along discrete lines, the boundary condition (5) is satisfied only on these lines.

Shock-wave conditions.- The shock-wave shape is initially unknown and must be determined through an iteration procedure as described subsequently. The flow variables behind the shock are found from the shock jump conditions. (See appendix B.)

Attached shock at wing leading edge.- In the present paper the method is applied to delta-wing configurations with the shock wave attached along the sharp leading edges. Under these conditions, the slope of the shock wave and the flow variables at the leading edge are determined directly from the shock conditions and the wing geometry. (See appendix B.) Hence, the flow at the leading edge is completely determined without recourse to the integration of the system of differential equations. The leading-edge condition takes the place of the symmetry properties for closed bodies in the leeward plane of symmetry.

Determination of the Shock Shape

The form of the shock-wave cross section is given by the unknown function $\eta = \eta_s(\tau)$. If η_s and $d\eta_s/d\tau$ were known, all the information concerning the shock-wave geometry would be known, and the values of the functions p, ρ, u, v, and w at the shock wave ($\zeta = 1$) could be evaluated from the shock jump conditions. These values could be used to start the numerical integration at $\zeta = 1$ and proceed down to the body surface at $\zeta = 0$. Only the correct shock function η_s will cause the flow-tangency condition (5) to be satisfied; thus, there must be a relation between the function $\eta_s(\tau)$ and the normal component of velocity at the surface, $v(0,\tau)$. This is the basis, then, for determining the correct shock shape.

Newton iteration for shock shape.- The number of unknown values of η_s is equal to the number of normal components $v_i(0) = v(0,\tau_i)$. A Newton-type iteration procedure is used for adjusting the N values of $\eta_{s,i}$ to achieve $\max_i |v_i(0)| \leq \epsilon$ where ϵ is the prescribed accuracy criterion. The steps in the procedure, which are straightforward and easily automated, are as follows:

(1) Assume an initial set of values $\eta_{s,i}$ ($i = 1, \ldots, N$) based on experience, approximate solutions, or previously computed cases with conditions close to those desired.

(2) Compute $\dfrac{d\eta_{s,i}}{d\xi}$ at each line with the use of the polynomial expression for the derivatives.

(3) With $\eta_{s,i}$ and $\dfrac{d\eta_{s,i}}{d\xi}$ from steps (1) and (2), solve the shock jump conditions for p_i, ρ_i, u_i, v_i, and w_i ($i = 1, \ldots, N$).

(4) Use the results of step (3) for initial values to start a numerical integration of the system of 5N equations from $\zeta = 1$ to $\zeta = 0$, and evaluate the surface normal components $v_i(0)$.

(5) Test $\max_i |v_i(0)|$. If $\max_i |v_i(0)| \leqq \epsilon$, the shock shape is satisfactory and the problem is considered to be solved. Otherwise, the following perturbation cycle is used.

(6) Perturb each parameter $\eta_{s,j}$ independently and in order. That is, change $\eta_{s,j}$ to $(1 + \delta)\eta_{s,j}$, where δ is a small number (for example, 10^{-6}), and repeat steps (2) to (4). This procedure results in small changes in each of the $v_i(0)$ due to the perturbation in $\eta_{s,j}$. Hence, the jth column of an N by N matrix of influence coefficients or partial derivatives $\frac{\partial v_i(0)}{\partial \eta_{s,j}}$ (j = 1, . . ., N) is generated with each perturbation.

(7) Solve the usual first-order linear system

$$\sum_{j=1}^{N} \frac{\partial v_i(0)}{\partial \eta_{s,j}} \Delta\eta_{s,j} = -v_i(0) \qquad (i = 1, \ldots, N) \tag{6}$$

to obtain the increments $\Delta\eta_{s,i}$ required to correct the shock shape and drive all $v_i(0) \to 0$.

(8) Use the new shock parameters $\eta_{s,i} + \Delta\eta_{s,i}$ to start a new cycle at step (2). Note that a complete cycle requires N + 1 integrations: one "pivotal" and N perturbations.

Modified Newton iteration procedure.- The regular Newton iteration procedure calls for a reevaluation of the Jacobian influence matrix at the beginning of each new cycle (step 6). Since most of the computation time is taken up in this step, a modification which bypasses this step on subsequent cycles (if they are required) was introduced. Once the surface velocities are within some preassigned magnitude (considerably larger than the final convergence criterion), the components of the Jacobian are not recomputed after each pivotal integration; only the right-hand member of equation (6) is updated at each cycle. Although more cycles are necessary for convergence, each cycle with the constant Jacobian consists of only one integration, and a considerable saving in the total number of integrations, and hence computer time, is obtained.

It should be noted here that the modified Newton procedure can diverge in certain cases where the regular Newton procedure converges. The situation is easily visualized in the one-dimensional case where the first guess is too far away from the solution and

the second derivative is large. Figure 3 is an illustration of two sequences of modified Newton iterations to determine the zero of a function f: the unprimed sequence starts

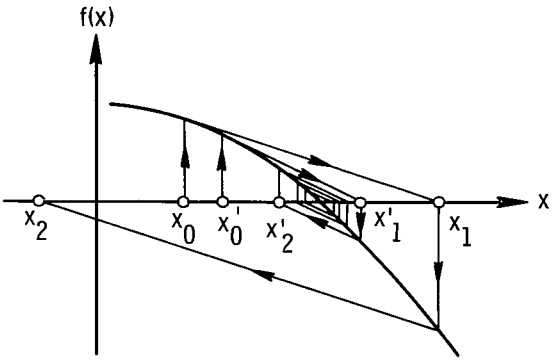

Figure 3.- Converging and diverging sequences of modified Newton iterations.

at x_0 and diverges, but the primed sequence converges. If the slope had been recomputed one more time at x_1, the unprimed sequence would also converge. For this reason the option is retained to use the regular Newton for more than one cycle if the surface velocities are still too large after the first iteration. In nearly all cases computed by the authors, the modified Newton procedure converged if the $\max_i |v_i(0)|$ was in the range of 0.03 to 0.05. Examples can be given where the regular Newton procedure also diverges. The sufficient conditions for convergence of both procedures are the same (ref. 46), but the graphical example of figure 3 demonstrates that the necessary conditions (for convergence) are clearly different.

The shock-wave determination procedure of reference 2 differs somewhat from the present one, in that the shock function is given by a trigonometric polynomial, and the coefficients are chosen to minimize the sum of squares of the normal components at the surface.

Approximate starting shock shapes.- Usually a very good estimate of the shock shape is required for a successful calculation and convergence. The exceptions are circular cones at moderate relative incidences, $\frac{\alpha}{\theta_0} \lessapprox 0.5$, and delta wings at large supersonic Mach numbers, $M_\infty > 3.0$. For most other cases, however, considerable care must be exercised in choosing the initial shock shape to start the iterations previously described. A poor initial estimate can result in any of several program failures, such as negative pressures or vanishing denominators. The latter difficulty is caused by excessive supersonic cross flow and introduces characteristic-type singularities in the differential equations (that is, when a line ζ = Constant is tangent to a conical characteristic).

In order to obtain a good initial estimate of the shock shape for such cases as elliptic cones at incidence, a "simpler" case is computed first and then the input parameters are changed in a series of steps toward the desired configuration, a new converged shock shape being obtained with each change of the input parameters (for example, γ, M_∞, θ_o, α, and a/b). The history of the set of $\eta_{s,i}$ as a function of the set of input parameters is incorporated in an extrapolation procedure to predict the new shock shape for the new set of input parameters. The converged values of $\eta_{s,i}$ for the initial value of the parameter are used as the input values corresponding to a small variation of the input parameter; for example, the parameter may be changed to 1.05 times its initial value. Once the converged solution for this value of the parameter is obtained, the inputs $\eta_{s,i}$ for a new value of the parameter are computed by linear extrapolation of the two previous sets. After three sets of converged $\eta_{s,i}$ have been obtained corresponding to three values of the input parameter, including the set with the small variation of the parameter, a quadratic extrapolation is employed. Such a procedure was found to be essential for efficient computation. The procedure is completely automated in the computer program for circular and elliptic cones, and variation of any of five different input parameters is allowed. The program for the conical delta wings has not been so automated.

If, during a sequence of calculations in which a parameter is incremented, the calculation encounters difficulties (such as negative pressure), the program halves the increment and attempts a restart from the last parameter value for which the solution converged. If difficulties are encountered again, the parameter increment is halved again and this process is automatically repeated until the increment is smaller in magnitude than a preassigned value, or until successful convergence is achieved.

The initial estimate for the delta-wing shock shape can be made directly for any angle of attack α (up to that causing detachment from the leading edge), sweep angle Λ, and M_∞. The estimate used is an even function in ξ which requires only an estimate of $\eta_{s,1}$ (the value of η_s in the plane of symmetry). The function is contrived to give $\eta_{s,N+1} = 0$ (the condition of attachment at the leading edge) and the correct value for $\left(\frac{d\eta_s}{d\xi}\right)_{N+1}$, which is calculated from the shock conditions. The function is

$$\eta_{s,i} = \left[1 - \left(\frac{\xi_i}{\xi_{N+1}}\right)^2\right]\left\{\eta_{s,1} - \left(\frac{\xi_i}{\xi_{N+1}}\right)^2\left[\eta_{s,1} + \frac{\xi_{N+1}}{2}\left(\frac{d\eta_s}{d\xi}\right)_{N+1}\right]\right\} \tag{7}$$

where $\frac{d\eta_s}{d\xi} = -\frac{h}{\xi\tau}\tan\sigma$ and σ is evaluated from the wing geometry and stream conditions. (See appendix B.) The value of $\eta_{s,1}$ used in equation (7) is a tangent-cone

approximation, increased by a factor 1.2 to avoid the Mach wave condition for very thin wings at small α as follows:

$$\eta_{s,1} \approx 1.2(\beta - \theta_o - \alpha)$$

where (ref. 47)

$$\sin^2\beta = \frac{\gamma + 1}{2} \sin^2(\theta_o + \alpha) + \frac{1}{M_\infty{}^2}$$

In a few cases, the value of $\eta_{s,1}$ was so far off that the required corrections $\Delta\eta_{s,i}$ were sizable, too much "roughness" in the shock shape resulted, and subsequent iterations failed. It happens that in this event, the first correction for $\eta_{s,1}$ is very good so that using that value in equation (7) and restarting the iteration has always been successful.

Extrapolation to Surface

At the surface, $\zeta = 0$, the derivatives $du/d\zeta$ and $dw/d\zeta$ are infinite because of the well-known vortical layer adjacent to the surface in the conical flows. (See ref. 8.) The derivatives $dp/d\zeta$ and $dv/d\zeta$ however are finite, and this fact allows extrapolation of the functions p and v to the surface from $\zeta > 0$. In fact, it is only v_i that is extrapolated during the integrations in order to evaluate the magnitudes of $v_i(0)$ $(i = 1, \ldots, N)$. When the convergence criterion is met, the pressure p is also extrapolated to $\zeta = 0$.

Corrected isentropic surface values.- The surface entropy is a constant on the surface, and if the value is known, the isentropic surface density can be calculated as a function of the extrapolated pressure and the surface entropy. The Bernoulli equation relates p, ρ, u, v, and w; since $v = 0$ at the surface and p and ρ are known, there is only one equation with two unknowns, u and w. The other equation needed for determining u and w is the differential equation for the u-momentum. This equation on the body becomes

$$w(0,\xi) = \xi_\tau \frac{\partial u(0,\xi)}{\partial \xi} \tag{8}$$

Substitution of equation (8) into the Bernoulli equation gives the set of nonlinear differential equations which are to be satisfied at each line:

$$\frac{2\gamma}{\gamma - 1}\frac{p_i}{\rho_i} + u_i{}^2 + \left(\xi_\tau \frac{\partial u_i}{\partial \xi}\right)^2 = \frac{\gamma + 1}{\gamma - 1} \qquad (i = 1, \ldots, N) \tag{9}$$

The Lagrange derivative formula is used for evaluating the ξ-derivatives, and the set of equations (9) is solved by Newton iteration. When convergence is achieved, equation (8) gives w_i; hence, the isentropic surface values are completely determined. This procedure is essentially the same as that of reference 2.

The derivatives $\partial v/\partial\zeta$ and $\partial p/\partial\zeta$ at $\zeta = 0$ can be evaluated from the corrected surface values. The reduction of the continuity equation and the v and w momentum equations at $\zeta = 0$ gives the relations

$$\frac{\partial v}{\partial \zeta} = -\eta_s \left[\left(1 - \frac{w^2}{c^2} \right) \xi_\tau \frac{\partial w}{\partial \xi} + u \left(2 - \frac{w^2}{c^2} \right) \right]$$

$$\frac{\partial p}{\partial \zeta} = -\eta_s K_B \rho w^2$$

The relations show, as stated previously, that $\partial v/\partial\zeta$ and $\partial p/\partial\zeta$ are finite at the surface. The finiteness of these quantities is one of the principal merits of the coordinate system employed.

Computation of the surface entropy.- For the circular cone, the surface entropy is the value that occurs in the windward symmetry plane, line $i = 1$. For the elliptic cone with the free-stream velocity vector lying in the plane of the minor axis, the surface entropy is assumed to be the maximum value at the shock wave. When the free-stream vector is in the plane of the major axis, the surface entropy is piecewise constant for some flow conditions; that is, it has the value of the windward symmetry plane on the surface segment where $w(o,\tau) > 0$; and it has the value of the leeward symmetry plane on the rest of the surface. The surface entropy for the delta wings with convex surfaces is the same as the leading-edge value.

Stability and Error Growth

In practical numerical computations by the present method, it is found that there exists a maximum number of lines (or minimum spacing between lines) beyond which instabilities swamp the solution. This result is by no means surprising, in light of Hadamard's (ref. 48) famous example of the inherent instability of the Cauchy (initial-value) problem for Laplace's equation. The example demonstrated that certain types of initial data, described by vanishing amplitude and increasing frequency, are magnified exponentially as the distance from the initial line increases. No matter how close to zero amplitude the initial data become, the solution can contain unbounded oscillations at some finite distance from the initial line; hence, the Cauchy problem is poorly posed, in general, for elliptic equations. This feature has been evidenced in numerical solutions of the blunt-body inverse problem (ref. 22, p. 452) as well as in the present problem.

When the method of lines is applied to the solution of Laplace's equation in a rectangular region one finds that the solution is composed of a complementary part which is a sum of exponential eigenfunctions, and a particular integral. The largest eigenvalue of the complementary part is proportional to the number of lines so that round-off errors can grow exponentially like $10^{-j} \exp(Nx)$, where j is the number of decimal figures carried in the computation, N is the number of lines and x is the distance along lines from the initial data line, the lines being parallel to the X-axis. Hence, there exists an optimum number of lines which represents a compromise between decreasing discretization errors and increasing round-off error growth. Such a compromise is contained in most numerical procedures for the solution of differential equations. For example, in a standard solution by the grid relaxation method for Laplace's equation, the discretization error is $O(h^2)$ whereas the round-off error is $O(h^{-2})$ (ref. 49, p. 482). Hence, the grid method has an algebraic round-off error growth whereas the method of lines has exponential error growth.

The discussion is not intended to discourage the use of the method of lines; rather, it is intended to provide an understanding of difficulties if they arise in applications to nonlinear problems. One should expect to encounter instability where (1) the shock wave is a large distance from the body, a condition which occurs at low Mach number ($M_\infty \lesssim 1.5$) and on the leeside of the body at large incidence; (2) when cross-flow gradients are large and require a fine spacing of lines, which increases the eigenvalues; and (3) when a small number of figures is carried in the computation. These three conditions correspond to x large, N large, and j small, respectively, in the linear problem.

In the conical flow problems treated so far, it appears that $N = 19$ is about the maximum number of lines which can be used without encountering sudden error growth. This observation applies to cases involving moderate-to-large Mach numbers ($M_\infty \gtrsim 2$), angles of attack up to relative incidence of one, and a 60-bit computer word length (about 15 decimal figure accuracy). Usually, a much smaller number of lines ($N \approx 9$) provides sufficient accuracy for, say, circular cones, elliptic cones of moderate axis ratio ($1.0 \leqq a/b \leqq 1.5$), and delta wings at large Mach numbers ($M_\infty \gtrsim 3$). For investigations of cases which are more severe, for example, low Mach numbers, one will have to be content with the accuracy provided by a smaller number of lines in order to avoid the large eigenvalues and thus suppress the error growth.

Force Coefficients

The force coefficients are computed by numerical integration of the surface pressures. The equations for these coefficients are given in appendix C. The reference area for the force coefficients is taken as the base area for the elliptic and circular cones and the plan area for wings. No force coefficients are presented in the results.

RESULTS AND DISCUSSION

Circular Cone

The circular cone is perhaps the most basic conical configuration and, as a consequence, has received more extensive treatment in the literature than other conical bodies. At small incidence it is one of the simplest conical flows to calculate and good experimental data are available to assess the validity of the computations. Moreover, at large values of incidence it exhibits the features which often complicate the computation of many conical flows. An extensive tabulation of the flow about circular cones, not only surface quantities but the flow variables throughout the field as well, is presented in references 13 and 50. The latter results have been computed by the method of lines as presented in reference 2. Computations by the present method give comparable results.

Tracy (ref. 51) presents results of an experimental study of a circular cone with semiapex angle of 10° at a Mach number of 7.95. Included are the measurements which delineate the shock structure and the viscous boundary; the region between the body and the viscous boundary is dominated by viscous effects. Figure 4 shows these measured boundaries and the shock shape computed by the method of lines for $N = 15$ at angles

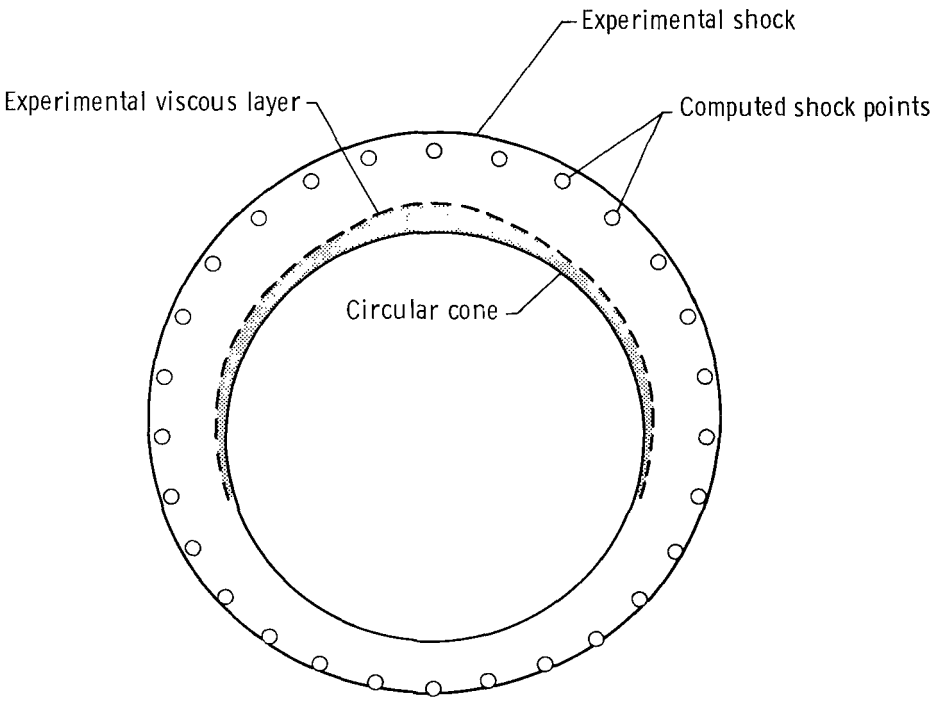

(a) $\alpha = 4^{\circ}$.

Figure 4.- Cross section of shock for circular cone at incidence. $M_{\infty} = 7.95$; $\theta = 10^{\circ}$; $N = 15$. Experiment from reference 51.

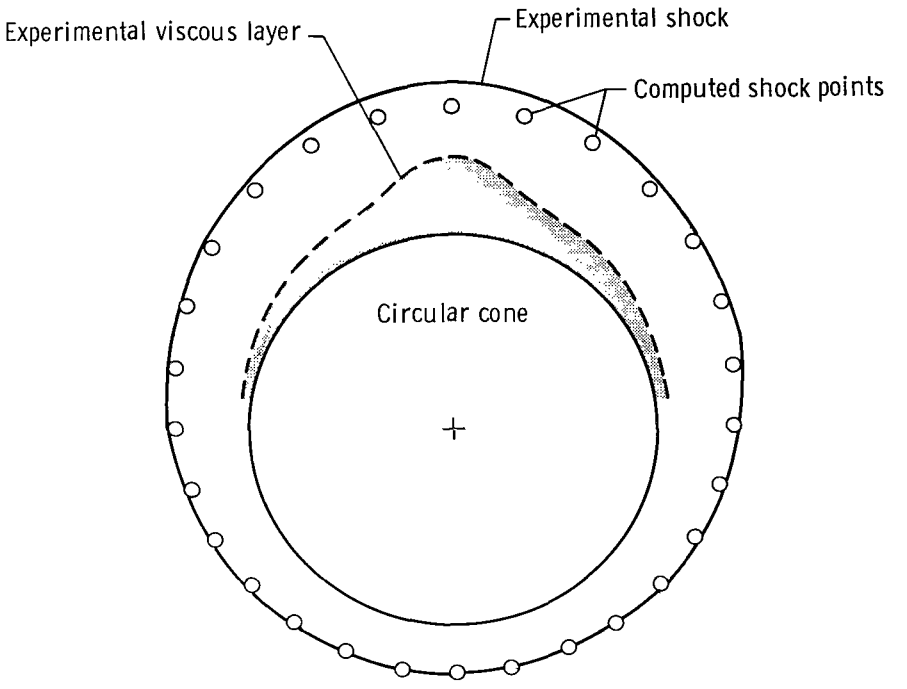

(b) $\alpha = 8^{\circ}$.

Figure 4.- Concluded.

of attack of 4° and 8°. It is seen that the computed shock shape is in good agreement with the measured results over the windward side but is less satisfactory on the leeward side where the viscous effects distort the flow. The experimental results show that the viscous region becomes more prominent as the angle of incidence increases and the computed shock wave on the lee side departs more from the measured values at the higher incidence. The corresponding surface pressure distributions are shown in figure 5 as a function of the circumferential angle ϕ where ϕ is -90° in the windward plane of symmetry. Agreement with experiment is less satisfactory in regions where viscous effects are significant. Thus, the measured and calculated values show poorer agreement on the lee side and depart more at the larger angle of attack.

Difficulties at large relative incidence.- As the angle of incidence is increased, conditions are encountered where it becomes difficult to obtain a converged solution. These conditions generally occur where α/θ_o is near or exceeds unity. Three factors, singly or together, contribute to the difficulty in obtaining a solution: (1) the shock wave on the lee side approaches tangency with the stream Mach cone, (2) the cross flow becomes locally supersonic, (3) the computed pressure in the flow field or on the body becomes very small. It may be seen in figure 5 that the surface pressure on the lee side is tending toward the free-stream value $C_p = 0$ at $\alpha = 8^{\circ}$. Similarly, the shock-wave pressure coefficient (not shown) at the leeward symmetry plane is also near zero; hence,

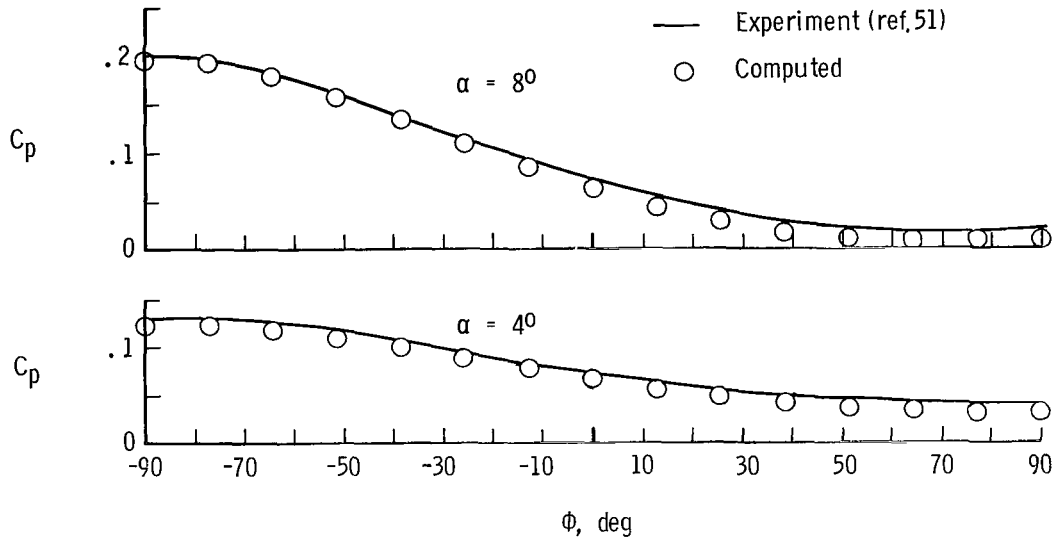

Figure 5.- Circumferential pressure distributions on circular cone at incidence. $M_\infty = 7.95$; $\theta = 10^\circ$; $N = 15$.

that portion of the shock is approaching tangency with the free-stream Mach cone, which is, in turn, a characteristic surface. The result is that the expressions for the ζ-derivatives approach the indeterminate form (0/0) and the problem becomes very ill-conditioned. The particular sequence of runs for these calculations with 15 lines was made in increments of 1° in α for values of α up to 9° by using the previously described extrapolation routine for generating the initial values of η_s for the pivotal computation. The routine made an attempt at $\alpha = 10^\circ$ and encountered difficulty; as explained earlier, the 1° α-increment was halved, and successful convergence was achieved for $\alpha = 9.5^\circ$. Then it was necessary to halve the increment twice more to avoid difficulties, so that $\alpha = 9.625^\circ$ was the next converged solution, and so on. Thus, the calculations became very sensitive for $\alpha \geq 9.5^\circ$; that is, a high degree of accuracy in the shock shape is required to satisfy the convergence criterion. The cross-flow Mach number M_c at the shock surface is shown in figure 6 for $\alpha = 4^\circ$, 8°, and 9.5°. It may be seen that M_c becomes 1 at the shock for $\alpha = 9.5^\circ$ to add to the difficulty in obtaining a converged solution in this instance. Once difficulty is encountered, the computations can often be continued by reducing the number of lines. Thus, as previously discussed, there is generally some trade-off between the resolution and the range of the computations. The reduction of the number of lines from 15 to 13 permitted calculations for increments in α of 1° up to 10°, and by half-degree increments up to 11°. Thereafter, smaller increments were required. The cross-flow Mach numbers M_c at both the body and shock are shown in figure 7 for the circular cone with 13 lines at $\alpha = 11^\circ$. It may be seen that a fairly extensive supersonic cross flow has developed, the largest values of the Mach number being at the body; at the shock the cross-flow Mach number does not substantially exceed one.

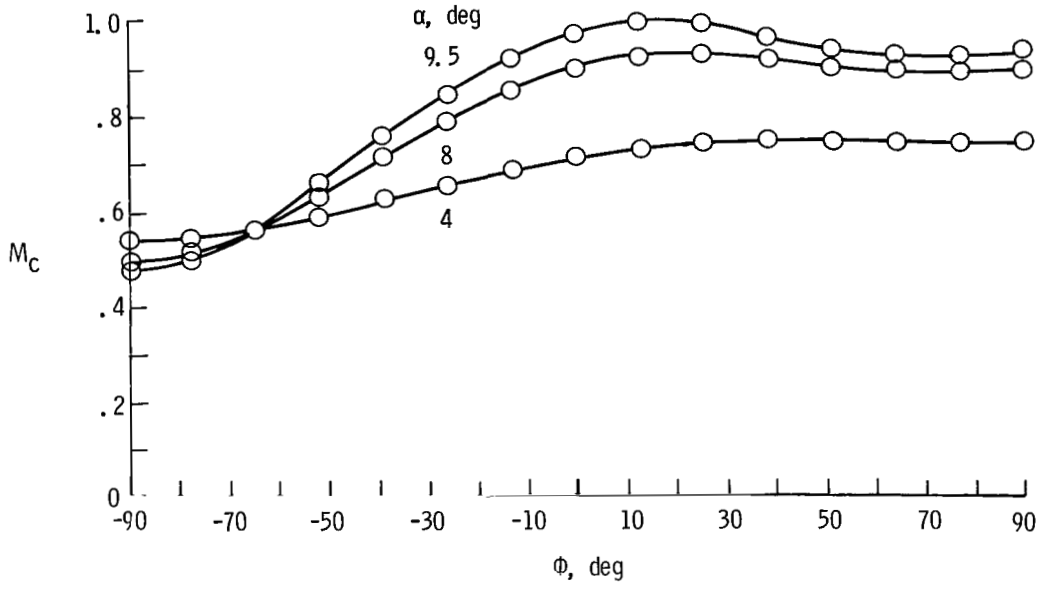

Figure 6.- Circumferential distribution of cross-flow Mach number at shock wave for circular cone at moderate incidences. $M_\infty = 7.95$; $\theta = 10^\circ$; N = 15.

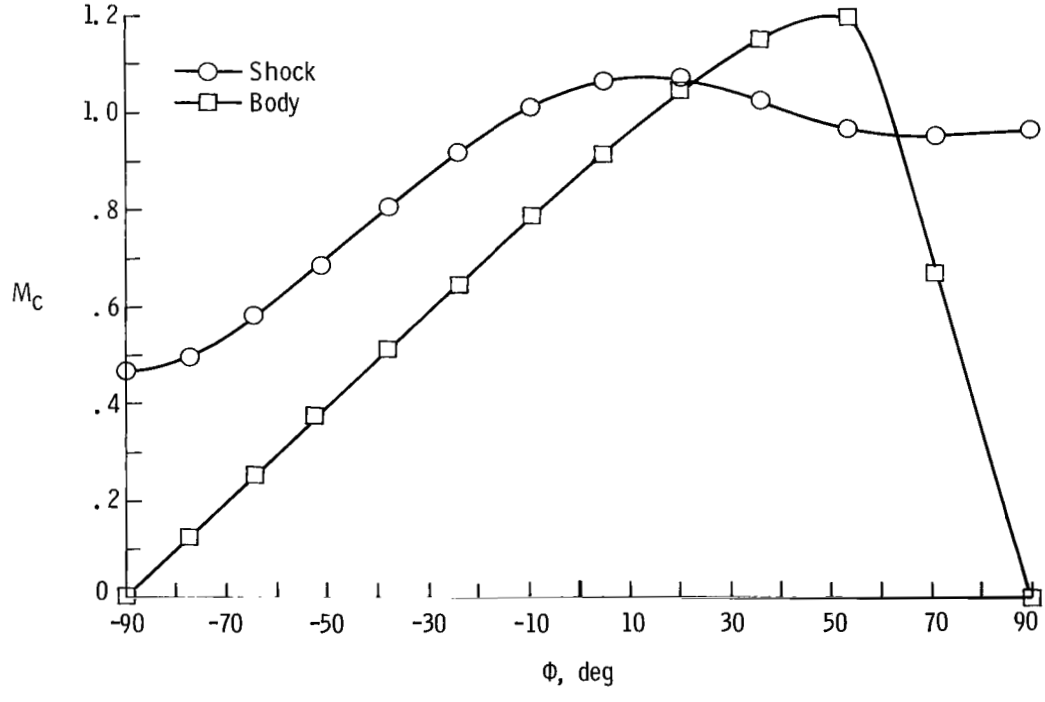

Figure 7.- Computed cross-flow Mach number at shock wave and surface for circular cone at relative incidence equal to 1.1. $M_\infty = 7.95$; $\theta = 10^\circ$; N = 13.

A pressure minimum on the circular cones generally occurs away from the plane of symmetry, and the pressure coefficient becomes negative at the larger values of incidence. The sensitivity of the calculations to the accuracy of the shock location coupled with the small values of the pressures often lead to failure of the method through computation of a negative value of the pressure under these circumstances.

Extrapolation of surface pressures to large angles of incidence.- Even though the computations break down at some value of α near or beyond θ_c, useful results on the windward side can be obtained for larger values of α. Extrapolation of the results has proven practical with the present program as also in the similar computations of Jones (ref. 2). In figure 8 extrapolated values of the surface pressure coefficients on the windward side of the circular cone are compared with the experimental values measured by Tracy. The extrapolated values at $\alpha = 12^\circ$, 16°, 20°, and 24° computed with the use of the Lagrange formula from calculations by the method of lines at $\alpha = 6^\circ$, 8°, and 9.5° are in excellent agreement with experiment.

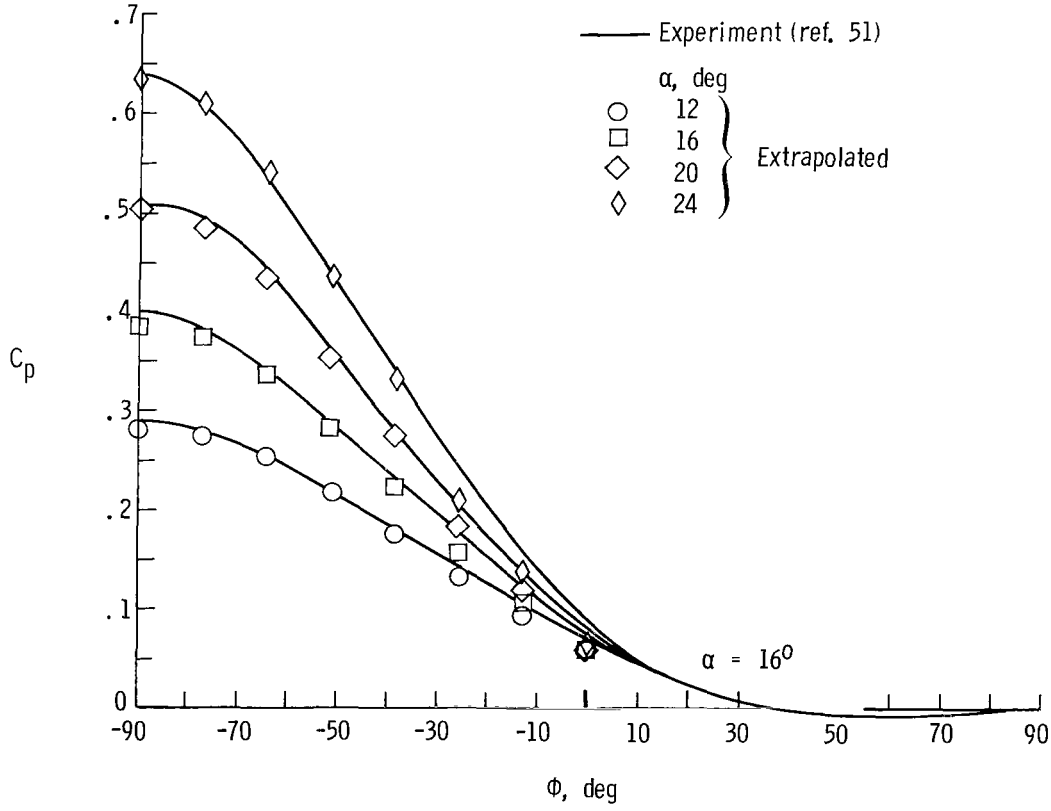

Figure 8.- Comparison with experiment of large-incidence windward-side pressures extrapolated from calculations at $\alpha = 6^\circ$, 8°, and 9.5°. $M_\infty = 7.95$; $\theta = 10^\circ$; $N = 15$.

Artificial hump on leeward side.- An alternate method of extending the calculations to large angles of attack is to alter the geometry on the lee side of the body to avoid some of the computational difficulties already discussed. The success of such an approach hinges on the fact that the flow on the windward side of the body is, to a large extent, independent of the flow on the lee side. Thus, the flow on the windward side of the specified body can be computed by selecting the shape on the lee side in such a way that one source of the computational difficulties is avoided; that is, the pressures are raised on the lee side. It may be noted that a supersonic cross flow may still exist along the sides but does not appear to limit the computations. For a conical body that was semicircular on the windward side and semielliptic on the leeward side, labeled bielliptic herein, computations have been made for angles of incidence much larger than is possible for a circular cone. The ratio of the major axis to the minor axis of the ellipse was taken sufficiently large to avoid computational problems and was sometimes taken as a linear function of the angle of attack for simplicity. Results of these computations at angles of attack of 12° and 16° for a stream Mach number of 7.95 and a semicone angle of 10° are shown in figure 9. Figure 9 displays the circular body, the experimentally determined viscous boundary, and the shock contour (ref. 51). The body shape on the lee side

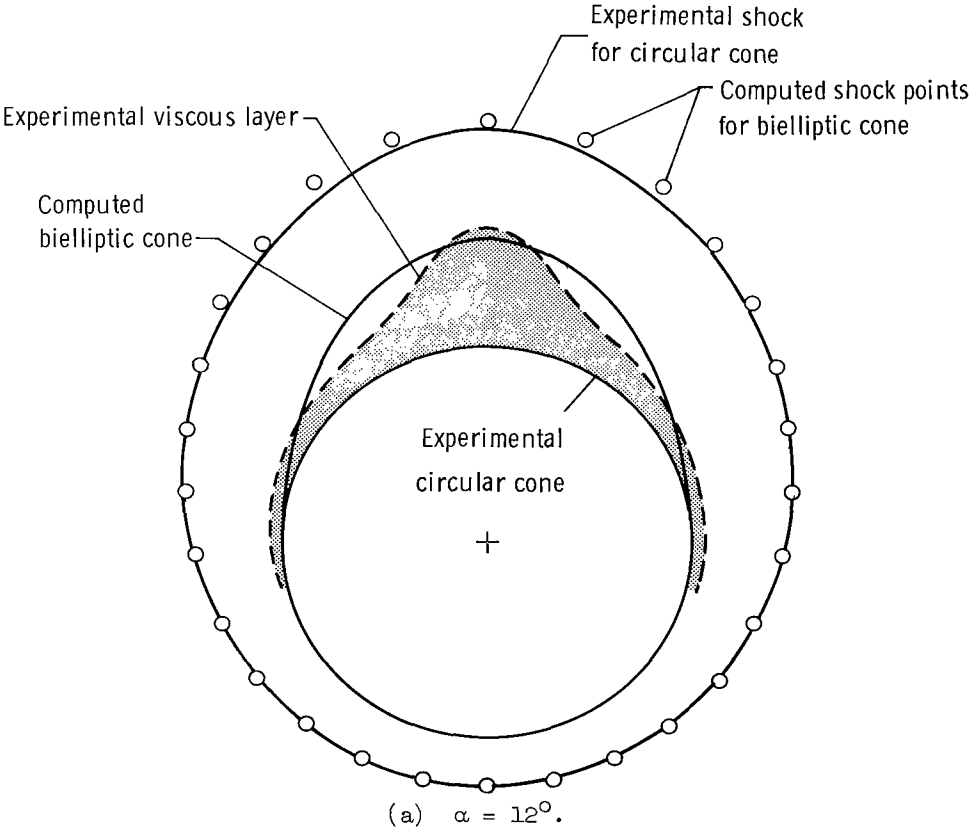

(a) $\alpha = 12^{\circ}$.

Figure 9.- Comparison of shock shape computation for bielliptic cone with experiment (ref. 51) for circular cone at large incidences. $M_{\infty} = 7.95$; $\theta = 10^{\circ}$; $N = 15$.

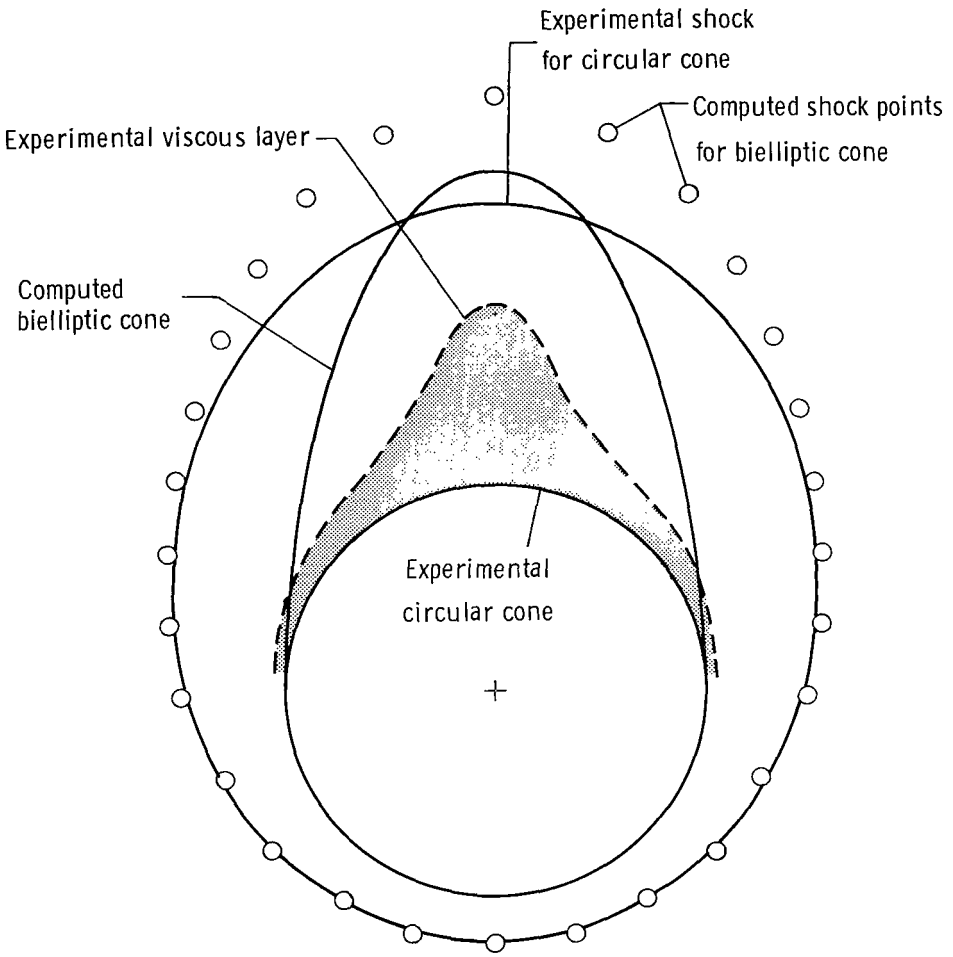

(b) $\alpha = 16^{\circ}$.

Figure 9.- Concluded.

used for the computations is also shown as well as symbols for the computed shock shape. For both computations the calculated shock shape on the windward side is in excellent agreement with the experimental values. The reasonably good agreement between experimental and computed values of the shock location on the lee side for $\alpha = 12^{\circ}$ is apparently due to a fortuituous choice of the axis ratio a/b of the ellipse (1.52) and was not selected essentially to duplicate viscous boundary. The axis ratio for the case at $\alpha = 16^{\circ}$ was 2.52. The corresponding values of the surface pressures are shown in figure 10. The computed values are in good agreement with experiment on the windward side at $\alpha = 12^{\circ}$ but show some deterioration at the more extreme case with $\alpha = 16^{\circ}$. It should be noted that the elliptic hump has held the leeward pressures at a "safe" positive level.

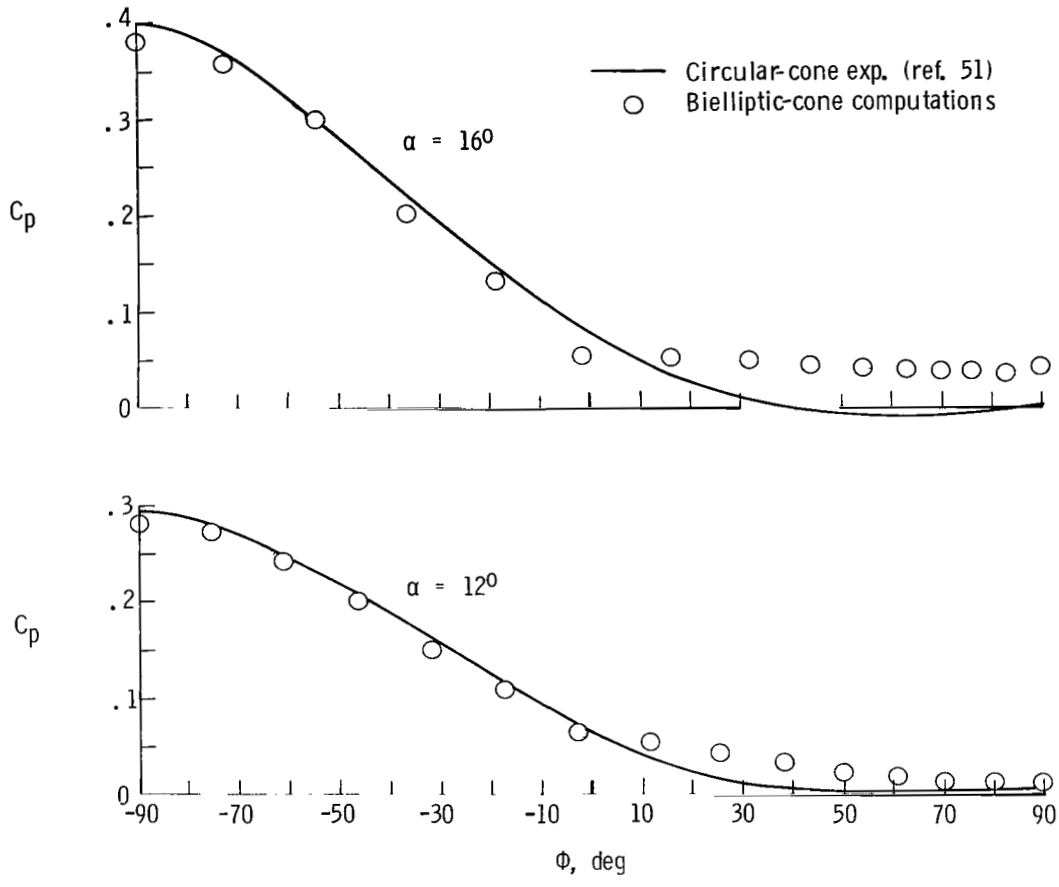

Figure 10.- Comparison of pressure computation for bielliptic cone with experiment for circular cone at large incidence.

Entropy Layer and Vortical Singularities

In the inviscid flow about a conical body, there exists a thin layer adjacent to the surface where the entropy gradients are large (in fact, unbounded). This so-called entropy or vortical layer was first recognized by Ferri (ref. 8) and has been studied analytically in many subsequent papers (refs. 9 to 11 and 52 as well as additional papers referenced therein). The pattern of the isentropes, or cross-flow streamlines, is shown in figure 11 as projected onto a plane Z = Constant, and illustrates the nature of the entropy layer for a circular cone at small incidence. In this case the streamline in the windward symmetry plane wets the entire cone surface, and it carries the maximum entropy. All other cross-flow streamlines rapidly approach the surface, form a thin layer of large (unbounded) entropy gradients, and converge in the leeward symmetry plane at a nodal point of the isentropes, where the entropy is multivalued. The nodal point is called the "vortical singularity."

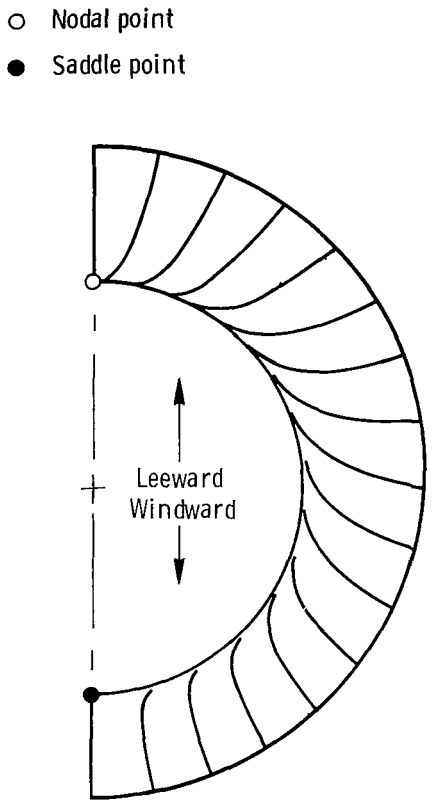

Figure 11.- Cross-flow streamline pattern for circular cone at small relative incidence. $M_\infty = 5^\circ$; $\theta_o = 10^\circ$; $\alpha = 2^\circ$; N = 17.

Entropy layer.- As explained in an earlier section entitled "Extrapolation to Surface," it is not necessary to account directly for the entropy layer. Nevertheless, because the independent variable ζ is continuous in the present method, it is possible to refine the integration near the surface and resolve some of the detail of this thin layer. Similarly, the "BVLR" method[4] can be used to resolve such details close to the surface, since the implicit nature of the method allows a nearly unlimited refinement of the grid size normal to the surface; such computations have been presented in reference 53 for an elliptic cone at zero incidence. Using a semidiscrete method somewhat similar to the present one, Ndefo (ref. 3) has also obtained some entropy layer calculations for a circular cone.

The computation of the flow in the entropy layer with the method of lines is tedious because ϵ must be very small in order to carry the integration very close to the surface. This requirement, in turn, demands that the shock shape be precisely determined. The necessary precision of the computation requires many iteration cycles and the calculation is generally feasible only with the use of the modified Newton iteration technique previously described. For the final computations presented here, ϵ was 10^{-10}.

[4]After Babenko, Voskresenskii, Lyubimov, and Rusanov, the co-authors of reference 13.

Calculations within the entropy layer were made for a circular cone with a semi-cone angle of 10°, $\alpha = 2^{\circ}$, and $M_{\infty} = 5$. The density distribution between the body and shock for $\phi = 0$ (along the side of the cone) is shown in figure 12. The density

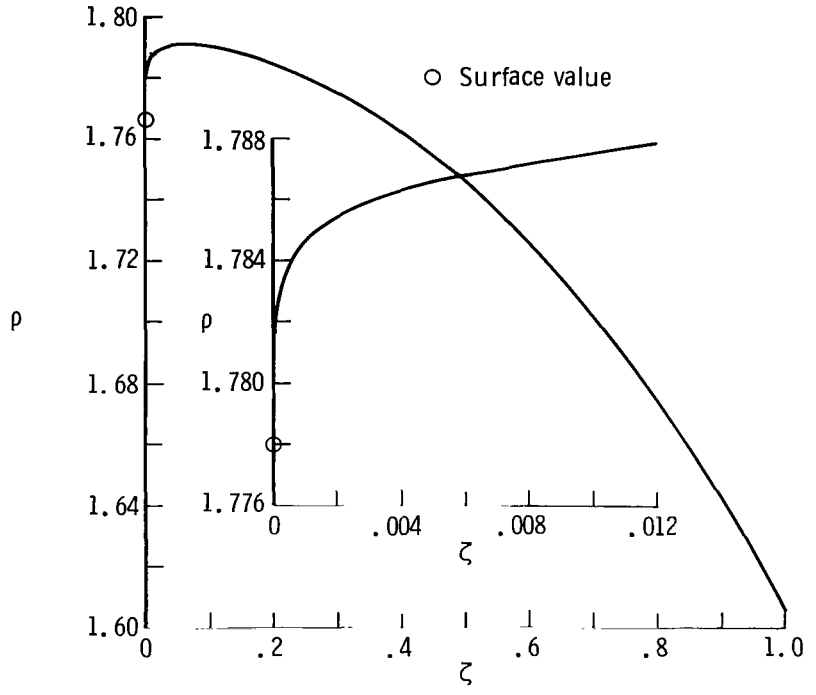

Figure 12.- Density distribution across shock layer and entropy layer of circular cone. $M_{\infty} = 5.0$; $\theta = 10^{\circ}$; $\alpha = 2^{\circ}$; $\phi = 0^{\circ}$.

monotonically increases from the shock to a region near the body where, in the entropy layer, the density decreases. The inset in figure 12 expands the abscissa by a factor of 50 and the ordinate by a factor of 10 to display the variation near the conical surface.

The results for several values of ϕ are presented in figure 13 where the quantity $\rho - \rho_0$ (ρ_0 is the surface value of the density) is presented as a function of ζ on a log-log plot. Those results show that deep in the entropy layer, the density variation is of the form

$$\rho(\phi,\zeta) = \rho_0(\phi) + C(\phi)\zeta^{\nu}$$

From figure 13, $\nu \approx 0.19$. Dr. R. E. Melnik has supplied the authors with an estimate of ν based on his asymptotic analysis of the entropy layer (ref. 9). His estimate for this case is $\nu = 0.22 \pm 0.04$ which is consistent with the present numerical results. The possible error indicated is a result of neglecting terms which are $O\left[(\alpha/\theta_0)^2\right]$ in the estimate.

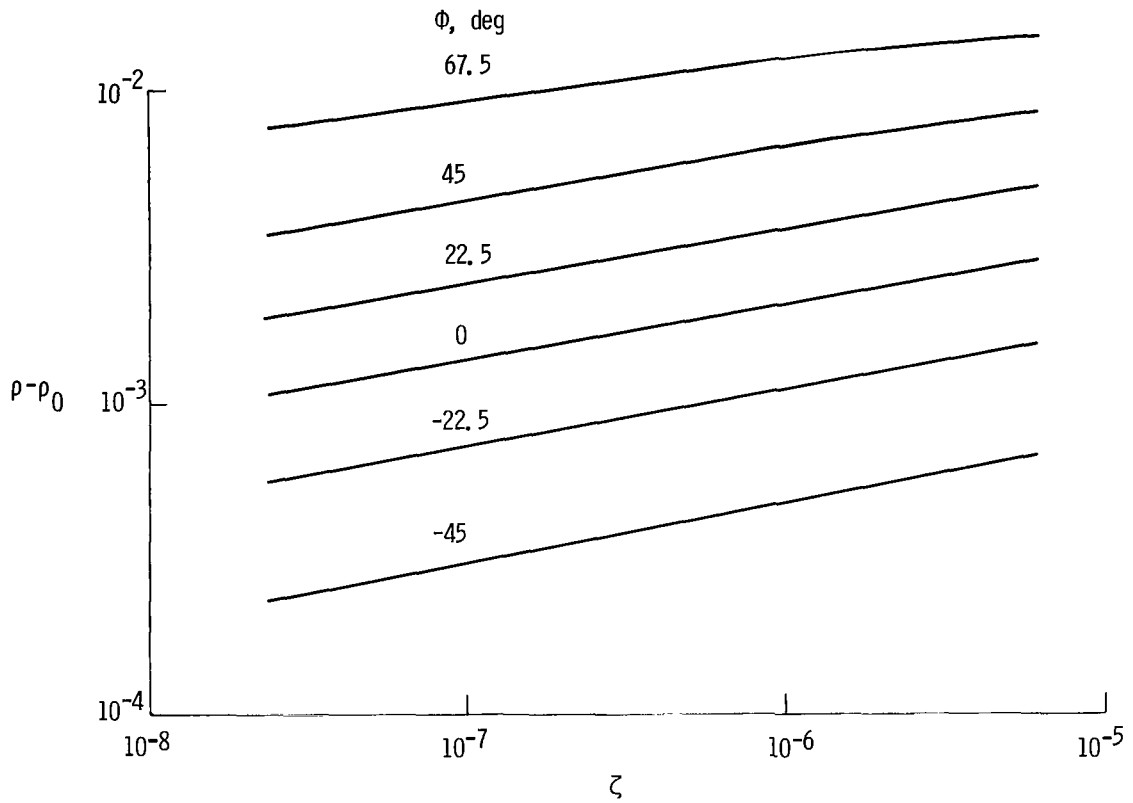

Figure 13.- Density variation in the entropy layer. $M_\infty = 5.0$; $\theta = 10^\circ$; $\alpha = 2^\circ$.

Vortical singularity lift-off.- Ferri (ref. 8) suggested the possibility that the nodal singularity could lift off the conical body at large angles of incidence. Several authors have attempted to develop analytic solutions in the neighborhood of the nodal point; Melnik (ref. 52) and others have concluded from their analyses that the vortical singularity can, in fact, lift off the surface.

Some effort has been expended to verify the lift-off phenomenon by exact numerical solutions, with questionable results. Gonidou (ref. 16) has attempted such calculations with the BVLR method, but his results indicated numerical instability, and hence were in doubt. It has been shown (ref. 53) that the conditions for lift-off are just those which cause the BVLR method to be unstable. Jones (ref. 2) has made computations which indicate that the vortical singularity was off the conical surface. His calculations are for a circular cone with a semivertex angle of 12.5° at a stream Mach number of 1.797. Jones presents computations for α/θ_0 up to 1.4 and his results indicate that lift-off occurs for α/θ_0 between 1.1 and 1.2. His integration step size was one-tenth of the shock-layer thickness and extrapolation to the surface was made from the last step. Thus, he extrapolated across the nodal point for the angle-of-incidence conditions where the vortical singularity is off the surface.

Computations have been made with the method of lines presented herein in an attempt to verify Jones' results. The calculations were made for α/θ_0 up to 1.2. Sonic velocity was attained at the shock in the lee plane of symmetry for this condition and the computations could not be carried to larger values of α because of the sensitivity of the calculations to the shock shape. One set of computations was made with an integration step size of 0.1 with extrapolation to the surface from 0.1 to nearly duplicate the calculations of Jones. A second set carried the integration to a value of 0.05 with extrapolation from that value of ζ to the surface. Both calculations indicated that lift-off had just barely occurred for $\alpha/\theta_0 = 1.2$. The results of the latter computations are shown in figure 14 where $dv/d\zeta$ and v in the leeward plane of symmetry are plotted against ζ. The values of $dv/d\zeta$ were extrapolated (shown dashed) to $\zeta = 0$ with the use of the Lagrange formula and the corresponding values of v were found by integration of $dv/d\zeta$. The incipient lift-off condition occurs for $\frac{dv}{d\zeta} = 0$ at $\zeta = 0$; at angles of incidence beyond the lift-off condition, $\frac{dv}{d\zeta} > 0$ at the surface and a zero value of v occurs off the body (nodal point) as well as on it. Precise lift-off computations are

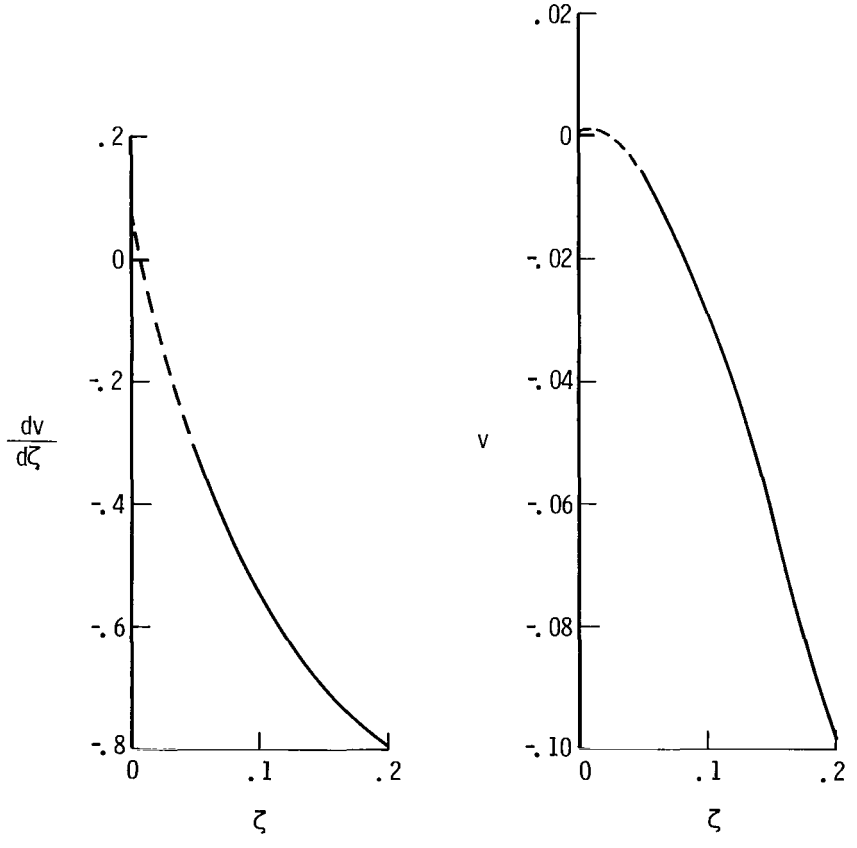

Figure 14.- Extrapolation of the normal velocity component and its derivative in the lee plane of symmetry of a circular cone near the condition for vortical singularity lift-off. $M_\infty = 1.797$; $\theta = 12.5^\circ$; $\alpha = 15^\circ$; $N = 13$.

difficult to make since the shock must be located with great accuracy in the region near the leeward plane of symmetry. In practice, computations are made for several values of α near or beyond the incipient lift-off condition. In cases where the nodal singularity is off the surface, the quantity $dv/d\zeta$ is extrapolated across the singular point.

The calculation of the flow beyond the incipient lift-off condition in this manner is questionable. The extrapolation of the derivative $dv/d\zeta$ across the singular point in the leeward symmetry plane is one facet open to criticism since the discontinuity in the entropy across the singularity is not taken into consideration. That is, the entropy should be that of the leeward symmetry plane between the shock and the nodal point and that of the windward symmetry plane between the body and the nodal point. Likewise, there is a discontinuity in both ρ and u across the nodal point. From the second of equations (2), in the plane of symmetry ($w = 0$) and in the neighborhood of the nodal point ($v \to 0$), the expression for the derivative becomes

$$\frac{dv}{d\zeta} = -2\eta_s u$$

Thus, $dv/d\zeta$ is discontinuous like u at the nodal point and extrapolation of $dv/d\zeta$ across it is invalid.

The method of lines could be adapted to account properly for the discontinuity in the variables across the vortical singularity although it is not known whether it would indeed be successful because of the computational difficulties that are encountered at the large incidences where lift-off is supposed to occur. The computations would require extrapolation from some integration step to a value of ζ at which the v component of velocity vanishes in the leeward symmetry plane, that is, to the location of the nodal point. The jump in entropy across the singularity is known and the jump in ρ and u can be computed. The integration could then be continued with the new initial values and finally extrapolated to the surface in the normal fashion. No attempt has been made to carry out such a sequence of computations. In view of the incorrectness of the extrapolation across the nodal point which has been used in the method of lines, and the instability of the BVLR method when incipient lift-off conditions occur, it is felt that the existence of a nodal point off the surface has not yet been conclusively demonstrated by numerical computation.

Elliptic Cone

Calculations have been made by the method of lines for the supersonic flow over an elliptic cone to compare with the experimental results of Chapkis (ref. 54). The cone angle θ_0 in the vertical plane of symmetry is 5.97°, the axis ratio a/b is 2, and the

stream Mach number is 5.8. The computed and experimental surface pressure coefficients are shown in figure 15 for α of 0°, 2°, 4°, and 6°. The agreement between the

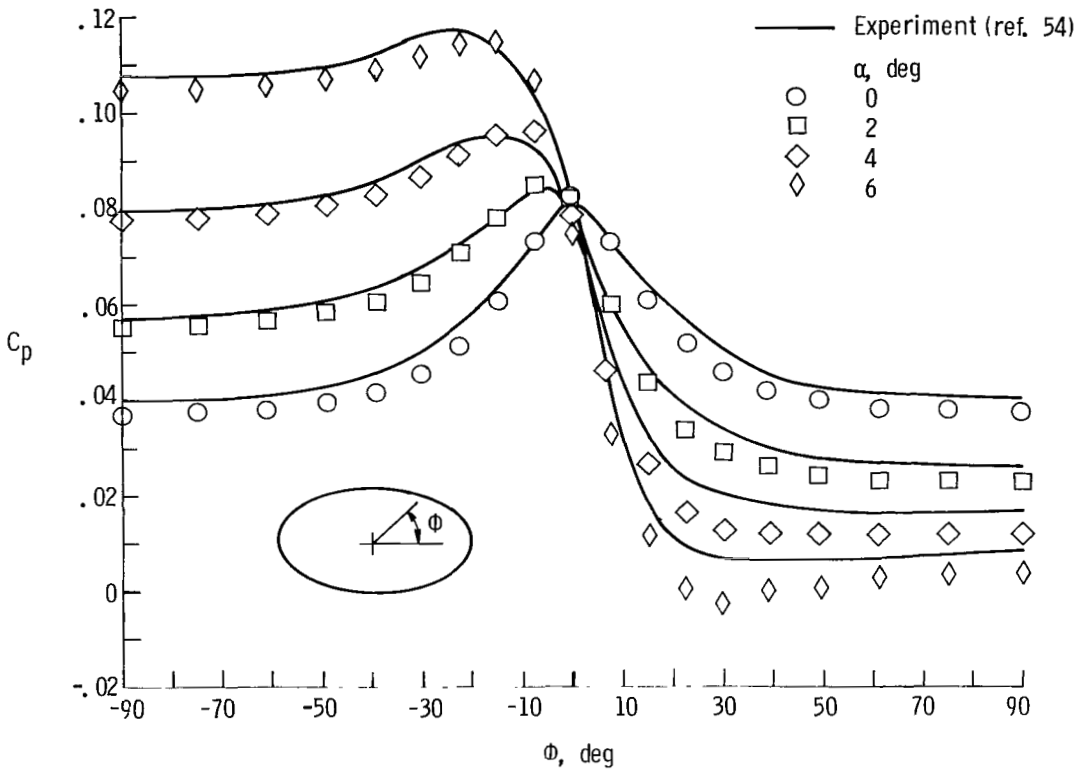

Figure 15.- Computed and experimental circumferential pressure distributions for elliptic cone at incidence. $M_{\infty} = 5.8$; $\theta_o \approx 6^{\circ}$; $\frac{a}{b} = 2$; $N = 19$.

computations and experiment is generally good but is less satisfactory on the leeward side where the viscous buildup raises the level of the measured pressures. Both the computed and experimental results show a relatively constant value of the pressure on the windward side and a rapid expansion around the side of the elliptic body, a supersonic cross flow occurring for the case at an angle of attack of 6°. Typical of the inviscid calculations for both the circular and elliptic cones is the pressure minimum which occurs away from the horizontal plane of symmetry when the relative incidence α/θ_o approaches unity. Convergence of the solution for angles of incidence beyond 6° becomes difficult, similar to the case of a circular cone for $\frac{\alpha}{\theta_o} \geqq 1$, since the imbedded regions of supersonic cross flow and low pressures are encountered.

Extrapolated surface pressures.- Extrapolated values of the surface pressure coefficient on the windward side of the elliptic cone, using the C_p values for $\alpha = 2^{\circ}$, 4°, and 6°, are compared with the experimental results of Chapkis in figure 16. The agreement is excellent at $\alpha = 8^{\circ}$ and 10° but shows some deterioration at $\alpha = 14^{\circ}$.

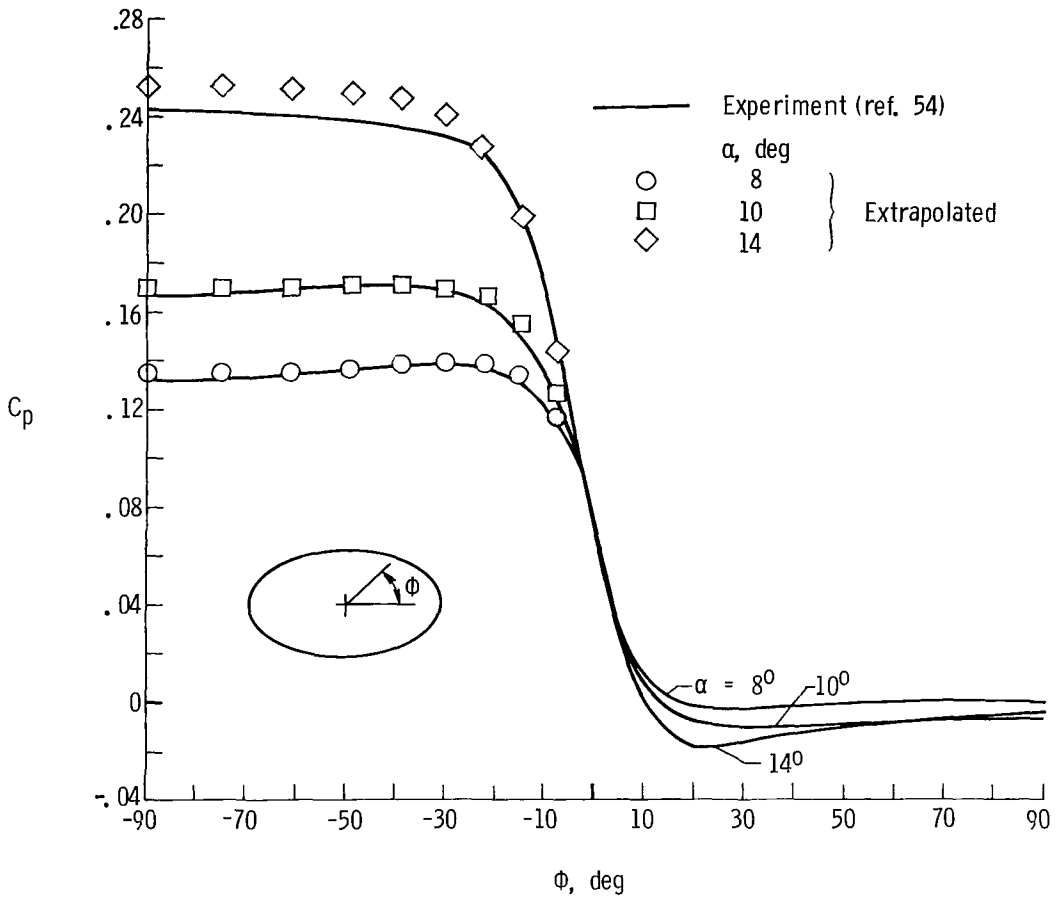

Figure 16.- Comparison with experiment of large incidence windward-side pressures extrapolated from calculations at $\alpha = 2^\circ$, 4°, and 6°. $M_\infty = 5.8$; $\theta_o \approx 6^\circ$; $\frac{a}{b} = 2$; $N = 19$.

Cross-flow streamline pattern.- In figure 17 the cross-flow streamlines together with the cross section of the body and shock are shown for the elliptic cone at angles of incidence of 2° and 6°. At an angle of attack of 6° the relative incidence α/θ_o is about 1. The streamline contours, which correspond to constant values of the entropy, were obtained by linear interpolation. Those contours either near the windward saddle point or the leeward nodal point are difficult to obtain with precision and are shown dashed in some cases where their location is uncertain. It may be seen that a nodal point (shown with an open symbol) occurs in the windward and leeward planes of symmetry and a saddle point singularity (shown with a filled symbol) on the windward side. At zero incidence the saddle point lies on the major axis and moves to the windward side with increasing incidence. The cross-flow streamline patterns are similar on the windward side for the two cases; however, the general character of the stream lines on the leeward side changes as the relative incidence is increased.

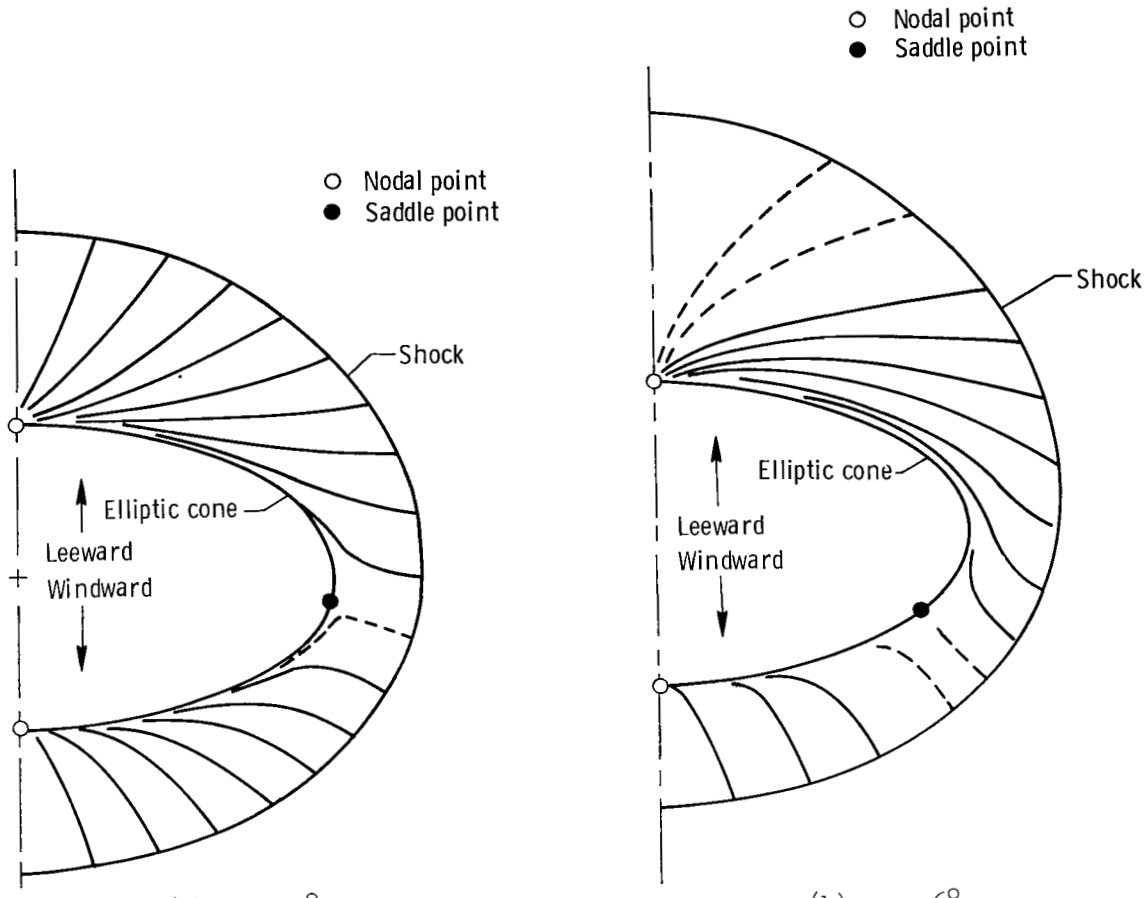

(a) $\alpha = 2^{\circ}$.

(b) $\alpha = 6^{\circ}$.

Figure 17.- Cross-flow streamline pattern for elliptic cone at incidence.
$M_{\infty} = 5.8$; $\theta_o \approx 6^{\circ}$; $\frac{a}{b} = 2$; $N = 19$.

Computation history.- The elliptic cone calculations at $\alpha = 0^{\circ}$ were made by starting from a circular cone (a/b = 1) with semiangle equal to the desired semiangle (11.8°) in the plane of the major axis of the ellipse. The axis ratio a/b was changed in increments until the desired configuration was obtained. The solutions for various angles of attack were then computed, beginning with zero angle of attack. Table I gives the history of the automatic increases in α together with the number of Newton iteration cycles (N + 1 integrations) and the number of integrations of the coupled 5N differential equations required to converge the shock shape for each α by using the regular Newton iteration. The convergence criterion for the normal velocity component was set at $\epsilon = 10^{-3}$ and the final value of $\max_i |v_i(0)|$ is also shown. Each integration from the shock to the body was made in 12 integration steps with a step size of 0.1 to a value of ζ of 0.1, and steps of 0.05 and 0.025 thereafter. The total central processing time, excluding compilation, was 740 seconds (Control Data 6600 computer). Table II gives the

TABLE I.- COMPUTATION HISTORY FOR ELLIPTIC CONE WITH REGULAR NEWTON ITERATION

$\left[N = 17;\ M_\infty = 5.8;\ \frac{a}{b} = 2;\ \theta_o = 6^o\right]$

Angle of incidence, α, deg	Number of Newton cycles	Number of integrations	$\max_i \lvert v_i(0) \rvert$
0	0	1	7.7×10^{-4}
.05	1	19	3.7×10^{-5}
1	1	19	5.7×10^{-4}
2	2	37	4.9×10^{-5}
3	1	19	3.8×10^{-5}
4	1	19	2.6×10^{-5}
5	1	19	1.6×10^{-4}
6	2	37	1.7×10^{-5}
Total		170	

TABLE II.- COMPUTATION HISTORY FOR ELLIPTIC CONE WITH MODIFIED NEWTON PROCEDURE

$\left[N = 17;\ M_\infty = 5.8;\ \frac{a}{b} = 2;\ \theta_o = 6^o\right]$

Angle of incidence, α, deg	Number of Newton cycles	Number of modified Newton cycles	Number of integrations	$\max_i \lvert v_i(0) \rvert$
0	0	0	1	7.7×10^{-4}
.05	1	0	19	3.7×10^{-5}
1	1	0	19	5.7×10^{-4}
2	1	2	21	2.6×10^{-4}
3	1	0	19	4.2×10^{-5}
4	1	0	19	4.2×10^{-5}
5	1	0	19	1.6×10^{-4}
6	1	1	20	2.9×10^{-4}
Total			137	

computation history for the same set of computations except that the modified Newton procedure was employed; that is, the partial derivatives employed in the Newton iteration were not recomputed in cases where more than one iteration was required. The central processing time in this case was 595 seconds. Comparison of tables I and II shows that worthwhile savings in computing can be obtained with the use of the modified Newton method. The superiority of this method is more dramatic for sequences of computations where the regular Newton method requires two or more cycles for each value of the parameter. Tables I and II show an increase in the number of integrations for angles of attack of 2° and 6°. The increase at an angle of attack of 2° is due to the fact that the initial values of η_s are found by linear extrapolation of those for $\alpha = 0^{\circ}$ and $\alpha = 1^{\circ}$ whereas the initial values of η_s at larger angles of incidence are obtained by quadratic extrapolation and consequently provide a better estimate for the pivotal computation. At the angle of attack of 6°, α/θ_0 is approximately one, a supersonic cross flow has developed and convergence, as already discussed for the case of the circular cone, is more difficult to achieve.

Effect of number of lines.- In problems involving severe cross-flow gradients, it would be desirable to use a relatively large number of lines to resolve the detail of a solution. However, the maximum number that can be used profitably in a given computation is restricted by the computing time and by instabilities that enter the solution, as explained in an earlier section. A maximum of about 19 lines has proven feasible for the method of lines in the form presented herein.

Figures 18 and 19 illustrate the changes in the solution with a change in the number of lines for the elliptic cone with $a/b = 2$, $\alpha = 2^{\circ}$, $\theta_0 = 5.97^{\circ}$, and a stream Mach number of 5.8. The surface pressure distribution is shown in figure 18 for $N = 5$, 9, and 17 and the corresponding shock shapes, together with the body shape, are shown in figure 19. It may be seen that the results for $N = 5$ and $N = 9$ oscillate about those for $N = 17$. The computations for $N = 5$ clearly establish the trend of the solution whereas those for $N = 9$ are in very good agreement with the 17-line case. The central processing time, excluding compilation, for the same sequence of computations beginning with a circular cone was 46, 103, and 322 seconds for $N = 5$, 9, and 17, respectively.

Elliptic cone with large axis ratio.- The pressure gradients in the cross-flow direction for the elliptic cone become large as a/b becomes large; thus, a relatively large number of lines to construct the solution to good accuracy are dictated. However, the instabilities which arise with a large number of lines force the use of fewer lines than would otherwise be desirable. Computations for an elliptic cone with $N = 17$ at zero incidence are compared with the experimental results of Martellucci (ref. 55) in figs. 20 and 21; the semicone angle in the plane of the major axis is 30.05°, $a/b = 3.68$, and $M_{\infty} = 3.09$. The general agreement of the computed and measured pressures (fig. 20) is

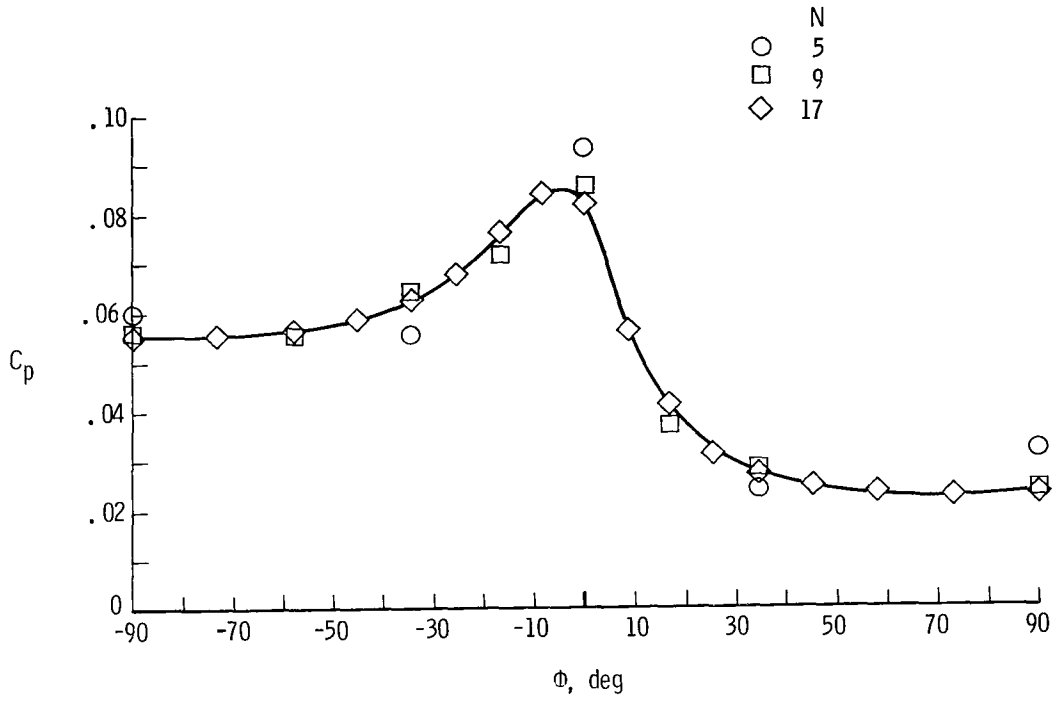

Figure 18.- Convergence with increasing N for pressure distribution on elliptic cone. $M_\infty = 5.8$; $\theta_o = 6^\circ$; $\frac{a}{b} = 2$; $\alpha = 2^\circ$.

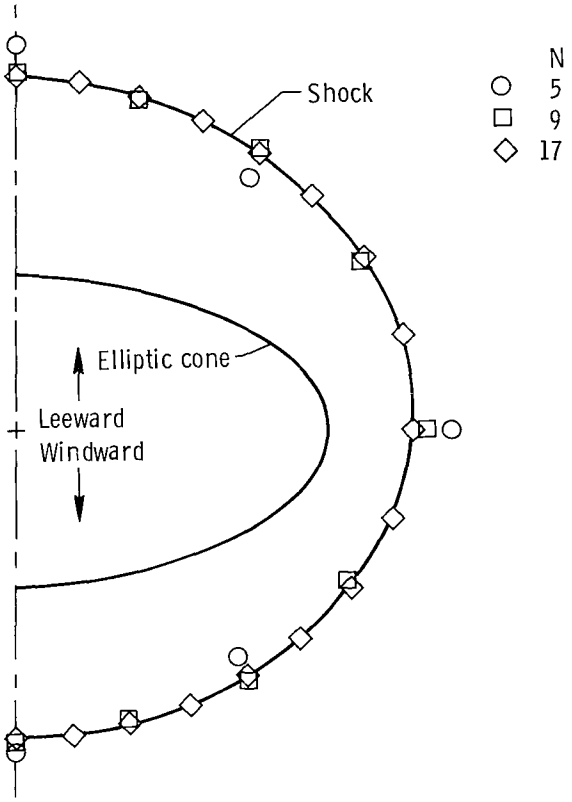

Figure 19.- Convergence with increasing N for shock shape on elliptic cone. $M_\infty = 5.8$; $\theta_o \approx 6^\circ$; $\frac{a}{b} = 2$; $\alpha = 2^\circ$.

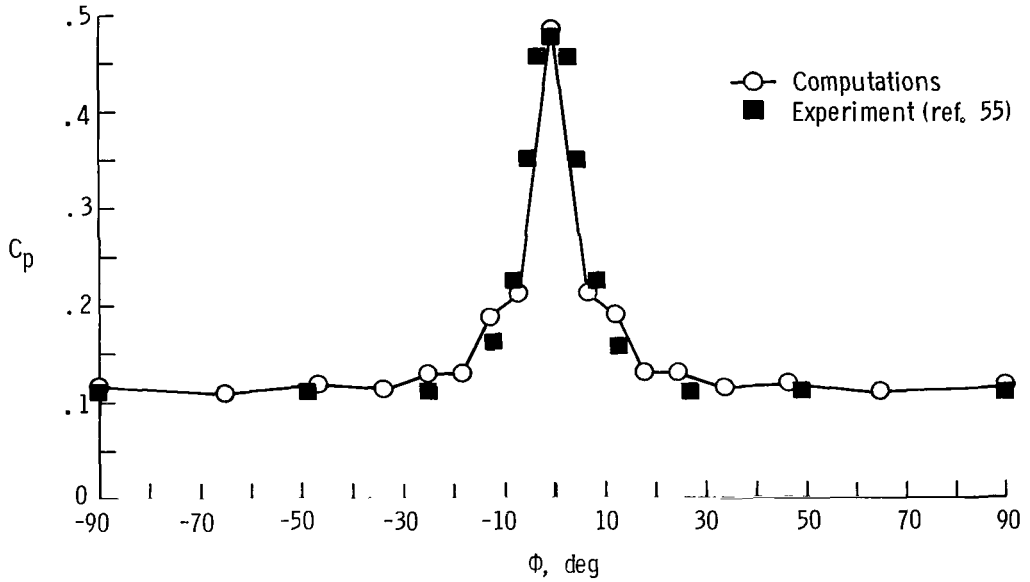

Figure 20.- Computed and experimental circumferential pressure distribution on elliptic cone at zero incidence. $M_\infty = 3.09$; $\theta_o \approx 8.9$; $\frac{a}{b} = 3.68$; $N = 17$.

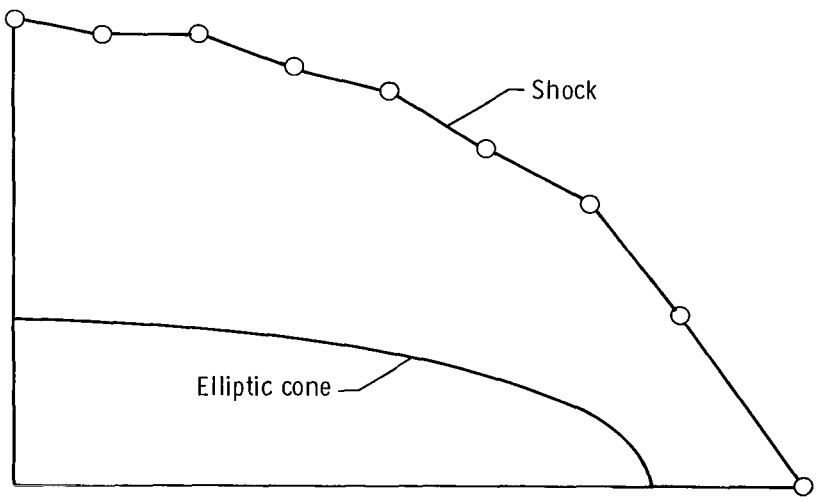

Figure 21.- Computed shock shape for elliptic cone at zero incidence. $M_\infty = 3.09$; $\theta_o \approx 8.9$; $\frac{a}{b} = 3.68$; $N = 17$.

good but the computed results clearly exhibit some roughness. The roughness of the shock shape (fig. 21), and, in particular, the too large value of the shock coordinate in the plane of symmetry of the major axis is typical of cases where too few lines have been employed. (See fig. 19.) It is possible to continue the solutions to larger values of a/b but converged solutions become more difficult to obtain, the "roughness" of the solution becomes more pronounced, and program failure ultimately follows.

Comparison of an elliptic cone computation with other methods.- The saddle and nodal point singularities, as seen in figure 17, arise when the w-component of velocity on the body vanishes. This component of velocity, which is one of the three velocity components of the coordinates used herein, is normal to a ray from the apex. Babenko (ref. 53) employed a cylindrical coordinate system to compute the flow about an elliptic cone and erroneously concluded that a singularity occurred where the circular-cylindrical component of velocity w_c vanished and thereby computed a discontinuity in the other two cylindrical velocity components. Jones (ref. 2) similarly used a circular-cylindrical coordinate system but calculated the solution correctly. The semicone angle in the plane of the major axis is 35°, $a/b = 2$, $\alpha = 0$, and $M_\infty = 10$ for this case. The circular-cylindrical velocity components computed by Babenko, Jones, and by the present method are shown in figure 22. The results of Jones and the present calculations are in agreement.

Elliptic cone at yaw.- The designation "elliptic cone at yaw" refers to one for which the stream velocity vector is in a plane parallel to the major axis; ψ is the yaw angle for this configuration. Chapkis (ref. 54) has made measurements of the surface pressures for the yawed cone. The conical body is the same one for which the angle-of-attack measurements were made; the semicone angle in the plane of the minor axis is 5.97°, $a/b = 2$, and the stream Mach number is 5.8. The computed surface pressure coefficients are compared with the experimental results in figure 23 for angles of yaw of 2°, 4°, 6°, and 8°. The fairing of the experimental data was taken from reference 54. Note that this faired data does not have a zero slope at $\phi = 0^\circ$ and 180° as should be the case. The pattern of the flow is somewhat different from that of the elliptic cone at incidence. The w component of velocity for the 4° yaw condition is shown in figure 24. The nodal point, which is located where the w component of velocity vanishes outside the plane of symmetry, is located on the leeward side of the conical body. The cross-flow streamlines together with the body and shock shape are shown in figure 25 for yaw angles of 2°, 4°, 6°, and 8°. The streamline contours near the nodal singularity are difficult to establish accurately and consequently are shown dashed. The saddle points are shown with a filled symbol and the nodal point with an open symbol in the figures. At zero yaw the nodal point is located in the plane of the minor axis and as the yaw angle is increased, it moves toward the leeward plane of symmetry. The surface entropy is discontinuous across the nodal singularity; the surface entropy in the region from the

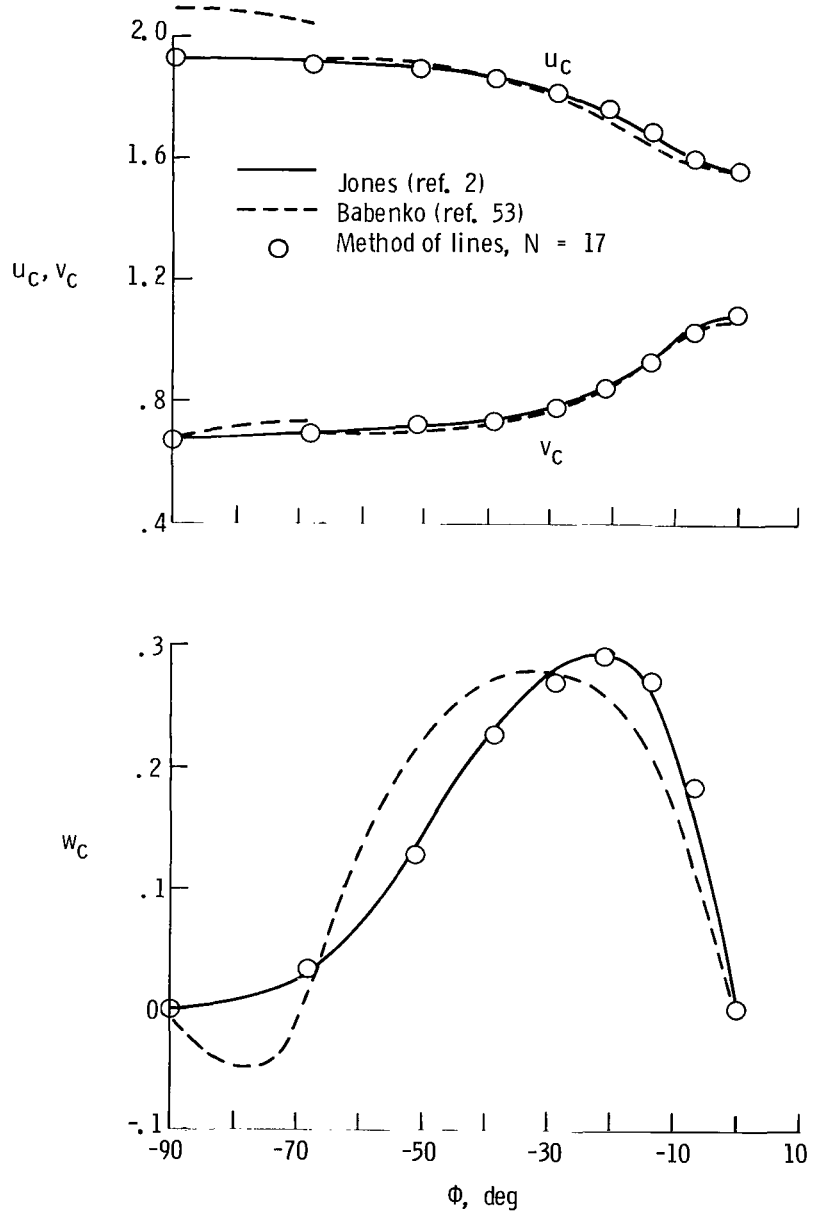

Figure 22.- Comparison of results of various computational methods for the cylindrical velocity components at the surface of an elliptic cone at zero incidence. $M_\infty = 10$; $\theta_o \approx 19.3$; $\frac{a}{b} = 2$; $N = 17$.

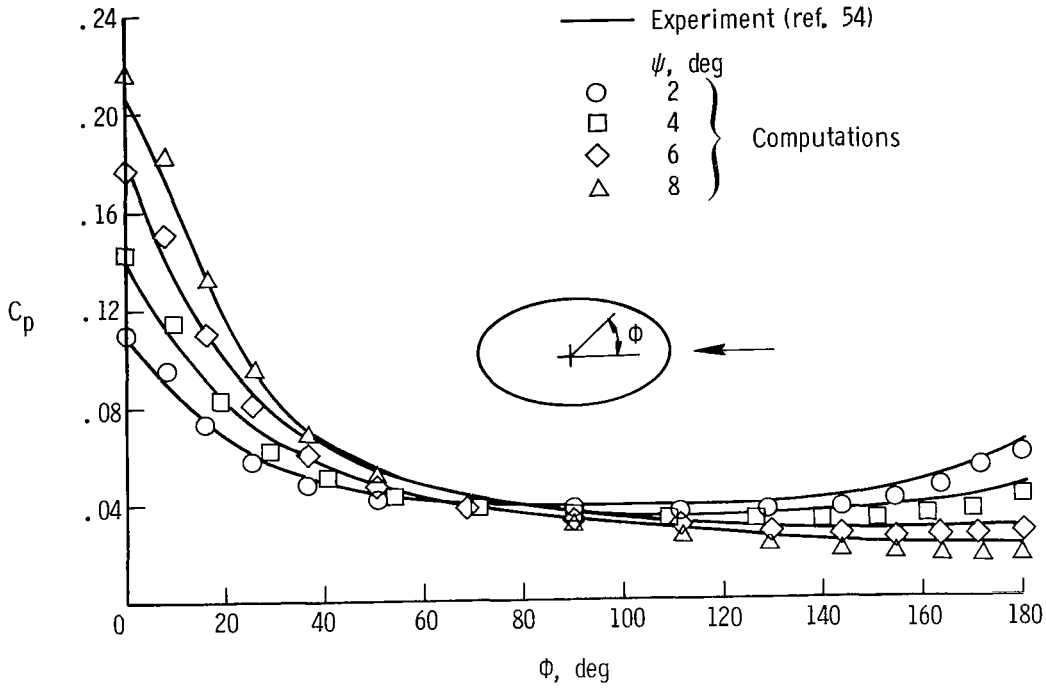

Figure 23.- Computed and experimental pressure distributions on a yawed elliptic cone. $M_\infty = 5.8$; $\theta_o = 11.8^\circ$; $\frac{a}{b} = 2$; $N = 15$.

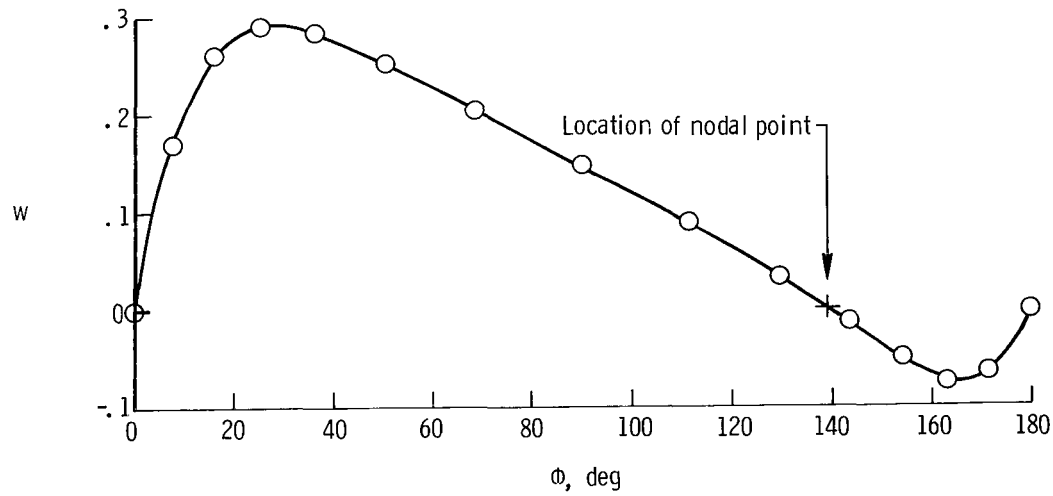

Figure 24.- Computed distribution of surface cross-flow velocity on a yawed elliptic cone. $M_\infty = 5.8$; $\theta_o = 11.8^\circ$; $\frac{a}{b} = 2$; $\psi = 4^\circ$; $N = 15$.

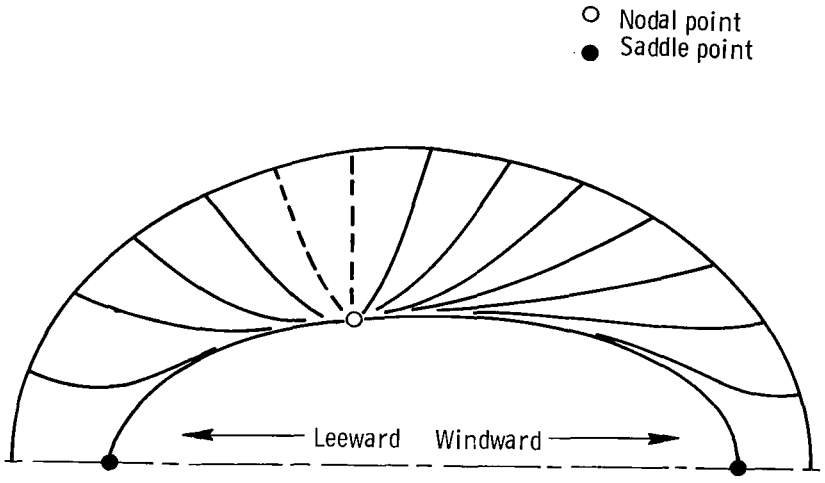

(a) $\psi = 2^{\circ}$.

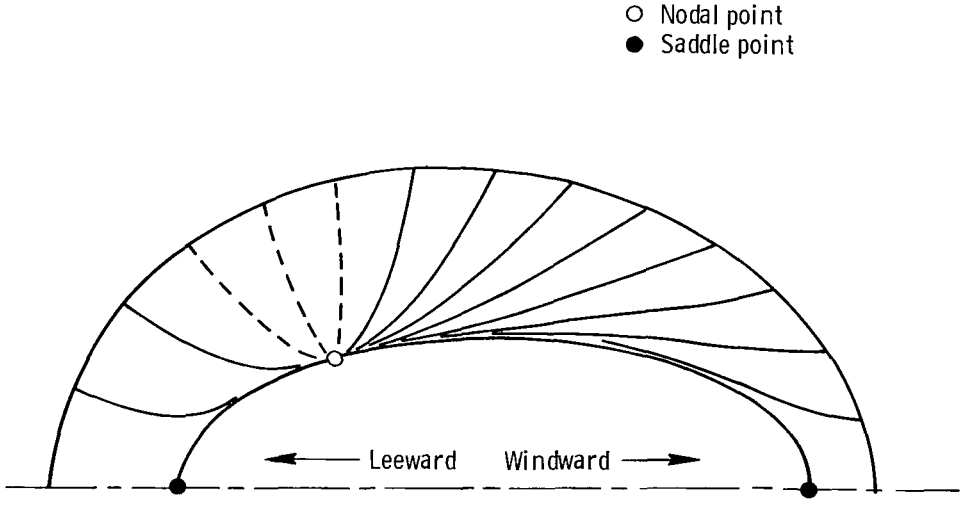

(b) $\psi = 4^{\circ}$.

Figure 25.- Cross-flow streamline pattern for yawed elliptic cone. $M_{\infty} = 5.8$; $\theta_{o} = 11.8^{\circ}$; $\frac{a}{b} = 2$; $N = 15$.

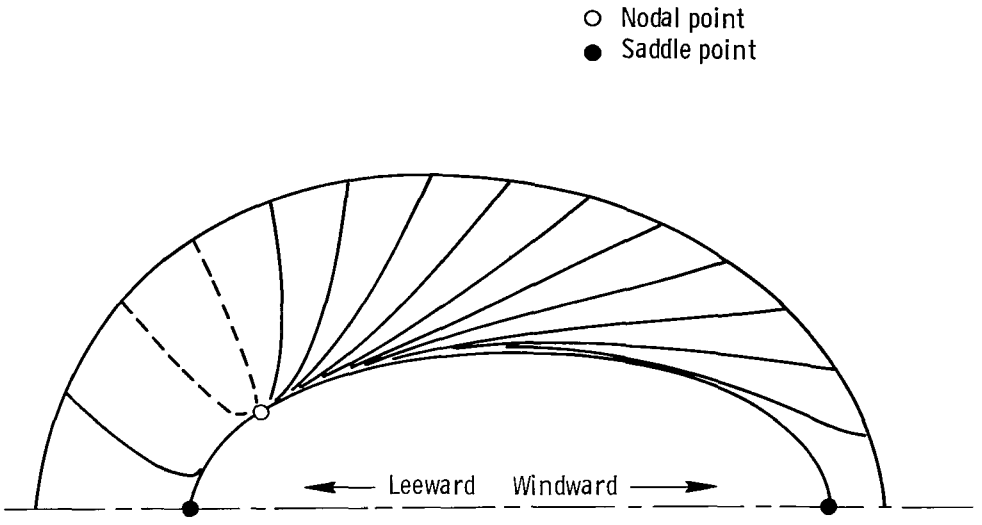

(c) $\psi = 6^{\circ}$.

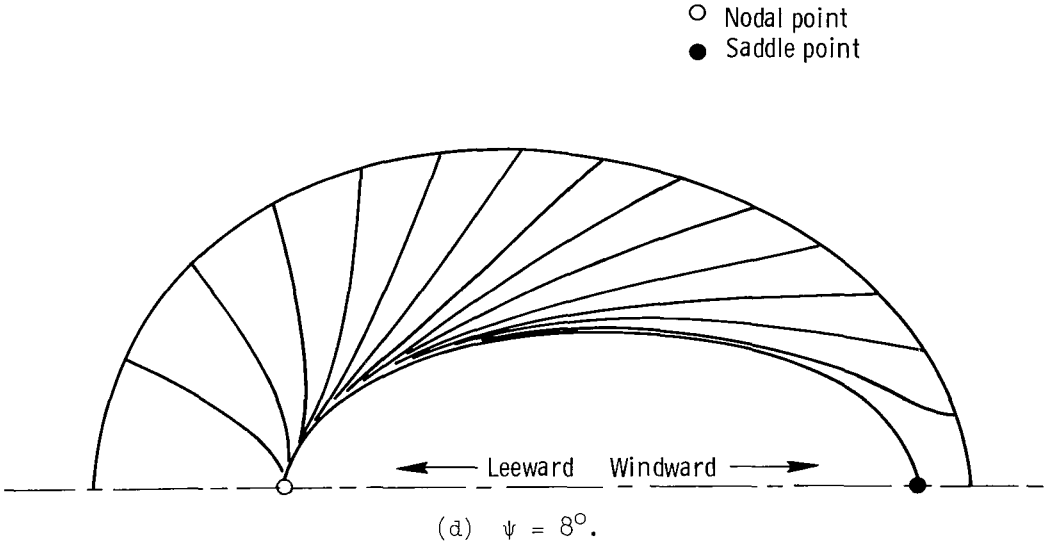

(d) $\psi = 8^{\circ}$.

Figure 25.- Concluded.

windward saddle point to the nodal point ($w > 0$) corresponds to the value of the entropy in the windward plane of symmetry whereas that from the nodal point to the leeward plane of symmetry ($w < 0$) corresponds to the value in the leeward plane of symmetry. Along with the discontinuity in surface entropy is a discontinuity in the u-component of velocity and the density. The surface distribution of the u-component of velocity for the 4° yaw is shown in figure 26. As the angle of yaw increases, the nodal point continues to move toward the leeward side and at some yaw condition apparently moves to the leeward plane of symmetry. At an angle of yaw of 8° (fig. 25), the nodal point appears to have coalesced with the leeward saddle point; however, it is impossible to obtain any resolution of the transition from the present computations.

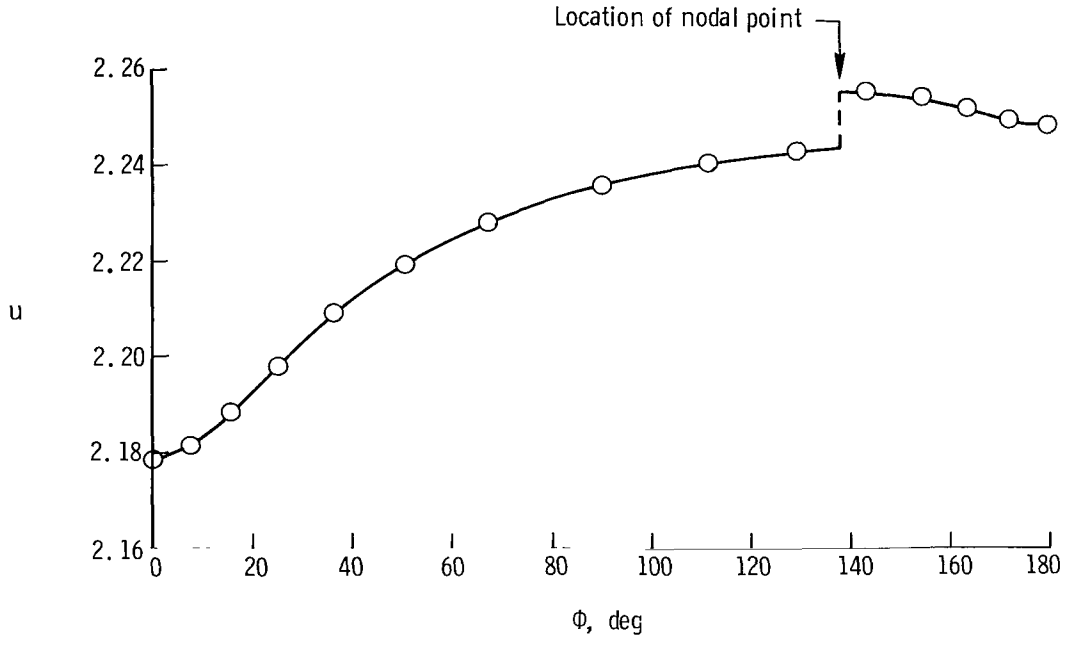

Figure 26.- Circumferential distribution of u-component of velocity at surface of yawed elliptic cone, illustrating discontinuity at nodal point. $M_{\infty} = 5.8$; $\theta_o = 11.8^{\circ}$; $\frac{a}{b} = 2$; $\psi = 4^{\circ}$; $N = 15$.

Conical Delta Wings

The present method has been applied to the problem of conical delta wings with the shock wave attached at the sharp leading edges. In this problem the compression surface is independent of the other surface, and the two can be treated separately. The method of lines, as formulated herein, is only applicable to the compression side where the shock wave forms the outer boundary. Nevertheless, the compression-side results are valuable from both theoretical and practical standpoints. As mentioned earlier, the results from the present method provide a check for more complex three-dimensional

calculation methods, and it will be seen that they corroborate results from other conical methods and experiment, too. Practically speaking, at large supersonic Mach numbers nearly all the aerodynamic-force contribution comes from the compression side.

In these problems the cross-flow component $\sqrt{v^2 + w^2}$ is supersonic at the leading edge and remains supersonic for some distance toward the wing center line. The partial differential equations governing the conical flow are of the hyperbolic type in regions where the cross flow (that is, the velocity component on the spherical surface) is supersonic, and a two-dimensional conical method of characteristics can be used to construct the exact flow in such regions. Maslen (ref. 28) was the first to describe this approach for conical delta wings, and it has been exploited extensively in reference 41 for the flow about elliptic cones at large angles of attack. A conical method of characteristics has been developed by Chiang and Wagner (ref. 56); they supplied the conical characteristic results presented in this paper.

Vincenti and Fisher (ref. 57) proposed an approximate method which can also be used in regions of supersonic cross flow; it is analogous to the familiar shock-expansion method for two-dimensional and axisymmetric flows. The approximation reduces to a pair of nonlinear ordinary differential equations that are numerically integrated along the surface in the spanwise direction from the leading edge inward to the cross-flow sonic point. Results obtained by Richard D. Wagner, Jr., by that method are presented and are referred to as a "conical shock expansion" method.

The supersonic cross flow in the delta-wing problems presents no difficulties for the method of lines; this result is contrary to the case of the circular or elliptic cone at incidence where convergence becomes more difficult when a region of supersonic cross flow occurs.

Parabolic-arc cross section.- Reference 17 presents calculated results for a number of conical delta wings obtained by the "BVLR" method. Computations for delta wings with both flat and parabolic-arc cross sections presented in reference 17 are compared herein with results from the present method and other methods. Planform and section views of a thin parabolic cross-section wing are shown in figure 27 with the calculated shock shape for $\alpha = 10^{\circ}$. The conditions for this problem are $M_{\infty} = 4$, $\Lambda = 50^{\circ}$, $\theta_0 = 3^{\circ}$, and $N = 12$. The cross-flow sonic line is shown as a heavy dashed line in the section view.

Equal line spacing was used for the wing computations with the method of lines; that is, equal $\Delta\xi$ increments were used around the wing contour on the surface $r = 1$. Thus, when projected onto the plane $Z = 1$ in which the body cross section is prescribed, the lines appear to spread as the leading edge is approached. The solid curve for the shock (fig. 27) represents Voskresenskii's results, and the squares are the present

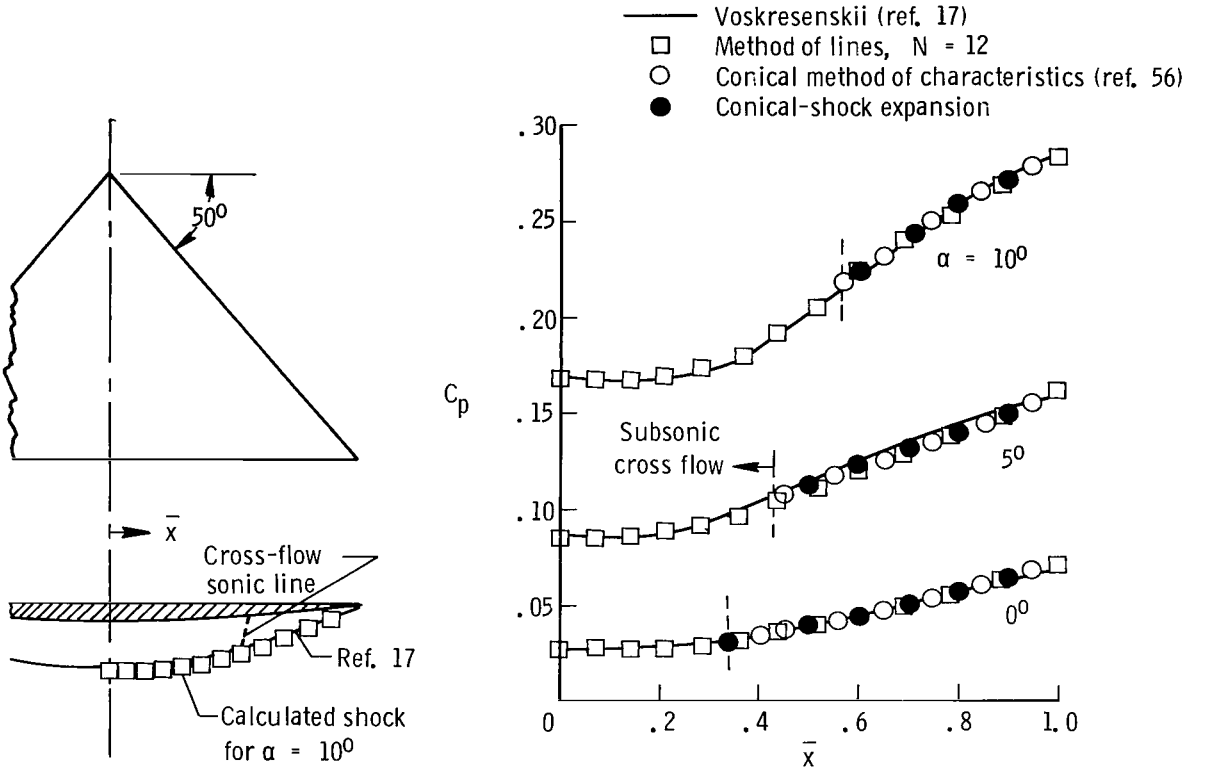

Figure 27.- Comparison of computations for shock shape and spanwise pressure distribution for a conical delta wing. Parabolic-arc cross section; $M_\infty = 4^\circ$; $\theta_o = 3^\circ$; $\Lambda = 50^\circ$; N = 12.

results for N = 12. The replotting of Voskresenskii's shock shape is probably not as accurate as that for the pressures because although Voskresenskii's shock appears to lie slightly inside the present result near the center line, shock pressures by both methods (not shown here) agree very well except near the leading edge. The conical method of characteristics also gives a shock shape from the leading edge to the cross-flow sonic lines, and the results (not shown) are in agreement with the present results.

The surface pressure coefficient is plotted against $\bar{x}$, a nondimensional spanwise coordinate; $\bar{x} = 0$ at the wing center line and $\bar{x} = 1$ at the leading edge. The vertical dashed lines indicate the spanwise location of the cross-flow sonic point[5] at the surface and, hence, the limit of applicability of both the conical method of characteristics (MOC) and the conical shock-expansion method. The method of lines, conical characteristics, and conical shock expansion agree very well in the supersonic cross-flow region. Voskresenskii's results are generally quite close to the present results. However, his results for $\alpha = 5^\circ$ are generally higher than the other computations in the outboard

[5]As the angle of attack is increased, the cross-flow sonic point moves toward the leading edge and reaches it slightly before leading-edge detachment occurs.

region except at the leading edge. At the leading edge, where the pressure and other variables can be calculated accurately from the algebraic shock conditions, results from all theories should agree exactly yet Voskresenskii's result for the pressure is noticeably low. His pressure calculation just inboard of the leading edge rises slightly above that of the three conical methods, but then appears to agree well with the present results in the central subsonic cross-flow region. It is not entirely clear whether the generally small discrepancies in the supersonic cross-flow region are due to the error in the leading-edge boundary condition. Of particular note is the very good agreement of the comparatively simple conical shock-expansion calculations with the other results.

Circular-arc cross section.- Reference 58 presents experimental data for various conical delta wings with attached leading-edge shocks; one of the models had a circular-arc cross section, a good test problem for the various computational methods. Figure 28 shows the shock shape computed by the method of lines for $N = 12$ and spanwise pressure distributions compared with experimental and other computed results. The wing thickness and the Mach number are both about twice that of the computations in figure 27. It can be seen that the cross-flow sonic line is closer to the wing center line; this result is due largely to the higher Mach number.

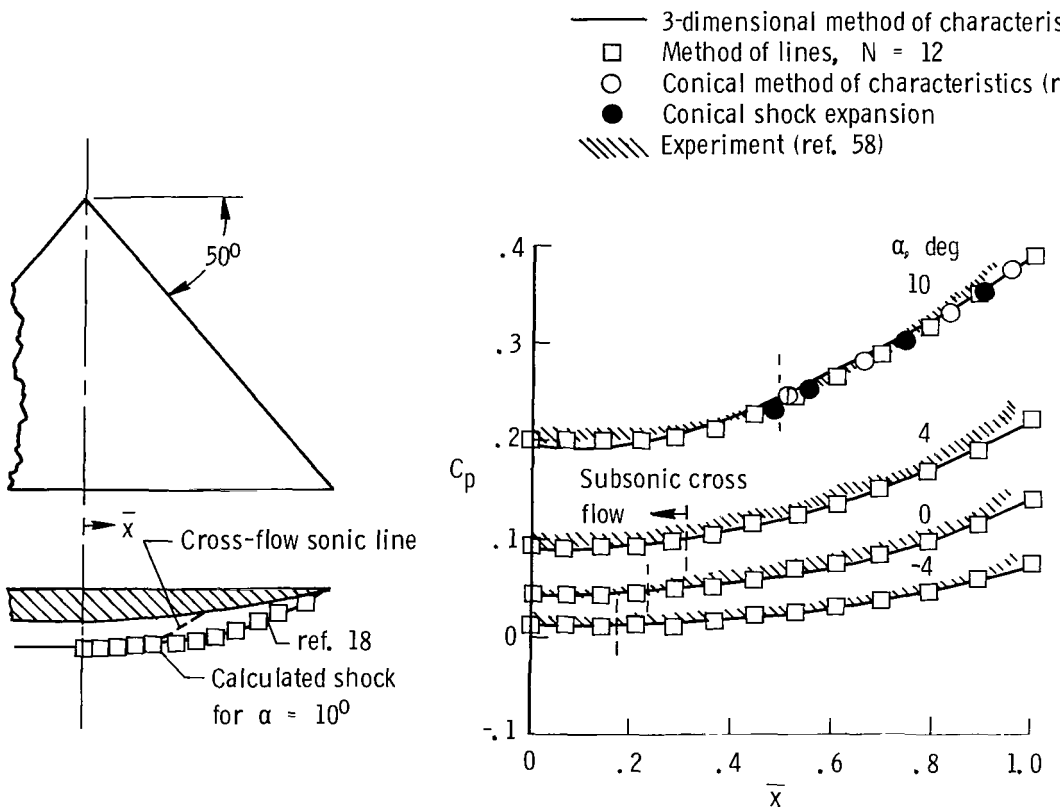

Figure 28.- Comparison of computations and experiment for shock shape and spanwise pressure distribution for conical delta wing. Circular-arc cross section; $M_\infty = 8.1$; $\theta_o = 6.54^\circ$; $\Lambda = 50^\circ$; $N = 12$.

Hatched bands are used to represent the measurements of reference 58 for several different Reynolds numbers and stations downstream from the wing apex. The measured pressures are higher than the inviscid predictions everywhere on the surface; however, the agreement is generally good except near the leading edge. The higher pressures are caused by the hypersonic boundary-layer displacement effect which is most pronounced near the leading edge ($\bar{x} = 1$). Computations by a three-dimensional method of characteristics described in reference 18, conical method of characteristics, and conical shock expansion are shown for $\alpha = 10^{\circ}$. The agreement is generally good in the supersonic cross-flow region; in the region of subsonic cross flow, three-dimensional method of characteristic calculations are generally lower than those computed by the method of lines. At the smaller angles of attack, the three-dimensional method of characteristics and method of lines computations are in excellent agreement and lie at the lower limit of the experimental data.

The cross-flow streamline pattern for the circular-arc delta wing is shown in figure 29. The streamlines show very little curvature; however, the computations were

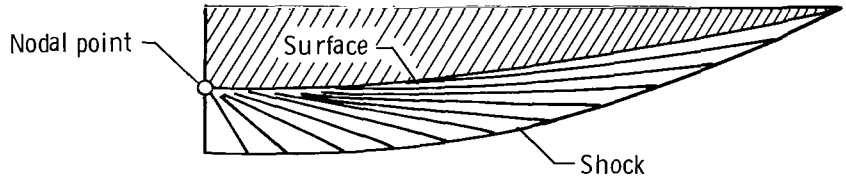

Figure 29.- Cross-flow streamline pattern for conical delta wing. Circular-arc cross section; $M_{\infty} = 8.1$; $\theta_o = 6.54^{\circ}$; $\Lambda = 50^{\circ}$; $\alpha = 10^{\circ}$; $N = 12$.

made by linear interpolation and consequently the finer detail may be lost, particularly in the region of the nodal point. The nodal point (shown with an open symbol) lies in the plane of symmetry and the surface entropy is equal to that at the wing leading edge.

Spanwise pressure distributions for the circular-arc delta wing for $M_{\infty} = 5.08$ are shown in figure 30. Both the three-dimensional method of characteristic calculations and those by the method of lines ($N = 10$) are in good agreement with the experimental results of reference 58 over most of the wing and the agreement near the leading edge is better than that shown in figure 28 since the viscous interaction effects are not as severe at the lower Mach number. The shock shapes for $\alpha = 4.5^{\circ}$ and $\alpha = -5^{\circ}$ are also shown in figure 30. The three-dimensional method of characteristic computations are in good agreement with those by the method of lines with some minor differences near the plane of symmetry.

Flat delta wing.- The classical problem of the flat-plate delta wing has several interesting features. There are three distinct regions to the flow field which exhibit different flow characteristics. The region bounded by the wing surface, the cross-flow

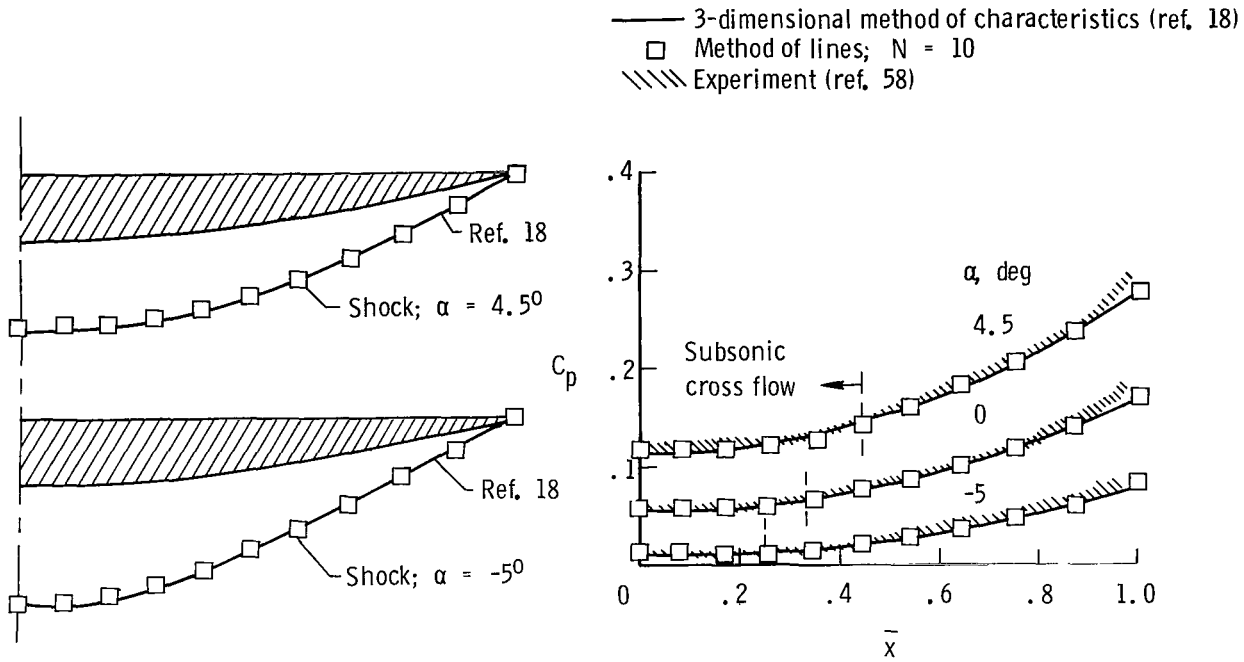

Figure 30.- Comparison of computations and experiment for shock shape and spanwise pressure distribution for conical delta wing. Circular-arc cross section; $M_\infty = 5.08$; $\theta_o = 6.54^\circ$; $\Lambda = 50^\circ$; N = 12.

sonic line, and shock is one in which all the flow quantities p, ρ, V, and S are constant since the shock wave is planar from the leading edge to the cross-flow sonic line. The isentrope extending from the intersection of the cross-flow sonic line with the shock is a boundary of the second region. The region bounded by this dividing streamline, the cross-flow sonic line, and the wing surface is one of varying flow properties but is isentropic. The third region bounded by the dividing streamline, the shock, and the plane of symmetry is one of variable entropy. The exact inviscid pressure distribution should exhibit a "corner" of discontinuous slope at the cross-flow sonic point. These weak singularities are not treated in any special way in the present method and the same is assumed to be true of reference 17.

The computations for the flat-plate conical delta wing shown in figure 31 are for $\Lambda = 50^\circ$ and $M_\infty = 4$. The method of lines computations and those of Voskresenskii produce nearly identical results. The open circles are used to show the actual location of the computational lines in the present method for N = 12; the results are surprisingly smooth around the sonic line. Although the assumed starting shock shape (eq. (7)) is analytic, the final converged shock points lie very close to a straight line between the leading edge and the cross-flow sonic line as they should. A comparison is made in reference 20 of the pressure distribution and the shock shape for this wing computed by the method of Kutler and Lomax and with the method of lines; the agreement is excellent.

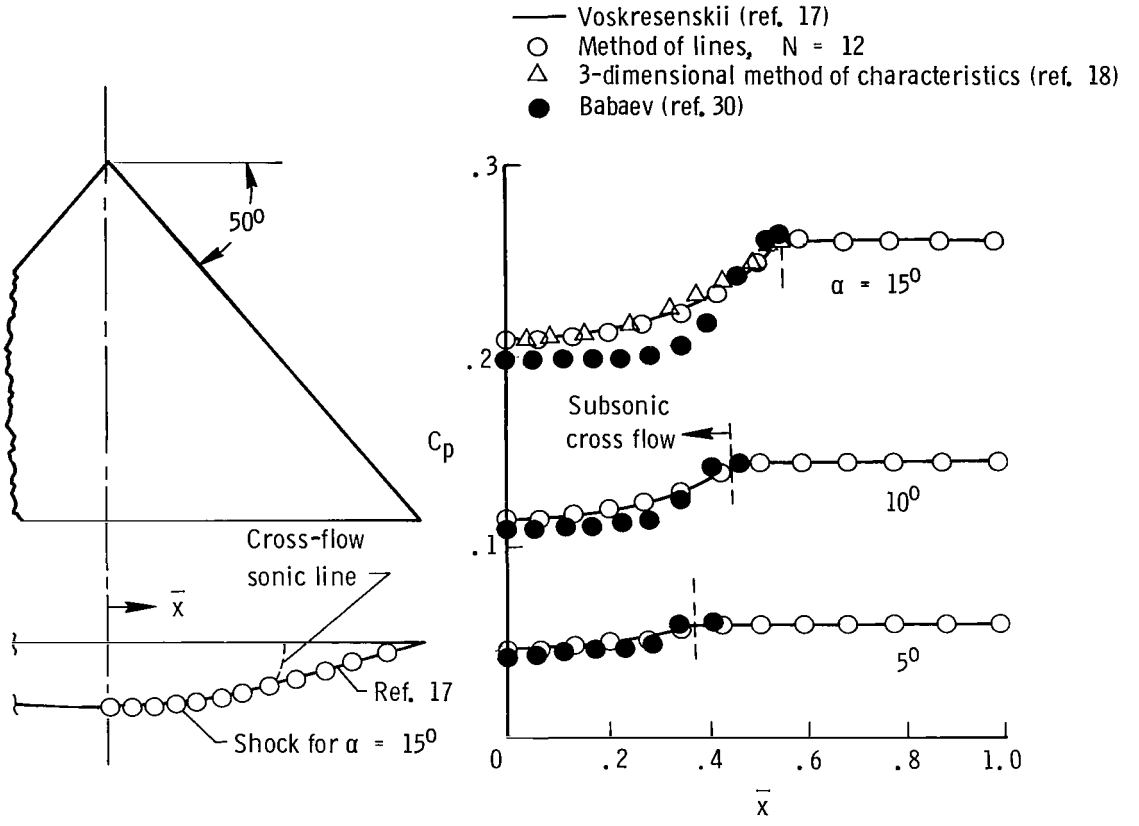

Figure 31.- Comparison of computations for shock shape and spanwise pressure distribution for conical delta wing. Flat-plate cross section; $M_\infty = 4$; $\theta_o = 0^\circ$; $\Lambda = 50^\circ$; N = 12.

In the methods of references 18 and 30, the flow properties are set constant in the supersonic cross flow and in reference 30, an effort was made to account for the weak singularities. Even so, the latter results (solid circles) are in considerable disagreement with the other methods, particularly at the larger values of α. It is also noteworthy that although Babaev (ref. 30) attempted to account for the singularities, his results for the surface pressure distribution appear to be very smooth at the sonic point, without a corner. Results by the method of reference 18 (three-dimensional method of characteristics) are shown in the C_p plot for $\alpha = 15^\circ$, and they are in general agreement with the present results and those of reference 17; apparently, the results of reference 30 are erroneous.

The cross-flow streamline pattern for the flat-plate delta wing at an angle of attack of 15° is shown in figure 32. The cross-flow streamline emanating from the intersection of the sonic line and the shock is the dividing streamline which separates the outboard constant entropy region from that of variable entropy. No attempt was made to trace the cross-flow streamlines in the constant-entropy region.

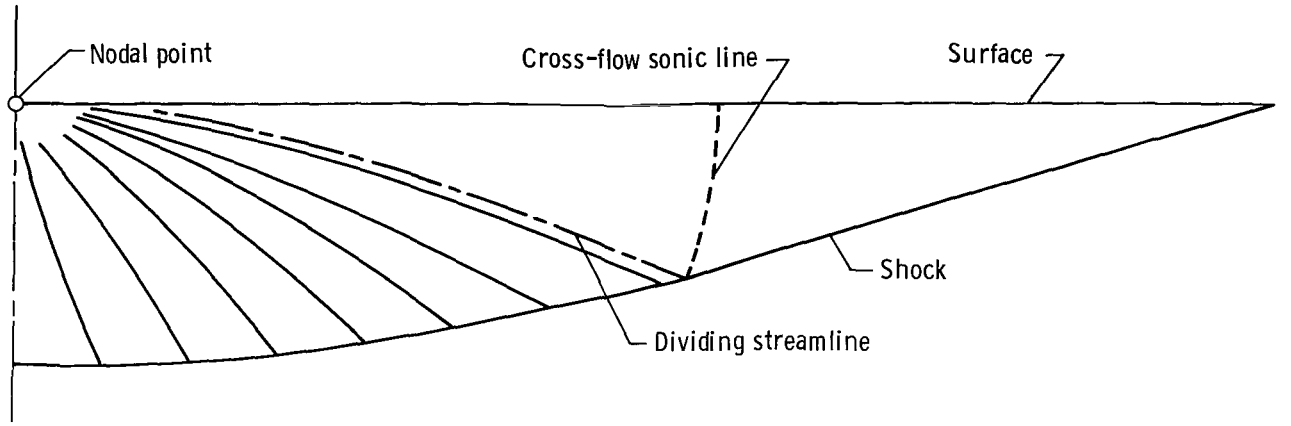

Figure 32.- Cross-flow streamline pattern for conical delta wing. Flat-plate cross section; $M_\infty = 8.1$; $\theta_o = 0^\circ$; $\alpha = 15^\circ$; $\Lambda = 50^\circ$; $N = 12$.

The method of lines computations for a flat conical delta wing are compared with experimental values of reference 58 for $M_\infty = 5.08$, $\Lambda = 50^\circ$, and $\alpha = 14^\circ$ in figure 33. The experimental values (shown hatched) are measurements from several streamwise stations. The method of lines computations generally fall at the lower limit of the experimental data.

The flow over a flat delta wing, $M_\infty = 4$, $\Lambda = 50^\circ$, has been computed for large angles of attack approaching the condition of shock detachment from the wing leading edge. Both the shock and surface pressures are shown in figure 34 for $\alpha = 15^\circ$, 20°, and 22.4°. The subsonic cross-flow region increases in extent as the angle of incidence increases and just before the shock detachment condition, the cross flow is everywhere subsonic. The shock detachment condition was attained for α slightly greater than

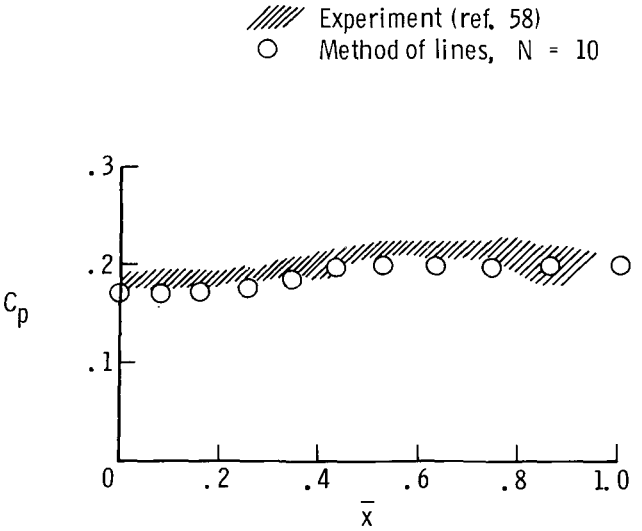

Figure 33.- Comparison with experiment for spanwise pressure distribution for conical delta wing. Flat-plate cross section; $M_\infty = 5.08$; $\theta_o = 0^\circ$; $\Lambda = 50^\circ$; $\alpha = 14^\circ$; $N = 10$.

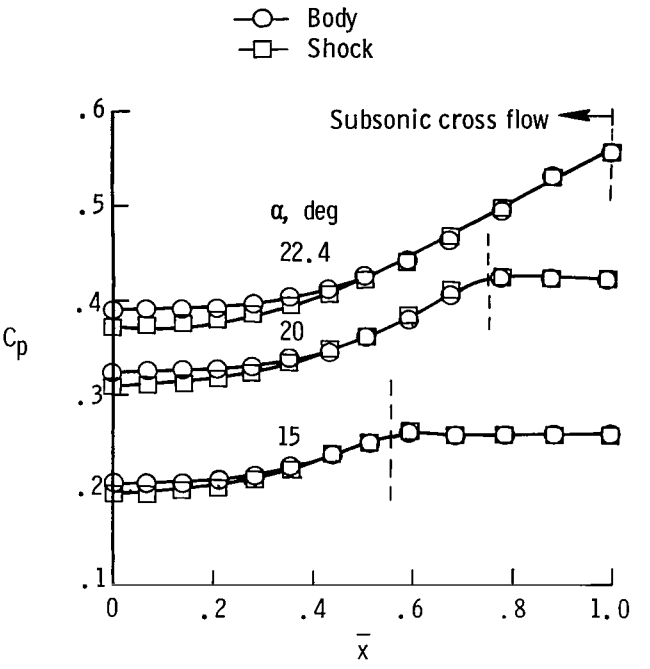

Figure 34.- Calculated spanwise pressure distribution on flat delta wing for conditions approaching leading-edge shock detachment. $M_\infty = 4^\circ$; $\theta_o = 0^\circ$; $\Lambda = 50^\circ$; $N = 12$.

22.4°. It may be seen that even when the cross flow is all subsonic, there is little variation of the pressure between the shock and wing surface at a given spanwise station.

Wing with reverse curvature.- Measurements of surface pressures are presented in reference 58 for a delta wing with a bell-shaped cross section that has a change in sign of the curvature. The cross-section shape is given by

$$y_o = -\tan\theta_o\left(1 - \Omega^2\right)^3$$

$$\Omega = \frac{x_o}{b}\tan\theta$$

where b determines the spanwise location at which y_o and its first two derivatives vanish. The results presented here are for the configuration designated $(B\text{-}W)_1$ in reference 58 with $b = 1$; thus, the slope goes to zero at the wing leading edge. The shock shape and pressure distributions are shown in figure 35. The conditions are $M_\infty = 8.1$, $\Lambda = 50^\circ$, $\alpha = 4^\circ$, with $\theta_o = 4.8^\circ$ and $\theta_o = 12.5^\circ$. The computations for $\theta_o = 4.8^\circ$ with $N = 12$ show a smooth shock shape and pressure distribution. The computations for $\theta_o = 12.5^\circ$ with $N = 9$ show some "roughness" in both the shock shape and the pressure distribution. The computed values of the shock coordinates for $\theta_o = 12.5^\circ$ are connected with straight lines to show more clearly the "roughness." The computed pressures follow

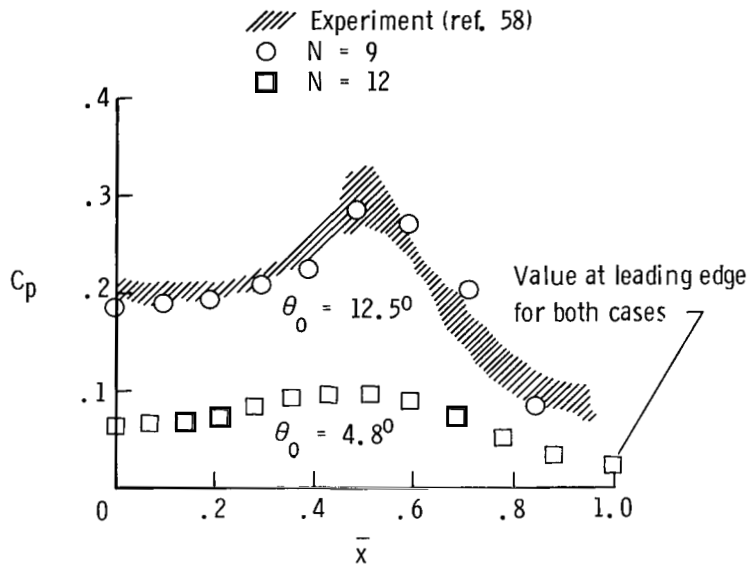

(a) Comparison of computations and experiment for spanwise pressure distribution.

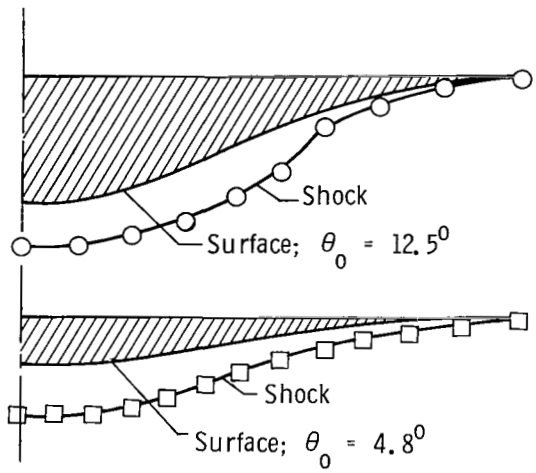

(b) Computed shock shape.

Figure 35.- Effect of increasing thickness on flow over a conical delta wing with reverse cross-section curvature. $M_\infty = 8.1$; $\Lambda = 50°$; $\alpha = 4°$.

the general distribution of the experimental data which is shown hatched. Noteworthy is the very abrupt thickening of the shock layer in the region where large pressure gradients occur. Mead and Koch (ref. 58) suggested that a shock occurs in the cross flow. This possibility seems likely, in which case the method of lines is unsuitable for computing this flow. Attempts to compute the $\theta_0 = 12.5°$ case for $N > 9$ failed since the computations showed increased roughness and convergence was not attained. The body-oriented coordinate system used here is not well adapted to configurations with reversed

curvature because the lines tend to converge as the shock is approached, with a resultant increase in computational difficulties. The question of an internal shock could probably be settled by tracing the characteristics in a cross-flow MOC computation. Kutler's method (refs. 19 and 20) would likewise be suitable for study of this case.

Convergence history.- Figure 36 illustrates the convergence history for the flat-plate delta wing at $\alpha = 15^{o}$ shown in figure 31. The surface pressure distribution

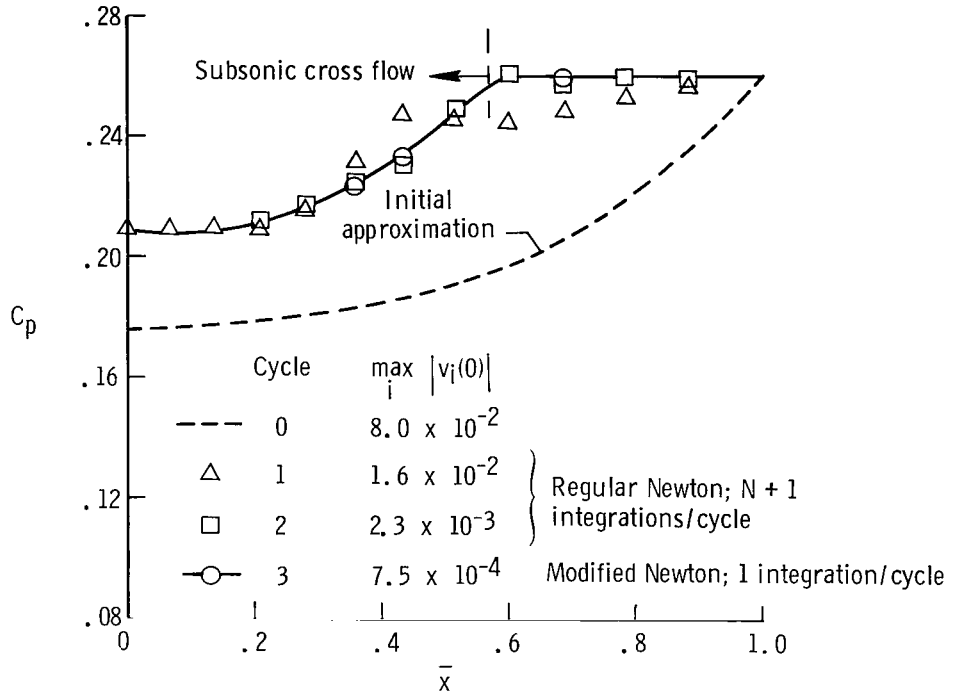

Figure 36.- Surface pressure convergence history for flat delta wing. $M_\infty = 4^{o}$; $\theta_o = 0^{o}$; $\Lambda = 50^{o}$; $\alpha = 15^{o}$; N = 12.

obtained with each new pivotal shock shape, including the initial approximation given by equation (7), is shown. The key of the figure gives the maximum normal velocity magnitude, at the end of each cycle and a designation indicating whether the cycle was a regular or modified Newton cycle.

Convergence with increasing N.- Figure 37 provides an illustration of the accuracy that can be achieved with small values of N. A comparison of the surface pressures and the cylindrical cross-flow velocity component w_c with N = 2, 4, and 8 is made with the computations of Voskresenskii for the flat delta wing at $\alpha = 15^{o}$. The pressure is a quantity that requires no correction after extrapolation to the surface whereas the velocity w_c is a surface-corrected quantity. With only one line placed between the leading edge and the wing center line (N = 2), the accuracy is surprisingly good. More lines are used, however, to give better resolution.

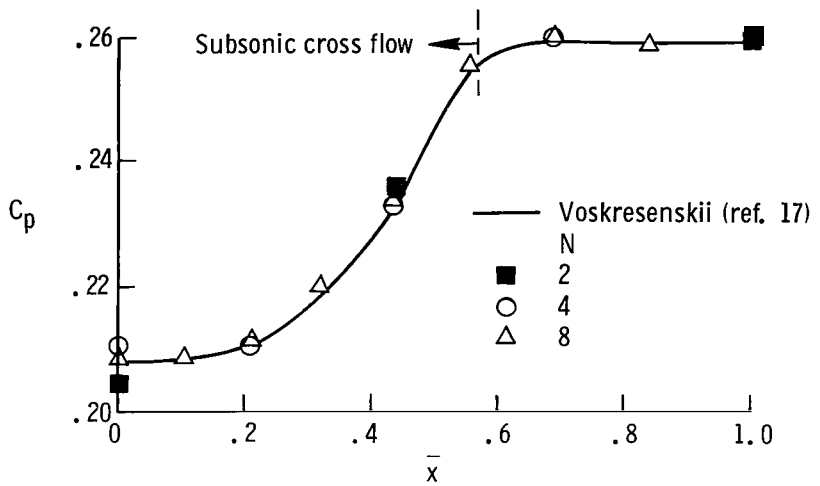

(a) Comparison of computations for spanwise pressure distribution.

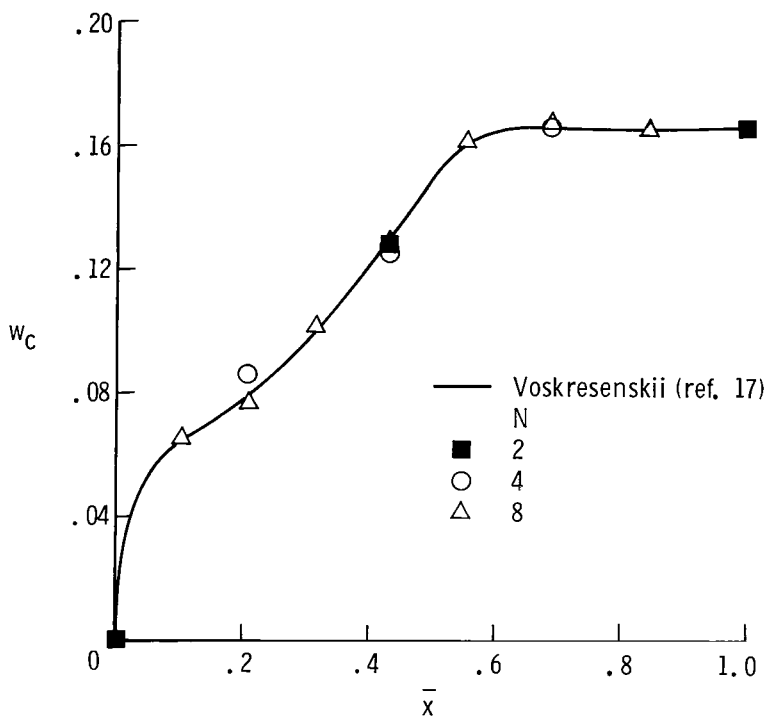

(b) Comparison of computations for spanwise distribution of cylindrical velocity component w_c.

Figure 37.- Convergence with increasing N for flat delta wing. $M_\infty = 4$; $\theta_o = 0^\circ$; $\Lambda = 50^\circ$; $\alpha = 15^\circ$.

Variable Line Spacing

The computations presented herein were made for an equal line spacing in the arc length coordinate τ; that is, the computational coordinate ξ was equal to τ. It would appear desirable to stretch the computational coordinate ξ compared with the arc length τ to bunch the lines in the region where the gradients are large and the coordinate transformation $\xi = \xi(\tau)$ was included in the program for this purpose. When the geometry and computational lines are projected onto a plane $Z = \text{Constant}$ to appear like a cylindrical coordinate system, the line spacing is nonuniform in the polar angle ϕ. The smallest values of $\Delta\phi$ on an elliptic cone do, in fact, occur in the region of maximum surface curvature and flow gradients, at the extremes of the major axis. The previously described instabilities that arise with very small line spacing impose a limit on the amount of local "bunching" of the lines which can be utilized. Since about 13 to 17 lines are required, in general, for elliptic cones, further bunching of the lines in the large curvature region can push the calculation beyond the stability limitation on $\Delta\tau$. Within this limitation some calculations have been made for elliptic cones in which the ξ coordinate was stretched in the region of the major axis; however, the results were inconclusive regarding the merit of using such a nonuniform line spacing in the present "natural" coordinates.

CONCLUDING REMARKS

The method of lines has proved to be a useful and versatile procedure for constructing the numerical solution to conical flow problems. It has the merit of a relatively simple mathematical formulation and can be adapted to compute the flow about a variety of conical bodies. The method has been applied to circular and elliptic cones at incidence and to the compression side of several conical delta wings with an attached leading-edge shock. Numerous comparisons have been made with experiment which serve to validate the method.

Several other approaches for calculating conical flows have been compared with the method of lines and were found to be in agreement. Two of these approaches are three-dimensional computations that attain the conical solution asymptotically, whereas two others are strictly two-dimensional conical methods. The conical flow problems provide excellent check cases for the more general three-dimensional computational methods because a conical flow is three dimensional but can be solved by two-dimensional methods.

Computations have been made for a circular cone to compare with experimentally determined values of both the shock shape and the surface pressures. The computed values are in good agreement with the measured results over the windward side but agreement is less satisfactory on the leeward side where a viscous buildup occurs to

raise the level of the measured pressures. The region dominated by the viscous buildup increases in extent with increasing incidence and the computed results for the leeward side show poorer agreement with experiment at the larger angles of attack. Comparison of computed and measured pressures for an elliptic cone of axis ratio $a/b = 2$ similarly show good agreement over the windward side.

Whenever a supersonic cross flow occurs around circular or elliptic cones, convergence of the normal components of velocity at the body surface to a zero value is more difficult at lines in that region. Convergence is possible, however, if the supersonic cross-flow region is not extensive. Low pressures, supersonic cross flow, and large cross-flow gradients are factors which limit the range of parameters for which computations can be made. These factors tend to limit the angle of attack to values such that the leeward side is not appreciably in wind shadow, the stream Mach number generally greater than 2 but dependent upon cone angle, and the axis ratio a/b for the elliptic cone generally less than approximately 3. These limits are very approximate and depend too on the convergence criteria one is willing to accept.

Cross-flow streamline patterns for the elliptic cone both at incidence and yaw are presented to illustrate the change in the flow as the incidence or yaw is altered. The method of lines has been used to provide resolution of the thin entropy layer in the neighborhood of the conical body and a study was also made in an attempt to provide verification for the lift-off of the nodal singularity. Computations were made up to the incipient lift-off condition but could not be carried to larger angles of attack because computational difficulties are encountered as the incipient lift-off condition is approached.

Comparisons have been made with experiment and other computations for the compression side of conical delta wings with attached leading-edge shocks. Computations for wings with parabolic, circular arc, and flat-plate cross sections are in good agreement with other calculations and with experiment except in the region of the leading edge where the viscous interaction effects are most important. Over the rest of the wing the calculated pressures fall at the lower limit of the experimental data. Large regions of supersonic cross flow occur on the conical wings but contrary to the case of circular and elliptic cones, this condition provides no limitation and the method is applicable with no difficulties. Some cross-flow streamline computations are presented to illustrate the flow pattern on the windward side of conical wings.

Langley Research Center,
National Aeronautics and Space Administration,
Hampton, Va., August 6, 1971.

APPENDIX A

GEOMETRICAL RELATIONS

In order to make use of the body-oriented conical coordinate system η,τ, it is necessary to relate the arc length τ (on the intersection of the unit sphere with the conical body) to the rectangular body coordinates x_o,y_o. Moreover, the direction cosines between the body-oriented coordinates and the Cartesian coordinates X, Y, and Z are required to relate the velocity components and the coordinates in the two systems. These relations have previously been given in reference 43 but are presented here in the notation of this paper for the sake of completeness.

Arc Length

The element of length ds in the η,τ,r coordinates and the Cartesian coordinates is given by

$$(ds)^2 = r^2\left[(d\eta)^2 + (hd\tau)^2\right] + (dr)^2 = (dX)^2 + (dY)^2 + (dZ)^2$$

where rh is the scale factor of the τ coordinate. On the conical body the rectangular coordinates x_o,y_o are related to the Cartesian coordinates by

$$\left.\begin{aligned} x_o &= (X/Z)_o \\ y_o &= (Y/Z)_o \end{aligned}\right\} \tag{A1}$$

where the subscript o denotes values on the conical body. In the body-oriented coordinates, $\eta = 0$ on the body and $h = 1$ at $\eta = 0$ since τ is the arc length on the conical body at $r = 1$. Thus, from the expression for the element of length

$$d\tau = \pm\left[1 + \left(\frac{dY}{dX}\right)_o^2 + \left(\frac{dZ}{dX}\right)_o^2\right]^{1/2} dX_o \tag{A2}$$

In order to integrate equation (A2), it is necessary to find relations between $\left(\frac{dY}{dX}\right)_o$, $\left(\frac{dZ}{dX}\right)_o$, dX_o and the differentials dx_o and dy_o in terms of the geometric parameters which describe the conical body. Differentiation of equations (A1) gives

$$\left.\begin{aligned} dx_o &= Z_o^{-1}\left[1 - x_o\left(\frac{dZ}{dX}\right)_o\right]dX_o \\ dy_o &= Z_o^{-1}\left[\left(\frac{dY}{dZ}\right)_o - y_o\left(\frac{dZ}{dX}\right)_o\right]dX_o \end{aligned}\right\} \tag{A3}$$

The intersection of the spherical surface $r = 1$ with the body, in Cartesian coordinates, is

$$X_o^2 + Y_o^2 + Z_o^2 - 1 = 0 \tag{A4a}$$

or

$$Z_o = A_1^{-1/2} \tag{A4b}$$

where $A_1 = 1 + x_o^2 + y_o^2$. Differentiation of equation (A4) gives

$$x_o + y_o\left(\frac{dY}{dX}\right)_o + \left(\frac{dZ}{dX}\right)_o = 0 \tag{A5}$$

Differentiation of the equation defining the conical body, $G(x_o,y_o) = 0$, together with equations (A3) gives

$$G_x + G_y\left(\frac{dY}{dX}\right)_o - \left(x_o G_x + y_o G_y\right)\left(\frac{dZ}{dX}\right)_o = 0 \tag{A6}$$

where the subscripts on G denote derivatives with respect to the indicated argument. Substitution from equations (A3), (A4), (A5), and (A6) into equation (A2) gives

$$d\tau = -A_1^{-1}A_2^{1/2}G_y^{-1}\,dx_o = A_1^{-1}A_2^{1/2}G_x^{-1}\,dy_o \tag{A7a}$$

$$d\xi = \xi_\tau\,d\tau \tag{A7b}$$

where

$$A_2 = G_x^2 + G_y^2 + \left(x_o G_x + y_o G_y\right)^2$$

Integration of equations (A7) provides the relation between the body rectangular coordinates x_o,y_o, the arc length τ, and the transformed coordinate ξ. The integration is

first carried out to determine $\tau(N)$ and $\xi(N)$. The line spacing is then specified in terms of ξ and subsequent integration of equations (A7) establishes the values of x_o and y_o at each line.

Direction Cosines

The unit vector along a ray of the body is

$$\bar{e}_{r,o} = A_1^{-1/2}\left(\bar{i}x_o + \bar{j}y_o + \bar{k}\right)$$

and the unit normal to the body $\bar{e}_{\eta,o}$ is

$$\bar{e}_{\eta,o} = \frac{\nabla G}{|\nabla G|} = A_2^{-1/2}\left[\bar{i}G_x + \bar{j}G_y - \bar{k}\left(x_o G_x + y_o G_y\right)\right]$$

where

$$\nabla = \bar{i}\,\frac{\partial}{\partial X_o} + \bar{j}\,\frac{\partial}{\partial Y_o} + \bar{k}\,\frac{\partial}{\partial Z_o}$$

Then the unit vector $\bar{e}_\tau$ normal to the plane τ = Constant is

$$\bar{e}_\tau = \bar{e}_{r,o} \times \bar{e}_{\eta,o}$$

The unit vectors $\bar{e}_r$ and $\bar{e}_\eta$ are found by a rotation of $\bar{e}_{r,o}$ and $\bar{e}_{\eta,o}$ through the angle η in the plane τ = Constant. Then the set of unit vectors $\bar{e}_\eta$, $\bar{e}_\tau$, and $\bar{e}_r$ is related to the Cartesian unit vectors by

$$\begin{bmatrix} \bar{e}_\eta \\ \bar{e}_\tau \\ \bar{e}_r \end{bmatrix} = \begin{bmatrix} a_{11} & a_{12} & a_{13} \\ a_{21} & a_{22} & a_{23} \\ a_{31} & a_{32} & a_{33} \end{bmatrix} \begin{bmatrix} \bar{i} \\ \bar{j} \\ \bar{k} \end{bmatrix}$$

where

$$A_3 = x_o G_x + y_o G_y$$

$$a_{11} = -x_o A_1^{-1/2} \sin \eta + A_2^{-1/2} G_x \cos \eta$$

$$a_{12} = -y_o A_1^{-1/2} \sin \eta + A_2^{-1/2} G_y \cos \eta$$

$$a_{13} = -A_1^{-1/2} \sin \eta - A_2^{-1/2} A_3 \cos \eta$$

$$a_{21} = -\left(A_1 A_2\right)^{-1/2} \left(G_y + y_o A_3\right)$$

$$a_{22} = \left(A_1 A_2\right)^{-1/2} \left(G_x + x_o A_3\right)$$

$$a_{23} = \left(A_1 A_2\right)^{-1/2} \left(x_o G_y - y_o G_x\right)$$

$$a_{31} = x_o A_1^{-1/2} \cos \eta + A_2^{-1/2} G_x \sin \eta$$

$$a_{32} = y_o A_1^{-1/2} \cos \eta + A_2^{-1/2} G_y \sin \eta$$

$$a_{33} = A_1^{-1/2} \cos \eta - A_2^{-1/2} A_3 \sin \eta$$

APPENDIX B

FLOW PROPERTIES BEHIND SHOCK WAVE

Once the shock wave shape is prescribed the flow properties behind the shock can be evaluated from the shock jump conditions. In the case of a wing with an attached leading-edge shock, the flow is completely determined at the leading edge from these relations since the shock shape is known from the geometry there and from the stream conditions.

Shock Conditions

A set of unit vectors is constructed normal and tangential to the shock to obtain relations for the pressure, density, and velocity components behind the shock. Let $\bar{n}_1$ be the unit vector along a ray at the shock surface, $\bar{n}_2$ be the outward unit normal to the shock, $\bar{n}_3 = \bar{n}_1 \times \bar{n}_2$, and σ be the angle between the shock normal and the unit

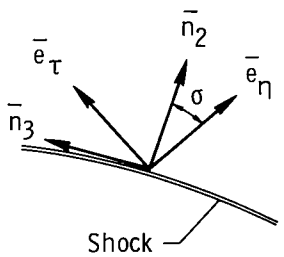

Figure 38.- Geometric relations between unit vectors at shock in a plane normal to a conical ray.

vector $\bar{e}_\eta$ (fig. 38). The angle σ is given by

$$\tan \sigma = -\frac{1}{h}\frac{d\eta_s}{d\tau}$$

$$= -\frac{\xi_\tau}{h}\frac{d\eta_s}{d\xi}$$

where the scale factor h is evaluated at $\eta = \eta_s$. This set of unit vectors is related to the set $\bar{e}_\tau, \bar{e}_\eta, \bar{e}_r$ by

$$\bar{n}_1 = \bar{e}_r$$

$$\bar{n}_2 = \bar{e}_\eta \cos \sigma + \bar{e}_\tau \sin \sigma$$

$$\bar{n}_3 = -\bar{e}_\eta \sin \sigma + \bar{e}_\tau \cos \sigma$$

The stream velocity vector $\bar{V}_\infty$ is taken of unit magnitude here for convenience. This vector, expressed in terms of the three sets of unit vectors, is

$$\bar{V}_\infty = \bar{j} \sin \alpha + \bar{k} \cos \alpha$$

$$= V_r \bar{e}_r + V_\eta \bar{e}_\eta + V_\tau \bar{e}_\tau$$

$$= V_1 \bar{\eta}_1 + V_2 \bar{\eta}_2 + V_3 \bar{\eta}_3$$

where

$$V_r = a_{32} \sin \alpha + a_{33} \cos \alpha$$

$$V_\eta = a_{12} \sin \alpha + a_{13} \cos \alpha$$

$$V_\tau = a_{22} \sin \alpha + a_{23} \cos \alpha$$

$$V_1 = V_r$$

$$V_2 = V_\eta \cos \sigma + V_\tau \sin \sigma$$

$$V_3 = V_\eta \sin \sigma + V_\tau \cos \sigma$$

and α is the angle of incidence. The direction cosines a_{ij} between the vectors $\bar{e}_\eta, \bar{e}_\tau, \bar{e}_r$ and $\bar{i}, \bar{j}, \bar{k}$ are given in appendix A. The stream velocity components V_1 and V_3 are tangential to the shock and V_2 is normal to the shock. The shock angle β then is given by

$$\sin \beta = -\bar{n}_2 \cdot \bar{V}_\infty = -V_2$$

and the pressure and density for an ideal gas are given by (ref. 59)

$$p = \frac{1}{\gamma(\gamma + 1) M_\infty{}^2 c^{*2}} \left[2\gamma M_\infty{}^2 \sin^2 \beta - (\gamma - 1) \right]$$

$$\rho = \frac{(\gamma + 1) M_\infty{}^2 \sin^2 \beta}{2 + (\gamma - 1) M_\infty{}^2 \sin^2 \beta}$$

From the Rankine-Hugoniot relations, the required velocity components behind the shock, referenced to the critical speed, are

$$u = \frac{V_1}{c^*}$$

$$v = \frac{1}{c^*}\left(\rho^{-1}V_2 \cos\sigma - V_3 \sin\sigma\right)$$

$$w = \frac{1}{c^*}\left(\rho^{-1}V_2 \sin\sigma + V_3 \cos\sigma\right)$$

Attached Shock at Wing Leading Edge

For the computation of the flow about wings with an attached leading-edge shock, the angle σ at the leading edge can be computed from the stream conditions and the wing geometry. Once σ is evaluated, all the flow quantities at the leading edge are computed directly from the foregoing shock relations. The wing leading edge lies in the X,Z-plane and makes an angle θ with the Z-axis $\left(\text{the sweep angle } \Lambda = \frac{\pi}{2} - \theta\right)$. To determine σ, it is only necessary to consider the flow quantities in a plane normal to the wing leading edge as shown in figure 39. The subscript n identifies values in this plane.

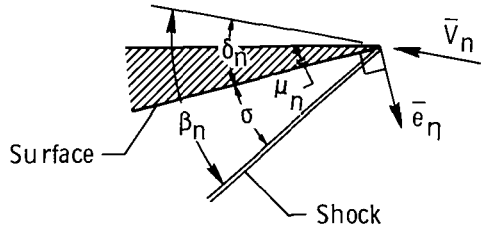

Figure 39.- Geometric relations at wing leading edge in a plane normal to edge.

The component of the stream velocity vector $\left(\bar{V}_\infty \text{ is of unit magnitude}\right)$ in the plane normal to the wing leading edge, $\bar{V}_n$, and its magnitude, V_n, are

$$\bar{V}_n = -\bar{i} \sin\theta \cos\theta \cos\alpha + \bar{j} \sin\alpha + \bar{k} \sin^2\theta \cos\alpha$$

$$V_n = \left(\sin^2\theta \cos^2\alpha + \sin^2\alpha\right)^{1/2}$$

The free-stream Mach number in this plane is $M_n = M_\infty V_n$.

Let μ be the opening angle of the wing leading edge (measured from the X-axis) in a plane Z = Constant. Then μ is computed from the geometry at the leading edge

by

$$\tan \mu = \frac{dy_o}{dx_o}$$

and the angle μ_n is found from

$$\tan \mu_n = \frac{\tan \mu}{\cos \theta}$$

From the wing geometry, the vector $\bar{e}_\eta$ is

$$\bar{e}_\eta = \bar{i} \sin \mu_n \cos \theta - \bar{j} \cos \mu_n - \bar{k} \sin \mu_n \sin \theta$$

and δ_n is given by

$$\sin \delta_n = -\frac{\bar{V}_n \bar{e}_\eta}{V_n} = V_n^{-1}\left(\sin \theta \cos \alpha \sin \mu_n + \sin \alpha \cos \mu_n\right)$$

The shock angle β_n is found from the equation relating the flow deflection δ_n and β_n (ref. 59)

$$\cot \delta_n = \tan \beta_n \left[\frac{(\gamma + 1)M_n^2}{2\left(M_n^2 \sin^2 \beta_n - 1\right)} - 1\right]$$

and $\sigma = \beta_n - \delta_n$. The flow quantities at the wing leading edge are computed from the shock relations with this value of σ and M_∞ replaced by M_n.

APPENDIX C

FORCE AND MOMENT COEFFICIENTS

Once the surface values of the pressure have been evaluated, the force and moment coefficients can be computed by numerical integration. The unit vector normal to the surface $\bar{e}_{\eta,o}$ (appendix A) is

$$\bar{e}_{\eta,o} = A_2^{-1/2}\left[\bar{i}G_x + \bar{j}G_y - \bar{k}\left(x_o G_x + y_o G_y\right)\right]$$

and the element of area on the conical surface is $r\, d\tau\, dr$. The normal force $\bar{F}_n$ on this elemental area is

$$\frac{d\bar{F}_n}{\rho_\infty V_\infty{}^2} = -\bar{e}_{\eta,o}\, c^{*2}\left(p - p_\infty\right) r\, d\tau\, dr$$

$$= -\bar{e}_{\eta,o}\, c^{*2}\left(p - p_\infty\right)\xi_\tau^{-1}\, r\, d\xi\, dr$$

where $p_\infty = \dfrac{1}{\gamma M_\infty{}^2 c^{*2}}$. Then the components of the force along the Y and Z directions are

$$\frac{dF_Y}{\rho_\infty V_\infty{}^2} = -c^{*2}\left(p - p_\infty\right) A_2^{-1/2} G_y \xi_\tau^{-1} r\, d\xi\, dr \tag{C1}$$

$$\frac{dF_Z}{\rho_\infty V_\infty{}^2} = c^{*2}\left(p - p_\infty\right) A_2^{-1/2}\left(x_o G_x + y_o G_y\right)\xi_\tau^{-1} r\, d\xi\, dr \tag{C2}$$

The integration is carried out over the conical body to the surface $Z_o = 1$. Now $r = z_o A_1{}^{1/2}$; thus, at $Z_o = 1$, $r = A_1{}^{1/2}$. The force coefficients then, after integration on r, are

$$C_Y = \frac{2c^{*2}}{A}\int_0^{\xi_u}\left(p - p_\infty\right) A_1 A_2^{-1/2} G_y \xi_\tau^{-1} d\xi$$

$$C_Z = \frac{2c^{*2}}{A}\int_0^{\xi_u}(p - p_\infty)A_1 A_2^{-1/2}(x_o G_x + y_o G_y)\xi_\tau^{-1}d\xi$$

where the upper limit $\xi_u = \xi_N$ for elliptic cones and $\xi_u = \xi_{N+1}$ for wing configurations and A is the reference area. The drag and lift coefficients are determined from

$$C_D = C_Y \sin\alpha + C_Z \cos\alpha$$

$$C_L = C_Y \cos\alpha - C_Z \sin\alpha$$

Expressions for the differential moments, or the center-of-pressure location measured from the apex, are found by multiplying equation (C1) by Z_o and equation (C2) by Y_o. Thus, with

$$Z_o = rA_1^{1/2}$$

$$Y_o = y_o Z_o$$

the coordinates of the center of pressure Y_{cp} and Z_{cp}, after integration on r, are

$$Y_{cp} = \frac{4c^{*2}}{3AC_Z}\int_0^{\xi_u}(p - p_\infty)A_1 A_2^{-1/2} y_o(x_o G_x + y_o G_y)\xi_\tau^{-1}d\xi$$

$$Z_{cp} = -\frac{4c^{*2}}{3AC_Y}\int_0^{\xi_u}(p - p_\infty)A_1 A_2^{-1/2} G_y \xi_\tau^{-1}d\xi = \frac{2}{3}$$

and the moment about the X-axis is

$$C_{m,x} = Y_{cp}C_Z - Z_{cp}C_Y$$

For the elliptic cone the reference area A is taken as the base area

$$A = \pi\left(\frac{b}{a}\right)\tan^2\theta$$

and for the wing the reference area is the plan area

$$A = \tan\theta$$

The integrals for the force coefficients and the coordinates of the center of pressure can be evaluated with the use of Simpson's rule if the number of increments $\Delta\tau$ is even; hence, it is required that the number of lines N is odd for elliptic cones and even for the wings with attached leading-edge shocks.

REFERENCES

1. Busemann, A.: Aerodynamic Lift at Supersonic Speeds. Ae. Techl. 1201, Rep. No. 2844, Brit. A.R.C., Feb. 3, 1937. (From Luftfahrtforschung, Bd. 12, Nr. 6, Oct. 3, 1935, pp. 210-220.

2. Jones, D. J.: Numerical Solutions of the Flow Field for Conical Bodies in a Supersonic Stream. Aeronaut. Rep. LR-507 (NRC No. 10361), Nat. Res. Counc. Can. (Ottawa), July 1968.

3. Ndefo, D. Ejike: A Numerical Method for Calculating Steady Unsymmetrical Supersonic Flow Past Cones. Rep. No. AS-69-11 (AFOSR Grant 268-68), U.S. Air Force, May 1969. (Available from DDC as AD 691 270.)

4. South, Jerry C., Jr.; and Klunker, E. B.: Methods for Calculating Nonlinear Conical Flows. Analytic Methods in Aircraft Aerodynamics, NASA SP-228, 1970, pp. 131-155; Discussion, pp. 156-158.

5. Stone, A. H.: On Supersonic Flow Past a Slightly Yawing Cone. J. Math. Phys., vol. XXVII, No. 1, Apr. 1948, pp. 67-81.

6. Staff of Comput. Section, Center of Anal. (Under dir. of Zdeněk Kopal): Tables of Supersonic Flow Around Yawing Cones. Tech. Rep. No. 3 (NOrd Contract No. 9169), Massachusetts Inst. Technol., 1947.

7. Taylor, G. I.; and Maccoll, J. W.: The Air Pressure on a Cone Moving at High Speeds. Proc. Roy. Soc. (London), ser. A, vol. 139, no. 838, Feb. 1, 1933, pp. 278-311.

8. Ferri, Antonio: Supersonic Flow Around Circular Cones at Angles of Attack. NACA Rep. 1045, 1951. (Supersedes NACA TN 2236.)

9. Melnik, R. E.: Vortical Layers in Supersonic Conical Flow. Hypersonic Boundary Layers and Flow Fields. AGARD CP No. 30, 1968, pp. 26-1 – 26-20.

10. Woods, B. A.: The Supersonic Flow Past an Elliptic Cone. Aeronaut. Quart., vol. XX, pt. 4, Nov. 1969, pp. 382-404.

11. Munsen, A. G.: A Uniformly Valid Solution for the Flow Over an Inclined Cone Using the Method of Matched Asymptotic Expansions. AFOSR 64-1056, U.S. Air Force, Apr. 1964. (Available from DDC as AD 603 154.)

12. Moretti, Gino: Inviscid Flowfield About a Pointed Cone at an Angle of Attack. AIAA J., vol. 5, no. 4, Apr. 1967, pp. 789-791.

13. Babenko, K. I.; Voskresenskii, G. P.; Lyubimov, A. N.; and Rusanov, V. V.: Three-Dimensional Flow of Ideal Gas Past Smooth Bodies. NASA TT F-380, 1966.

14. Rakich, John V.: A Method of Characteristics for Steady Three-Dimensional Supersonic Flow With Application to Inclined Bodies of Revolution. NASA TN D-5341, 1969.

15. Babenko, K. I.; and Rusanov, V. V.: Difference Methods of Solving Three-Dimensional Problems in Gas Dynamics. NASA TT F-10,827, 1967.

16. Gonidou, René: Supersonic Flows Around Cones at Incidence. NASA TT F-11,473, 1968.

17. Voskresenskii, G. P.: Chislennoe Reshenie Zadachi Obtekaniia Proizvol'noi Poverkhnosti Treugul'nogo Kryla v Oblasti Szhatiia Sverkhzvukovym Potokom Gaza (Numerical Solution of the Problem of a Supersonic Gas Flow Past an Arbitrary Surface of a Delta Wing in the Compression Region). Izv. Akad. Nauk SSSR, Mekh. Zhidk. Gaza, no. 4, 1968, pp. 134-142.

18. Powers, S. A.; and Beeman, E. R., Jr.: Flow Fields Over Sharp Edged Delta Wings With Attached Shocks. NASA CR-1738, 1971.

19. Kutler, Paul: Application of Selected Finite Difference Techniques to the Solution of Conical Flow Problems. Ph. D. Diss., Iowa State Univ., 1969.

20. Kutler, Paul; and Lomax, Harvard: A Systematic Development of the Supersonic Flow Fields Over and Behind Wings and Wing-Body Configurations Using a Shock-Capturing Finite-Difference Approach. AIAA Paper No. 71-79, Jan 1971.

21. Busemann, A.: Drücke auf Kegelförmige Spitzen bei Bewegung mit Überschallgeschwindigkeit. Z. Angew. Math. Mech., Bd. 9, Heft 6, Dec. 1929, pp. 496-498.

22. Hayes, Wallace D.; and Probstein, Ronald F.: Hypersonic Flow Theory. Vol. I – Inviscid Flows. Second ed., Academic Press, 1966.

23. Briggs, Benjamin R.: The Numerical Calculation of Flow Past Conical Bodies Supporting Elliptic Conical Shock Waves at Finite Angles of Incidence. NASA TN D-340, 1960.

24. Mauger, F. E.: Steady Supersonic Flow Past Conical Bodies. A.R.D.E. Rep. (B)3/60, Brit. War Office, May 1960.

25. Stocker, P. M.; and Mauger, F. E.: Supersonic Flow Past Cones of General Cross-Section. J. Fluid Mech., vol. 13, pt. 3, July 1962, pp. 383-399.

26. Eastman, E. W.; and Omar, M. E.: Flow Fields About Highly Yawed Cones by the Inverse Method. AIAA J., vol. 3, no. 9, Sept. 1965, pp. 1782-1784.

27. Makhin, N. A.; and Syagayev, V. F.: Numerical Solution of the Problem of Supersonic Flow Past Conical Bodies at an Angle of Attack. Fluid Dyn., vol. 1, no. 1, Jan.-Feb. 1966, pp. 100-101.

28. Maslen, Stephen H.: Supersonic Conical Flow. NACA TN 2651, 1952.

29. Babayev, D. A.: Numerical Solution of the Problem of Flow Round the Upper Surface of a Triangular Wing by a Supersonic Stream. U.S.S.R. Comput. Math. Math. Phys., no. 2, 1963, pp. 296-308.

30. Babaev, D. A.: Numerical Solution of the Problem of Supersonic Flow Past the Lower Surface of a Delta Wing. AIAA J., vol. 1, no. 9, Sept. 1963, pp. 2224-2231.

31. Dorodnitsyn, A. A.: A Contribution to the Solution of Mixed Problems of Transonic Aerodynamics. Vol. 2 of Advances in Aeronautical Sciences, Pergamon Press, Inc., 1959, pp. 832-844.

32. Belotserkovskiy, O. M.: Supersonic Gas Flow Around Blunt Bodies – Theoretical and Experimental Investigations. NASA TT F-453, 1967.

33. South, Jerry C., Jr.: Application of the Method of Integral Relations to Supersonic Nonequilibrium Flow Past Wedges and Cones. NASA TR R-205, 1964.

34. Chushkin, P. I.; and Shchennikov, V. V. (B. A. Woods, transl.): Calculation of Certain Conical Flows Without Axial Symmetry. Lib. Transl. No. 926, Brit. R.A.E., Dec. 1960.

35. Brook, John W.: The Method of Integral Relations for Conical Flow – Theoretical Analysis. Res. Mem. RM-193 (Contract No. AF 33(616)-6400), Grumman Aircraft Eng. Corp., Oct. 1961. (Available from DDC as AD 266 501.)

36. Liskovets, O. A.: The Method of Lines (Review). Differential Equations, vol. 1, no. 12, Dec. 1965, pp. 1308-1323.

37. Roslyakov, G. S.; and Telenin, G. F.: Survey of Computational Work on Steady Axisymmetric Gas Flow Carried out at the Computational Center of Moscow State University. Numerical Methods in Gas Dynamics, G. S. Roslyakov and L. A. Chudov, eds., NASA TT F-360, Israel Program Sci. Transl., 1966, pp. 1-11. (Available from CFSTI, U.S. Dep. Com.)

38. Telenin, G. F.; and Tinyakov, G. P.: A Method of Calculating the Three-Dimensional Flow Past a Body With an Attached Shock Wave. Sov. Phys. – Doklady, vol. 9, no. 2, Aug. 1964, pp. 132-133.

39. Tiniakov, G. P.: Investigation of the Three-Dimensional Supersonic Flow Around Ellipsoids of Revolution. Lockheed Missiles and Space Co. Transl. (From Izv. Akad. Nauk SSSR, Otd. Tekhn, Nauk, Mekhan, i Mashinostr., no. 6, 1965, pp. 10-19.)

40. Makhin, N. A.; and Syagayev, V. F.: Numerical Solution of the Problem of Supersonic Flow at an Angle of Attack Past Conical Bodies. NASA TT F-10,481, 1966.

41. Bazzhin, A. P.; and Chelysheva, I. F.: Primenenie Metoda Priamykh k Raschetu Obtekaniia Konicheskikh Tel pri Bol'shikh Uglakh Ataki [Application of the Straight-Line Method in the Calculation of Flows Past Conical Bodies at Large Angles of Attack]. Izv. Akad. Nauk SSSR, Mekh. Zhidk. Gaza, no. 3, 1967, pp. 119-123.

42. Bazzhin, A. P.; Trusova, O. N.; and Chelysheva, I. F.: Raschet Techenii Sovershennogo Gaza Okolo Ellipticheskikh Konusov pri Bol'shikh Uglakh Ataki [Calculation of Ideal-Gas Flows Around Elliptical Cones at Large Angles of Attack]. Izv. Akad. Nauk SSSR, Mekh. Zhidk. Gaza, no. 4, 1968, pp. 45-51.

43. Scheuing, Richard A.; Brook, John W.; Mead, Harold R.; Melnik, Robert E.; Hayes, Wallace D.; Donaldson, Coleman duP.; Gray, K. Evan; and Sullivan, Roger D.: Theoretical Prediction of Pressures in Hypersonic Flow With Special Reference to Configurations Having Attached Leading-Edge Shock – Pt. I. Theoretical Investigation. ASD TR 61-60, Pt. I, U.S. Air Force, May 1962.

44. McConnell, A. J.: Applications of Tensor Analysis. Dover Publ., Inc., 1957.

45. Nielsen, Kaj L.: Methods in Numerical Analysis. Macmillan Co., c.1956.

46. Mysovskih, I. P. (L. B. Rall, trans.): Lectures on Numerical Methods. Walters-Noordhoff Publ. (Groningen, Netherlands), c.1969.

47. Hord, Richard A.: An Approximate Solution for Axially Symmetric Flow Over a Cone With an Attached Shock Wave. NACA TN 3485, 1955.

48. Hadamard, Jacques: Lectures on Cauchy's Problem in Linear Partial Differential Equations. Dover Publ., Inc., c.1952.

49. Garabedian, P. R.: Partial Differential Equations. John Wiley & Sons, Inc., c.1964.

50. Jones, D. J.: Tables of Inviscid Supersonic Flow About Circular Cones at Incidence $\gamma = 1.4$. AGARDograph 137, Pts. I and II, Nov. 1969.

51. Tracy, Richard R.: Hypersonic Flow over a Yawed Circular Cone. Hypersonic Res. Proj. Mem. No. 69 (Contract No. DA-31-124-ARO(D)-33), Graduate Aeronaut. Lab., California Inst. Technol., Aug. 1, 1963.

52. Melnik, R. E.: Vortical Singularities in Conical Flow. AIAA J., vol. 5, no. 4, Apr. 1967, pp. 631-637.

53. Babenko, K. I.: Investigation of a Three-Dimensional Supersonic Gas Flow Around Conic Bodies. Applied Mechanics, Henry Görtler and Peter Sorger, eds., Springer-Verlag, 1966, pp. 749-755.

54. Chapkis, Robert L.: Hypersonic Flow Over an Elliptic Cone: Theory and Experiment. J. Aerosp. Sci., vol. 28, no. 11, Nov. 1961, pp. 844-854.

55. Martellucci, Anthony: An Extension of the Linearized Characteristics Method for Calculating the Supersonic Flow Around Elliptic Cones. J. Aerosp. Sci., vol. 27, no. 9, Sept. 1960, pp. 667-674.

56. Chiang, C. W.; and Wagner, Richard D., Jr.: Analysis of Supersonic Conical Flows. NASA TN D-5884, 1970.

57. Vincenti, Walter G.; and Fisher, Newman H., Jr.: Calculation of the Supersonic Pressure Distribution on a Single-Curved Tapered Wing in Regions Not Influenced by the Root or Tip. NACA TN 3499, 1955.

58. Mead, Harold R.; and Koch, Frank: Theoretical Prediction of Pressures in Hypersonic Flow With Special Reference to Configurations Having Attached Leading-Edge Shock – Pt. II. Experimental Pressure Measurements at Mach 5 and 8. ASD TR 61-60, Pt. II, U.S. Air Force, May 1962.

59. Ames Research Staff: Equations, Tables, and Charts for Compressible Flow. NACA Rep. 1135, 1953. (Supersedes NACA TN 1428.)

NASA-Langley, 1971 — 12 L-7813

"The aeronautical and space activities of the United States shall be conducted so as to contribute . . . to the expansion of human knowledge of phenomena in the atmosphere and space. The Administration shall provide for the widest practicable and appropriate dissemination of information concerning its activities and the results thereof."

—NATIONAL AERONAUTICS AND SPACE ACT OF 1958

NASA SCIENTIFIC AND TECHNICAL PUBLICATIONS

TECHNICAL REPORTS: Scientific and technical information considered important, complete, and a lasting contribution to existing knowledge.

TECHNICAL NOTES: Information less broad in scope but nevertheless of importance as a contribution to existing knowledge.

TECHNICAL MEMORANDUMS: Information receiving limited distribution because of preliminary data, security classification, or other reasons.

CONTRACTOR REPORTS: Scientific and technical information generated under a NASA contract or grant and considered an important contribution to existing knowledge.

TECHNICAL TRANSLATIONS: Information published in a foreign language considered to merit NASA distribution in English.

SPECIAL PUBLICATIONS: Information derived from or of value to NASA activities. Publications include conference proceedings, monographs, data compilations, handbooks, sourcebooks, and special bibliographies.

TECHNOLOGY UTILIZATION PUBLICATIONS: Information on technology used by NASA that may be of particular interest in commercial and other non-aerospace applications. Publications include Tech Briefs, Technology Utilization Reports and Technology Surveys.

Details on the availability of these publications may be obtained from:

SCIENTIFIC AND TECHNICAL INFORMATION OFFICE

NATIONAL AERONAUTICS AND SPACE ADMINISTRATION

Washington, D.C. 20546